UTS UNIVERSITY OF TECHNOLOGY SYDNEY

High Density Multiband Multi-Array Technologies for 5G Communication Antenna Systems

by Madiha Farasat

Thesis submitted in fulfilment of the requirements for

the degree of Doctor of Philosophy

under the supervision of

Principal Supervisor: Dr Yang Yang Co-Supervisor: Dr Dush Thalakotuna and Nathan Hu.

University of Technology Sydney

Faculty of Engineering and Information Technology

April 2024

Certification of Original Authorship

I, Madiha Farasat, declare that this thesis, is submitted in fulfilment of the requirements for the award of Doctor of Philosophy, in the Faculty of Engineering and Information Technology at the University of Technology Sydney.

This thesis is wholly my own work unless otherwise reference or acknowledged. In addition, I certify that all information sources and literature used are indicated in the thesis.

I certify that the work in this thesis has not previously been submitted for a degree nor has it been submitted as part of the requirements for a degree at any other academic institution except as fully acknowledged within the text.

This research is supported by the Australian Government Research Training Program.

Signature: Production Note:
Signature removed prior to publication.

Date: 26 April 2024

Abstract

A number of distinct concerns are driving the switch to multiband technologies for 5G communication, including the requirement for increased network capacity, the ability to handle a wide range of diverse use cases applications, and the opportunity to improve network performance. Multi-band and multi-beam arrays are good options, but they impose extra demands on the antennas. For instance, high performance antenna elements are necessary, however, cross-band scattering, a long-standing concern in multi-band antenna arrays, must be eliminated in order to preserve antenna system performance and stability. Secondly, wide operational bandwidth and consistent patterns with low side-lobe levels are sought for multi-band antenna arrays. All of these things are challenging to achieve. This thesis tackles the aforementioned issues by making four major contributions.

The first contribution is a detailed review article of base station antenna (BSA) technologies. The goal of this communication is to present a complete overview of recent BSA antenna designs and challenges, with a focus on lower microwave bands in the sub-6 GHz area. While there is a substantial amount of published work on BSAs, there is no unified discussion of BSA evolution with mobile technology. As a result, a brief overview of how BSA technologies have developed across mobile generations will benefit the antenna community.

The second contribution is the creation of novel methodology of HV dipoles (Horizontal vertical dipoles) for reducing cross-band interference in multi-band BSA arrays. The experimental results show that cross-band scattering is reduced and that both arrays exhibit stable radiation patterns over a wide range of operational bandwidths. The strategies proposed for controlling cross-band scattering ensure the coexistence of antennas for diverse services and promote communication standard development.

The third contribution is the development of a distinctive approach for common mode resonance suppression through filtering circuitry which helps to reduce the common mode resonance in multi-band BSA arrays. The experimental results verify the novel prototype and its significance. Hence, the proposed technique can be implemented for a wide range of multiband antenna where radiating elements are interspersed on same ground plane to supress pattern distortion.

The fourth contribution is the development of a compact antenna system as per modern day antenna requirements. There hasn't been much research conducted on how to maximise the directivity of wideband multiband antennas while catering size restrictions. The proposed designs can be utilised to boost system capacity in a variety of cellular base stations.

Acknowledgements

First of all, I would like to express my deepest gratitude to my principal supervisor Prof. Yang Yang for his continuous guidance and support throughout my PhD study. Prof. Yang has provided me with a remarkable research environment and has given me insightful advice. Furthermore, I am honoured to benefit from his personality and hard work, which I will treasure my whole life.

I am profoundly grateful to my co-supervisor Dr. Dush Thalakotuna for his valuable suggestions on this work, ongoing support and innovative ideas for my research projects. Dr Thalakotuna led me into the field of base station antennas and taught me how to combine scientific knowledge with industrial realizations. I am greatly inspired by his deep insights into technical issues. His attitude towards research left a deep impression on me, which will prove to be beneficial to my research career.

I would like to thank my co-supervisor Dr. Nathan Hu for his valuable suggestions on this work, support with testing and experiments.

Last but not least, I would like to express my forever thanks to my parents, my husband and especially my kids, for their unconditional love, unreserved support and encouragement throughout my journey.

Published and Under Review Papers

1. M. Farasat, D. Thalakotuna, Y. Yang, Z. Hu, and K. Esselle, "Suppression of Common-Mode Resonance in Multiband Base Station Antennas," *Sensors,* vol. 23, no. 6, p. 2905, 2023. **Chapter 4**.

2. M. Farasat, D. Thalakotuna, Z. Hu, and Y. Yang, "A Simple and Effective Approach for Scattering Suppression in Multiband Base Station Antennas," *Electronics,* vol. 11, no. 21, p. 3423, 2022. **Chapter 3.**

3. M. Farasat, D. N. Thalakotuna, Z. Hu, and Y. Yang, "A review on 5G sub-6 GHz base station antenna design challenges," *Electronics,* vol. 10, no. 16, p. 2000, 2021. **Chapter 2.**

4. M. Farasat, D. Thalakotuna, Z. Hu, and Y. Yang, " A Novel Cross-Interspersed Design of Multiband Antennas for Base Station Applications*," In* 2023 *IEEE International Symposium on Antennas and Propagation and USNC-URSI Radio Science Meeting Portland, Oregon,* USA. **Chapter 3.**

5. M. Farasat and Y. Yang, "Investigation of Radome Enclosed Antenna with Tilted Angles of 10° and 20° for Airborne Applications," *in 2020 4th Australian Microwave Symposium (AMS), 2020: IEEE*, pp. 1-2.

6. M. Farasat, D. N. Thalakotuna, and Y. Yang, " Compact Multi-Band Triangular Patch Antenna for 5G WLAN Applications," ready to submit, *2024 International Applied Computational Electromagnetics Society (ACES) Symposium*. **Chapter 5.**

7. M. Farasat, D. N. Thalakotuna, and Y. Yang, "Compact + 45 Dual Polarized Antennae for Triple Band Cellular Communication," Submitted to ACES *Journal*. **Chapter 5.**

To my Parents, Husband and

beloved Children

Table of Contents

List of Figures:

List of Table:

List of Abbreviations

BSA	Base Station Antenna
FBR	Front-to-Back Ratio
HB	High Band
HPBW	Half-Power Beamwidth
LB	Low Band
ME-dipole	Magneto-Electric Dipole
MIMO	Multiple-Input Multiple-Output
PDR	Power Division Ratio
RHCP	Right-Handed Circular Polarization
SLL	Side Lobe Level
CMSC	Common Mode Suppression Circuit
TCCD	Tightly-Coupled Cross-Dipole
XPD	Cross Polarization Discrimination
3G	Third Generation of Cellular Mobile Communications
4G	Fourth Generation of Cellular Mobile Communications
5G	Fifth Generation of Cellular Mobile Communications

Chapter 1: Multiband Technologies

1.1 Introduction

In the last few decades, mobile communication has seen rapid changes. Improvements in mobile communication have been noticeable from the first generation to the current fourth generation, also known as the Long-Term Evolution (LTE)/4G. If the network were updated, data transfer speeds, latency, capacity, and device compatibility would all improve. In order to ensure that future mobile communication technologies are compatible with the existing infrastructure, several studies focusing on various aspects of upgrading the existing system have been initiated.

The huge data rates that can be supported by 5G have made it the focus of a lot of academic and business attention recently. When it finally launches, 5G will use millimetre waves (in the 30GHz to 100GHz range) to cover the radio frequency spectrum. Many businesses are betting on the WLAN infrastructure and small cell idea, both of which will benefit from the use of mmWave in the future, by investing in R&D at the experimental stage. On the other hand, the same mmWave frequencies may be used to wirelessly broadcast ultra-high-definition (UHD) video to HDTVs, HD Game Consoles, and other HD video sources. The Wireless Gigabit Alliance (WiGig) is being studied for use in future gigabit-rate audio/video media devices. As an added bonus, this innovation improves conventional auto-motives while allowing for high-performance data transfer between computers and satellite communication.

When compared to its predecessors, the fifth-generation (5G) communication networks are expected to provide faster data rates, reduced latency, and more capacity. 5G networks are dependent on a number of cutting-edge technologies, including multiple input multiple output (MIMO), beamforming, and higher frequency bands, in order to accomplish these objectives. The usage of high-frequency bands does, however, come with a number of drawbacks, the most notable of which are restricted coverage, low penetration, and increased attenuation. Multiband technologies have evolved as a potentially useful option in response to the problems

presented above. The following paragraphs, discuss several key high-density multiband technologies used in 5G communication.

1.2 Technologies Essentials for High-Density Mobile Communication Systems

1.2.1 Antenna Systems

The coverage, capacity, and quality of the network are all determined by the antenna systems that are used in 5G communication. This makes antenna systems an extremely important component. Different kinds of antenna systems are implemented in 5G networks, such as massive MIMO and beamforming.

1.2.2 Massive MIMO

Massive Multiple Input Multiple Output, or Massive MIMO, is a major technique in 5G communication that makes use of a huge number of antennas to enhance spectral efficiency, boost capacity, and decrease interference. Massive MIMO is able to function in frequency ranges below 6 GHz as well as millimetre wave (mmWave) frequencies. Massive MIMO can utilise up to 32 antennas in frequency ranges below 6 GHz, while in mmWave frequencies, it can use up to 256 antennas simultaneously. The use of massive MIMO may greatly increase the performance of 5G networks, which is particularly beneficial in densely populated metropolitan areas with a high demand for data.

1.2.3 Beamforming

The capacity and quality of the network may both be improved using another antenna technique called beamforming, which is employed in 5G communications. The practice of directing radio waves towards a particular place or device, known as beamforming, may boost the signal's power while simultaneously lowering the likelihood of interference. Different antenna technologies, such as phased array antennas and digital beamforming, may be used to accomplish beamforming in various wireless networks.

1.2.4 Antennas Using a Phased Array

The creation of a directed beam from many antennas may be accomplished with the use of a phased array antenna, which is a specific kind of antenna system. Phased array antennas are able to be electrically guided in a variety of directions, which enables them to monitor and communicate with many devices at the same time. Phased array antennas are appropriate for applications that demand high data rates and minimal latency. These antennas may be employed in both sub-6 GHz and mmWave bands.

1.2.5 The Use of Digital Beamforming

The phase and amplitude of radio waves that are delivered by various antennas may be modified via the use of digital signal processing in the digital beamforming technology. Digital beamforming may be accomplished using a variety of antenna methods, such as sub-array beamforming and hybrid beamforming, and it can be employed in both the sub-6 GHz and the mmWave bands.

1.2.6 Small Cells

In 5G communication, small cells are an additional kind of antenna technology that is utilised to expand capacity and improve coverage in high-traffic regions. Small cells are low-power base stations with a limited range that may be deployed either inside or outside of a building. Small cells have the ability to function in a variety of frequency bands, including sub-6 GHz as well as mmWave bands. Various configurations of small cells, such as femtocells, picocells, and microcells, are all possible when using small cells.

1.2.7 Radomes

A radome is a specific kind of protective cover that is used for the purpose of shielding antenna systems from elements of the surrounding environment such as precipitation, wind, and debris. In most cases, radomes are crafted from materials such as fibreglass, carbon fibre, or Kevlar. Radomes may be engineered to give varying degrees of protection and transparency, and they can be employed in frequency ranges below 6 GHz as well as above 6 GHz for mmWave communications.

1.2.8 A Variety of Additional Multi-Band Technologies

In 5G communication, in addition to antenna systems and radomes, various multiband technologies are utilised. These technologies are used to increase the quality of the network as well as its capacity. These technologies include one of the following:

A. Distributed Antenna Systems, or DAS for short

Distributed antenna systems are a form of antenna technology that give wireless coverage over a vast region by using several antennas to cover the desired area. Both sub-6 GHz and mmWave frequencies are accessible to use with DAS.

1.3 The Utilisation of Multi-Band Technologies in 5G Communication Antenna Systems

The antenna systems utilised for 5G communications use a number of multiband technologies.

- MIMO (Multiple Input Multiple Output) technology is based on the use of several antennas for both transmission and reception, which increases throughput and strengthens signals.
- Beamforming technology is a method of boosting signal strength and decreasing interference by focusing a wireless signal in a narrow beam.
- Carrier aggregation is a method that uses several carriers together to boost available bandwidth and hasten the pace at which data may be sent.
- These antennas send out signals in two separate polarisations, increasing the intensity of the signal while decreasing the likelihood of interference.
- To enhance coverage and capacity in densely populated regions, small cells, which are low-power, short-range wireless access points, are increasingly being deployed.

Because of their ability to boost data transmission speeds, strengthen signals, and lessen interference, multiband technologies are crucial components of 5G communication antenna systems.

1.4 Research Objective

1.4.1 The Rationale for the Evolution of an Era Towards Multi-Band

The transition towards multiband technologies for 5G communication is being pushed by a number of distinct considerations, including the need for higher network capacity, the ability to accommodate a variety of diverse use cases and applications, and the capability to enhance network performance. In this response, we will go into these considerations more deeply and explain why multiband technology is quickly becoming an essential component of 5G communication.

To begin, one key motivation for the deployment of multiband technology in 5G communication is the need for higher network capacity. Mobile networks are coming under increasing amounts of pressure to deliver quicker and more consistent connection due to the proliferation of mobile devices and the rising demand for high-bandwidth applications such as video streaming and online gaming. As multiband technology makes it possible for network operators to expand the amount of spectrum that is accessible, this results in increased bandwidth for customers and an improvement in the network's total capacity.

Secondly, multiband technology has the potential to increase network performance, particularly in regions where signal strength is low or where there is congestion. The use of various bands within 5G networks enables load balancing over many frequencies, which in turn enables more effective utilisation of the spectrum that is now accessible. Especially in high-traffic regions such as stadiums, airports, and city centres, this may assist in minimising network congestion and increasing the dependability of the network.

Thirdly, multiband technology is essential because of its importance in enabling a wide variety of applications and use cases. Each of these use cases may have various needs in terms of bandwidth, latency, and reliability, and 5G is expected to allow a broad variety of new applications and services. These use cases span from driverless cars to industrial IoT. 5G networks, which make use of multiband technology, are able to accommodate a wide number of various use cases, hence providing for increased flexibility and adaptability.

Last but not least, the use of multiband technology is essential to the worldwide interoperability and standardisation processes. It is possible that various nations and areas could have access to different frequency bands for 5G. Using multiband technology is one way to assist in the assurance that devices and networks will be able to function across a variety of countries, regions, and networks. This is essential for guaranteeing that 5G can be implemented anywhere in the world and that consumers can have uninterrupted connection regardless of where they are located.

In the final analysis, multiband technology is becoming an increasingly significant component of 5G communication as a result of its capability to enhance network capacity, improve network performance, support a variety of various use cases, and maintain worldwide compatibility and standardisation. We may anticipate that multiband technology will play an increasingly crucial role in the delivery of connection that is quicker, more dependable, and more adaptable to people all around the globe, as 5G continues to develop and grow.

1.4.2 Requirements for Antennas Used in Multi-Band Base Stations

Antennas for multiband base stations are intended to function over many frequency bands, often spanning frequencies lower than 6 gigahertz in range. These antennas are required as a result of the constantly growing demand for wireless data transmission as well as the efforts made by service providers to improve the quality and speed of the services they deliver to their respective clients. When numerous frequency bands are used, the available spectrum may be utilised more effectively, which in turn results in improved coverage.

The following are some of the advantages of multiband base station antennas:

- Multiband antennas enable service providers to cover a broader area with fewer antennas, hence boosting the total coverage and lowering the number of sites necessary to serve a given region. This results in improved coverage.
- Greater signal quality: The use of various frequency bands makes it possible to achieve greater signal quality, which in turn may result in increased data transfer rates and a decrease in the number of signal dropouts.
- Reduced interference: As the number of wireless devices continues to proliferate, interference is becoming an increasingly significant problem. Making use of a number

of different frequency bands helps to cut down on interference, which ultimately leads to improved service quality.

- Utilisation of various frequency bands enables more effective utilisation of the available spectrum, which enables the more efficient usage of numerous frequency bands. This might result in higher capacity, enabling service providers to accommodate a greater number of customers and a greater volume of data traffic.

1.4.3 5G Base Station Antenna Incentive and Challenges

With more mobile users in the wireless network the spectrum utilization ratio increased, which demands more capacity. The need for more base station antennas impacted the mutual interference as the typical base station antenna covered a single narrow band. This has caused a cluster of antennas at a site. The maintenance and installation have become complicated. Dual band, dual polarization, multiband, double beam, multiband and dual polarized technologies have been used to reduce the above highlighted problems and to increase the spectrum efficiency. Different topologies are still being investigated using modern technology like combining two or more bands and extending bandwidth to meet the current telecommunication industry standards. The weight, load, compact size, and fabrication cost are realistic measures to consider in designing any antenna system.

The challenges associated with the BSAs are classified into three main categories, as shown in Figure 1.1. The challenges associated with the port measurements include the design challenges in achieving wide impedance bandwidths and meeting the port-to-port isolation requirements. The challenges in radiation patterns are mostly due to the interspersed nature of the multiband arrays. The radiating elements of other bands cause scattering and undesirable effects on the radiation patterns. Therefore, the radiating elements of one band have to be made almost transparent for the other band and vice versa. The size constraints are another challenge faced by the BSA designers. The real estate available on an antenna tower is very limited and costly; therefore, smaller compact antennas without any electrical performance degradation are always preferred.

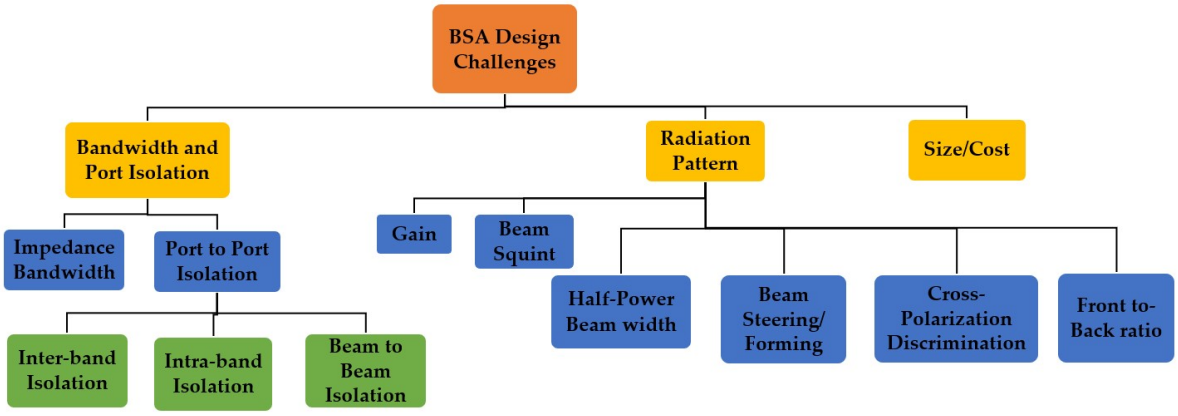

Figure 1.1 Classification of base station antenna challenges based on design.

1.4.4 Research Problems/Questions

From the studies discussed in the previous section and the highlighted research challenges for the design of 5G base station antenna, the questions identified for our research are as follows:

1. How to get a desirable pattern with multiband technologies?
2. What coupling techniques would improve performance for multiband antenna systems?
3. How can compactness be obtained in multiband antenna systems by keeping structure simple?

1.4.5 Research Gap

Based on the review of studies and challenges discussed in section 1.4.4 following are the research gaps finding:

Multiband arrays use is increasing in all communication systems due to the space saving it provides. However, sharing the same aperture leads to undesirable patterns: beam squint, beamwidth variation, ripples in pattern etc. This is due to coupling between antenna elements. There is some existing work on cloaking one band from another but this can result in complex radiating element designs. There is scope to look at different simple and effective techniques to reduce this coupling hence improve the patterns and other electrical performance on multi-band arrays.

1.5 Research Contents and Innovation with Thesis Outline

Based on the existing challenges in the advanced field of multiband technologies, the following objectives are set for the proposed research work for each chapter. The proposed research work is implemented in the following research content sequence

- **Chapter 1** gives a brief introduction of this report that includes multiband multi array technologies. It mentions the research objective, incentive along with the research gap that identifies the research aim, objectives and significance in the context of the challenges described.
- **Chapter 2** describes the relevant background of the research with one of the key multiband technology base station antenna (BSA) and its design challenges. It contains the history of the cellular mobile communication system along with evolution of BSA and their fundamental parameters and characteristics.
- **Chapter 3** addressed the design challenge of cross band scattering for multiband BSA systems. A simple and effective approach of HV (horizontal and vertical Dipoles) is demonstrated for scattering suppression.
- **Chapter 4** presents the novel technique to overcome common mode (CM) resonance effect challenges in multiband antennas. A common mode suppression filtering circuitry in matching network is introduced to reduce the CM effect for BSA application.
- **Chapter 5** addresses the compactness challenges in multiband antennas. Triple band dual polarized antenna for 5G MIMO capabilities are proposed followed by triangular split antenna for WLAN application.
- **Chapter 6** presents a further proposition towards multiband technology 5G antenna communication systems, in which mmW antennas as another solution towards 5G communication is discussed and implemented.
- **Chapter 7** reports the future works for 5G and next generation multiband technologies.

1.6 Aim and Significance

1.6.1 Research Aim

Base Station Antennas are fixed to the base stations which is a wireless system that uses microwave radio communication for cellular connectivity to users. It is usually mounted on towers. Different mobile communication systems have been nominated with different frequency bands. Modern mobile communication systems increase the demand for updated base station antennas. Base station antennas in addition to pragmatic and industrial measures/specifications going to new operational and economic advantages. The research aim is to have a detailed overview of these multiband technologies, and to consider the design specification. Developmental trends of multi-band antenna arrays with antenna elements at different bands.

1.6.2 Research Stakeholders

This research work will assist the national organization, manufacturer, service provider and developers to understand the essentials of 5G base station antenna system, its significance and the existing gaps. They may use it for design and development of 5G BSA and related infrastructure. Furthermore, this study would guide the researchers and academicians to improve their research knowledge and learn from existing voids of 5G base station antenna systems.

1.6.3 Social and Military Benefits

Our growing tech industry demands changing the maintenance of our antenna system with decreased budget and high performance. The aviation industry in particular is looking for advances in efficiency for inspection technology not only for safety, but also to make significant cost savings and avoidances. This indigenous research work would help in design and development of critical products which would generate revenue for our nation.

Chapter 2: Literature Review

2.1 Evolution of Cellular Mobile Communication Systems

The evolution of wireless communication technology started from first generation (1G) technology. However, the journey actually started many years ago in the17th Century when the first-time telegraph was used which was followed by the invention of the telephone in 1876. Moving from wired telephonic communication to wireless communication was a big revolution. This revolution is mobile radio telephone which was later called zero generation (0G) or pre-cellular mobile telephony that use PTT (Push to Talk), AMTS (Advanced Mobile Telephone system) technologies. 1G is the first generation of wireless mobile networks.1G of mobile communication opened wireless doors for everyone. From 1G to every successive generation of wireless standards has introduced astonishing advances in capacity, quality and speed for the communication channel and data transmission. The second generation (2G) technology, also called the Cultural Revolution lasted for quite a while from 1980's to 2003. In the 2G era there were numerous advancements made in access technologies to improve the channel capacity and to decrease the latency. Access technologies such as: GSM, GPRS and EDGE in 2G enabled data transfer at 30-35 kbps, 110 kbps and 135 kbps respectively. The 3G networks started rolling out in mid-2001. 2G was then replaced by 3G to significantly improve the data transmission up to speed of 2Mbps. The 3G widely based on CDMA2000 and EDGE technologies enables video streaming and more security. The jump from 3G to 4G networks was significant. 4G started in 2008 and enables faster communication with minimum at data rates of 100 Mbps. It also allows high definition streaming and increased portability.

Every jump to the next generation is to revolutionize the market and update the way of communications. What started simply as a network with only voice call and basic text messaging transformed to MMS that modified to fast speed video streaming. The process of this wireless communication technology evolution is still continuing. The network architecture simplified and modified day by day to achieve high speed and efficiency. The recent mobile applications, IoT devices, and other smart devices demand high data rates and more channel capacity. This demand leads the operator to update cellular data services and move to the next generation. 5G is finally making its debut and taking over from 4G. 5G is the latest generation

which is opening doors for new network architecture and planning for enabling technologies to be faster and more efficient. It is the next step in modern internet technology that changes everything from phone to field i-e self-driving cars and remote surgeries.

2.2 An Overview of the Evolution of Cellular Base Station Antenna Systems

One of the critical modules in a wireless mobile communication system is the base station antenna (BSA). The typical 1G base station antennas were Omni directional antennas since the coverage was more of a priority than the capacity in this first generation of mobile networks. With the increased users in the second generation 2G networks, operators started to consider ways to increase the capacity in their network. One of the techniques used for capacity improvement is sectorization in 2G networks. A common sectorization technique used in 2G is to divide the previous Omni cell into 3 sectors of 120^{o} each. As a result, three antennas, each having a half power beamwidth (HPBW) of 120^{o} are used in the Base Transceiver Station (BTS).

Another technique used in 2G networks to enhance capacity is the use of polarization diversity. The aim was to provide two orthogonal polarizations in the antenna array. The horizontal (H) and vertical (V) polarization were initially used, but ±45^{o}, otherwise known as slant polarization, has been widely adopted in many BTS antennas since 2G. In Figure 2.1 (a), (b) shows vertical and slant polarized dipole array configurations used in BSAs in 2G and following generations. The number of users increased rapidly, moving from 2G to 3G due to the introduction of mobile data services in 3G. As a result, operators had to explore further techniques to increase capacity. One solution was to further subdivide the sector into narrower sectors. This was done using narrow beam antennas with half-power beamwidth (HPBW) such as 65° or even 33°. One of the disadvantages was increased antenna loading on the tower.

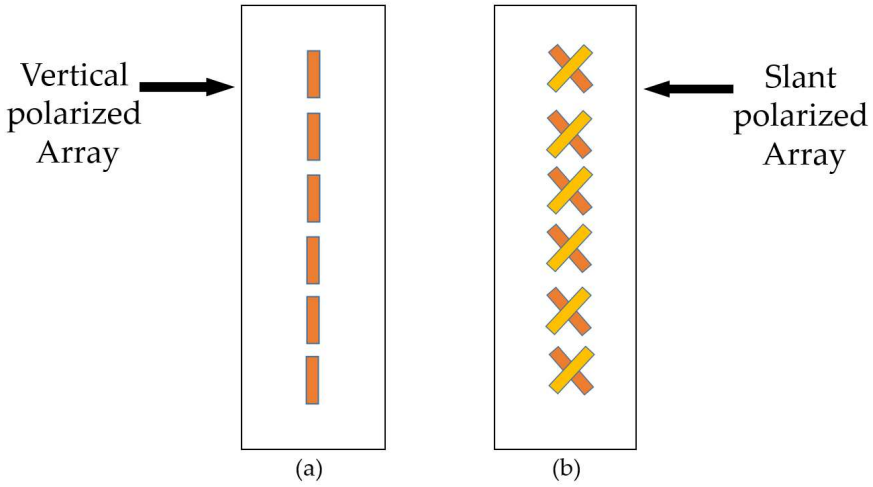

Figure 2.1 (a) Vertical polarized dipole array. (b) Slant polarized dipole array.

A solution to antenna loading was achieved by introducing multibeam panel antennas. Such antennas are similar in appearance to conventional sector antennas but have multiple narrow beams. As a result, increased capacity is achieved without the need for additional antennas, as shown in Figure 2.2. Narrow-beam base station antennas (BSAs) focus on transmitting or receiving signals within a narrow angle range, making them excellent for accurate targeting and long-range transmission. Twin-beam BSA antennas, on the other hand, can handle two different narrow beams at the same time, providing improved capacity and flexibility, particularly in highly populated regions or places where wireless access is in high demand. While narrow-beam BSAs are excellent at minimising interference and focussing signals, twin-beam BSAs provide improved multitasking capabilities, but with possibly more difficult design and implementation requirements. The twin beams or multibeam are achieved by introducing hybrid couplers into the feed network as shown in Figure 2.3. These multibeam antennas have been a prevalent choice among operators for mobile networks since then.

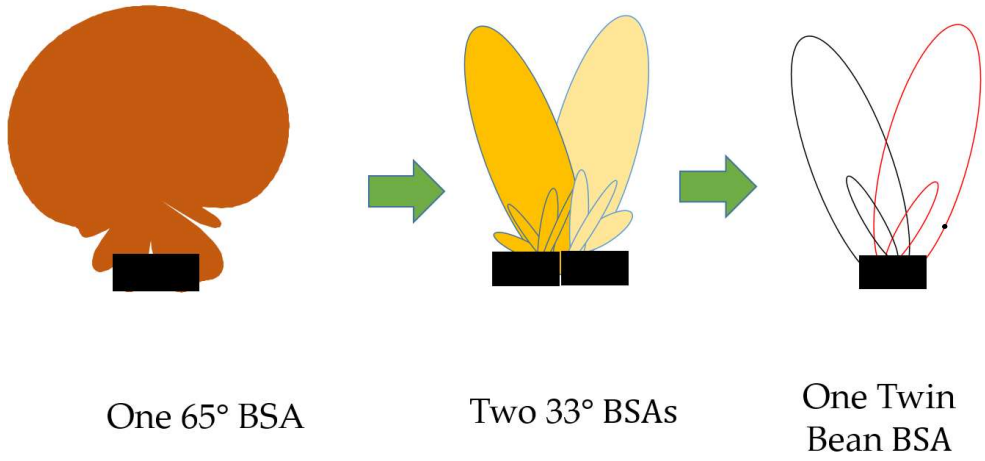

Figure 2.2 Patterns of a single-beam BSA, two narrow-beam BSAs, and a twin-beam BSA.

An increased number of cells/sectors requires comprehensive network planning to reduce cell edge interference and the need for operators to adjust the cell/sector coverage. This is achieved in a BSA antenna by providing beam tilting in the elevation plane. Most of the BSA antennas from 3G networks and later were equipped with a Remote Electrical Tilt (RET) feature, allowing the operator to remotely configure the elevation beam tilt in a 0–10° range to optimize the network. The elevation beam tilt in the antenna is achieved using a phase shifter that provides a phase gradient to the elements in the antenna array. Therefore, most of the BSA antennas from 3G networks and beyond had the capability of beam tilting in the elevation plane. However, the elevation beams steering feature achieved using such phase shifters is only suitable for network optimization, not for beamforming in the elevation plane. With 2G and 3G technologies, an additional spectrum was introduced beyond the previously used 800 MHz and 900 MHz bands. Primarily occupied higher frequency bands worldwide were in 1710–2100 MHz bands. With 4G LTE, additional spectra up to 2.6 GHz were used worldwide. In 5G, sub-6 GHz bands have an additional spectrum in 700 MHz bands and 3.4–3.6 GHz bands. Therefore, with every generation, the existing spectrum is reused, while additional bands are introduced.

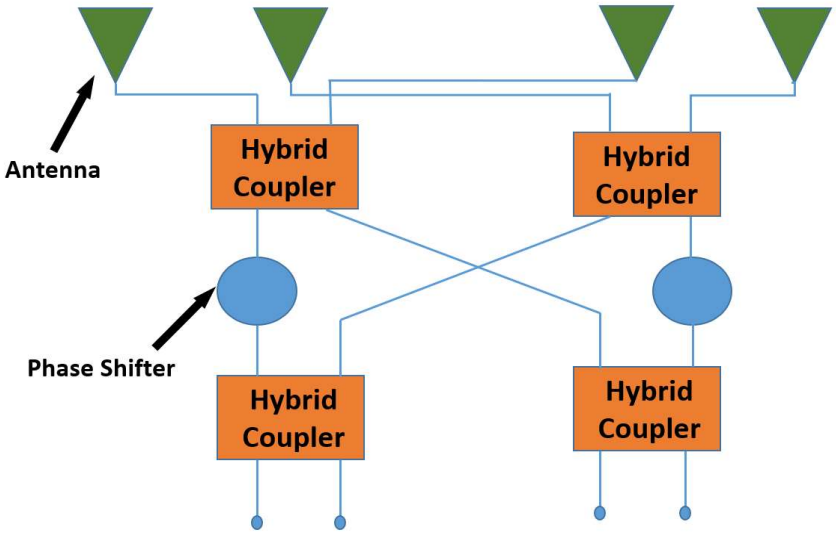

Figure 2.3 Hybrid coupler in MIMO antenna array.

The radiating antenna elements used in BSAs, however, have limited bandwidth. Hence, a single element cannot operate in multiple bands. The most common approach in BSAs is to have two to three distinct radiating elements to cover these bands, i.e., one radiating element to cover lower bands 650 MHz–960 MHz [1] and another for 1695 MHz–2760 MHz [1-3], and a third element type to operate in 3.4–3.6 GHz [4]. As a result, each of these bands is provided by a separate antenna array. Although early 2G networks used separate antennas for each band, later generations used antennas with multiple bands in one housing. This technology is called multiband antennas. A multiband antenna has multiple arrays, each serving a different band within one enclosure. In the initial generations of multiband antennas, the arrays were physically separated as shown in Figure 2.4a. These multiband antennas provided space and weight savings compared to two separate antennas.

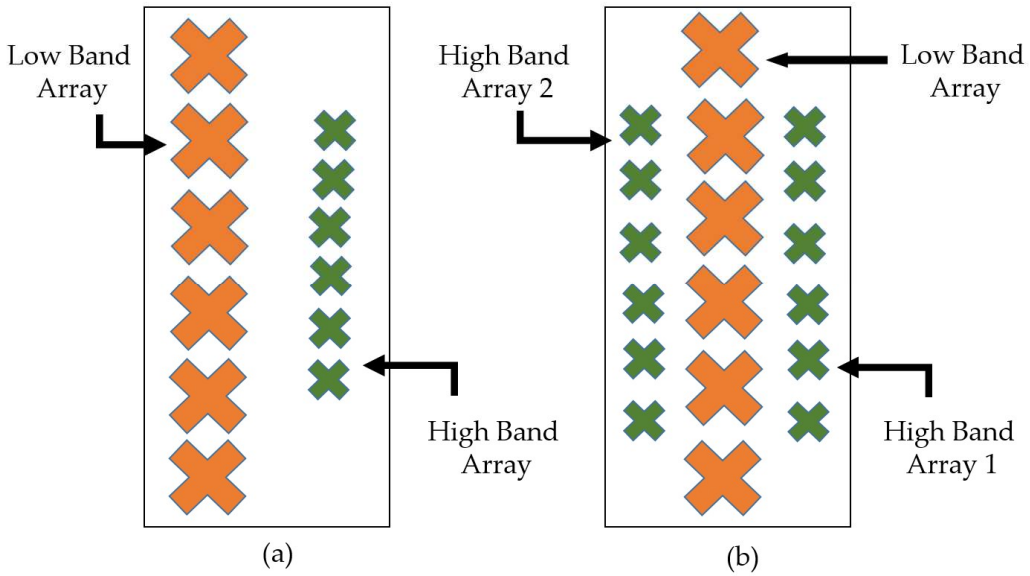

Figure 2.4 (a) Multiband antenna with physically separated arrays; (b) multiband antenna with interspersed arrays.

Later generations resulted in multiple interspersed arrays, as shown in Figure 2.4b, which further improved the space and weight savings. However, interspersed arrays present significant challenges during antenna designs, such as inter-band coupling and pattern distortions, discussed in detail in chapter 1 Section 1.4.3 of this work.

The antenna arrays in higher frequency bands occupy less area since the vertical element spacing is much smaller in higher frequencies compared to lower frequency bands. Therefore, multiple higher-frequency band arrays can be accommodated with one low band array, as shown in Figure 2.5. The most common configurations were a 1:2 or 1:4 array ratio between low band to high band. The antenna shown in Figure 2.5, has two ports for two polarizations used in low band array and two ports each for high band array, resulting in a total of 10 ports. This antenna architecture also allows multiple operators to share antenna arrays. As an alternative to such multiband arrays, antenna co-sharing was still practised among operators using a diplexer to combine multiple bands into one BSA, even with single-band antennas. Some advanced BSAs in the 3G era comprised dual polar multiband and multibeam antennas.

Notable changes compared to previous mobile network generations in the air interface are first introduced with LTE-A. A significant increase in data rates is achieved in LTE-A due to MIMO capability. Up to eight layers of MIMO are first introduced in 3GPP Release 10. MIMO transmit data in parallel both in time and frequency in segregated streams. The BSAs are

required to have spatially separated antenna arrays or polarization diversity to achieve the decorrelation in RF paths. The spatial separation has to be at least 0.7λ or more [5]. Some of the multiband antennas used in 3G networks at the time had 2–4 high band arrays already, and the operators could use them for MIMO operation without upgrading the BSA design. High band arrays are commonly used for MIMO operation, but some BSA designs can also support up to 4X MIMO for low band arrays [6].

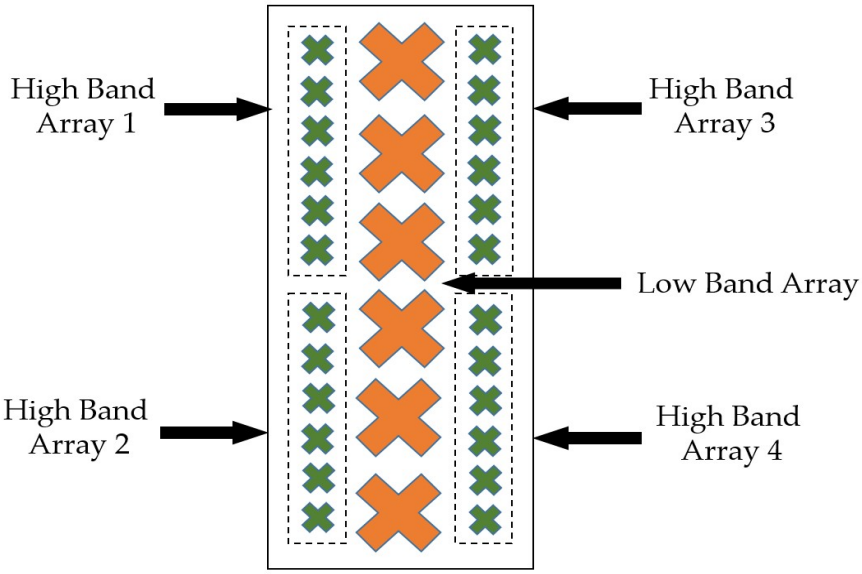

Figure 2.5 Low band to high band 1:4 antenna array configuration.

The 3GPP release 12 and 13 introduced active antenna systems (AAS) and massive MIMO (mMIMO) operation, which allowed real-time beamforming to provide increased capacity and reduced interference. These capabilities are adopted in the 5G air interface and are commonly referred to as 5G antennas among the antenna community. The mMIMO with AASs are extensively used in mm-wave bands due to advancements in the Antenna in Package (AiP) and millimeter-wave integrated circuit (MMIC) technologies. The smaller wavelengths at mm-wave require only small antenna footprints, allowing them to be directly integrated with the transceivers. However, the peak power limitations, efficiencies at mm-wave transceivers and propagation and penetration losses at mm-wave frequencies limit the use of mm-wave BSAs to indoor use and small cells. The mMIMO in sub-6 GHz is also used by the operators for outdoor coverage due to low propagation and penetration losses at these frequencies. The challenges of mm-wave antennas have significant differences to the sub-6 GHz BSAs. Within

the scope of this discussion, we present the challenges associated with the BSAs in sub-6 GHz and below, as these BSAs are the most widely used antennas by the operators to date.

The mMIMO aims to control the Signal-to-Noise Ratio (SNR) to each user by forming beams to each user unlike single-user MIMO and Multi-User MIMO in LTE and LTE-A. This requires a two-dimensional antenna array with control on the amplitude and phase to steer the beam in azimuth and elevation. The conventional beamforming antenna arrays require the element spacing to be 0.5λ to reduce the grating lobes. In contrast, the MIMO demands more spacing between the arrays to increase spatial diversity to at least 0.7λ or more. In practice, a compromise is made, and a 0.65λ column spacing is used in most of the mMIMO antennas. The need to form the beam requires a phase and amplitude control at each radiating element, which can be done using either analog beamforming architecture, digital beamforming architecture, or a hybrid beamforming architecture. The analog and digital beamforming architectures most commonly used are shown in Figure 2.6. Analog beamforming has a significantly lower power consumption than the digital beamforming technique due to a lack of active components. However, in practice, analog beamforming cannot provide true mMIMO capability because the beams formed by analog beamforming are either multiple fixed beams or steer at a much slower rate compared to the digitally formed beams. In practice, analog beamforming is achieved by either a beamforming network such as Butler Matrix [7] or using a lens [8]. Digital beamforming is the preferred architecture in Sub-6 GHz mMIMO antennas as most of the beamformers can provide IF outputs up to 6 GHz. Hybrid beamforming architecture is mostly used in mm-wave 5G realizations, in order to achieve power savings and reduce complexity in the designs. More details on the current sub-6 GHz adapted beamforming technologies and the challenges are discussed in section 2.4.

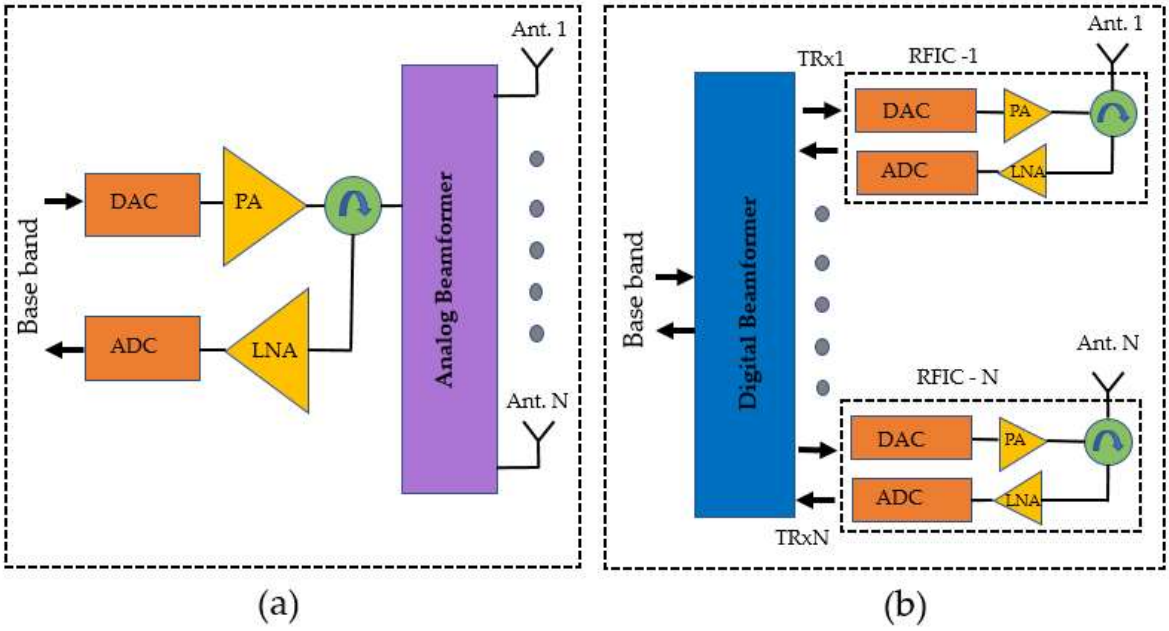

Figure 2.6 (a) Analog beamforming architecture; (b) Digital beamforming architecture.

2.2.1 Mobile Communication Architecture

The mobile communication network is structured using cells. Different possible techniques are adapted by mobile communication systems to increase the capacity and coverage of the network. To increase the capacity of the mobile communication network, each cell is divided into sectors. This process is called sectorization. Cells shape, size and orientation is directly related to the antenna's performance and coverage. The process of sectorization and use of different cell sizes can be adapted together to achieve the required coverage and capacity.

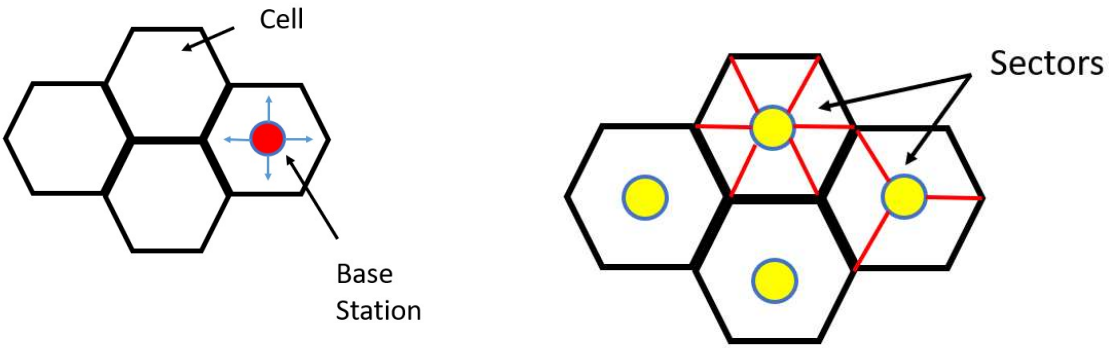

Figure 2.7 Cell topology of the mobile communication network.

In Figure 2.7 the cells are displayed as neighbouring hexagons, which is an appropriate model for an ideal cell topology, having well-defined borderlines and avoiding any overlapping of cells as well as any coverage gaps between cells.

When [7] using these technologies the three trends for BSA design to tackle 5G demands are reported as:

- Sectorization: to upgrade a cell site from a standard three sector to six or more sectors.
- Active antenna System: an antenna/radio combination connected back to the baseband with fibre e.g. hybrid active/passive BSA.
- Cell Shaping: beamforming technology used to sculpt overall cell coverage.

2.2.2 Important Communication Standards

Today's wireless and cellular communications use different digital communication standards in several frequency bands. Some important ones are shown in Table 2.1. Base stations are used in many different communication standards and can also be installed by public authorities. A wideband antenna that covers the above highlighted bands for base station applications is considered ideal for future 4G/5G and co-existing systems.

Table 2.1: Bands for different mobile communication system for BSA cover along with variation for sub-6 GHz range for 5G based on geographical locations/countries.

No.	Systems	Bands (MHz)	Geographical area	Bands (MHz)
1	FDD 1700	1690-1710	USA	3100 – 3550 3700 – 4200
2	DCS	1710-1880	USA	1900-2100
3	PCS	1850-1990	Korea	3400 – 3700 2100-2300
4	UMTS	1920-2170	India	3500-2300 1800-2100
5	LTE	2300-2400	Japan	3600 – 4200 1900 - 2100
6	LTE+	2570-2700	China	4800 – 4990 1800 - 2600
7	GSM850	880-915	China	4400 – 4500
8	GSM900	925-960	China	3300 – 3600
9	Sub-6	3300-3600	Europe	3400 – 3800
10	mm-Wave	(24000-28000) (37000-48000)	Australia	3500-2600 1800 -2600

2.2.3 Antenna with Several Frequency Bands Operating Below 6 Gigahertz

In the sphere of wireless communication, frequencies lower than 6 GHz are a popular choice due to the excellent coverage and penetration features they possess. However, these frequencies may become congested, making it difficult to locate a channel that is free of interference and can be used for communication. This problem may be remedied with the use of multiband antennas that operate at frequencies below 6 GHz. These antennas provide coverage across a wide range of frequency bands.

The Multiple Input Multiple Output, or MIMO antenna, is an example of a multiband antenna that can handle frequencies lower than 6 GHz. Antennas that employ the MIMO technique

broadcast and receive data simultaneously using many antennas, which results in an increase in capacity and an improvement in the signal's overall quality. In order to achieve higher data transmission rates and improved service quality, these antennas are often used in 4G and 5G networks.

The sector antenna is a further kind of multiband antenna that is suitable for frequencies lower than 6 GHz. These antennas may give coverage over a large region and are often used in settings that are exposed to the elements. They are built to function over a number of different frequency bands, and they are adaptable enough to be utilised in point-to-point as well as point-to-multipoint arrangements.

In a nutshell, in order to satisfy the growing demand for wireless data transfer, multiband base station antennas are required. They provide enhanced coverage, increased signal quality, less interference, and more effective utilisation of the spectrum. MIMO and sector antennas are examples of multiband antennas that operate at frequencies below 6 GHz and are critical for enabling greater data transfer rates and improved service quality in frequency bands that are already at capacity.

2.3 Base Station Antenna Fundamental Parameters

The antenna's performance is described by its characteristics, which include the spatial distribution of the radiated energy, the antenna's power efficiency, its efficiency in matching to the feed circuitry, and so on. There is a lot of correlation between these variables. Several factors, including antenna temperature and noise characteristics, are left unexplored. Later, we will talk about them in the context of radio wave propagation and system efficiency. In order to adequately characterise the performance of an antenna, we utilise a variety of criteria, some of which are interconnected.

- Radiation pattern, beam width
- Power
- Directivity, gain, aperture
- Radiation resistance

2.3.1 Radiation Pattern

An antenna radiation pattern or antenna pattern is defined as a mathematical function or a graphical representation of the radiation properties of the antenna as a function of space coordinates. The power pattern is the plot of the received/radiated power vs the angle at a fixed distance from the antenna.

The electric (or magnetic) field amplitude pattern is the record of the angular fluctuation of the field magnitude at a certain distance from the antenna.

- Designed for use in a broad context.
- Relative to a set of geographical coordinates.
- There are two types of field patterns: those characterized by the magnitude of the electric or magnetic field, and those characterized by the square of that magnitude, known as power patterns.
- Typically scaled down from their highest possible value.
- The power curve is often shown on a logarithmic scale or in decibels (dB).

Pattern:

$E(\vartheta,\phi)$.

$dA = r^2 \sin\vartheta d\vartheta d\phi$.

Azimuth: ϕ Elevation: $\pi/2-\vartheta$.

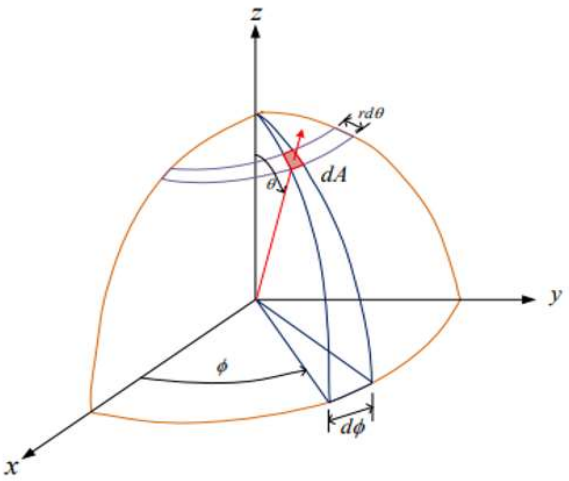

Figure 2.8 Power pattern plot of the received/radiated power of antenna vs the angle.

The use of spherical coordinates to depict radiation patterns is very practical. The angle formed by the two halves of a pattern's power, denoted by the notation HPBW, is 38.64 degrees for all three examples. The radiation pattern of an antenna describes how its energy is radiated in

space. For a base station antenna, it is important to have a radiation pattern that covers the desired service area and minimizes interference with neighbouring cells.

2.3.2 Radiation Pattern Lobes

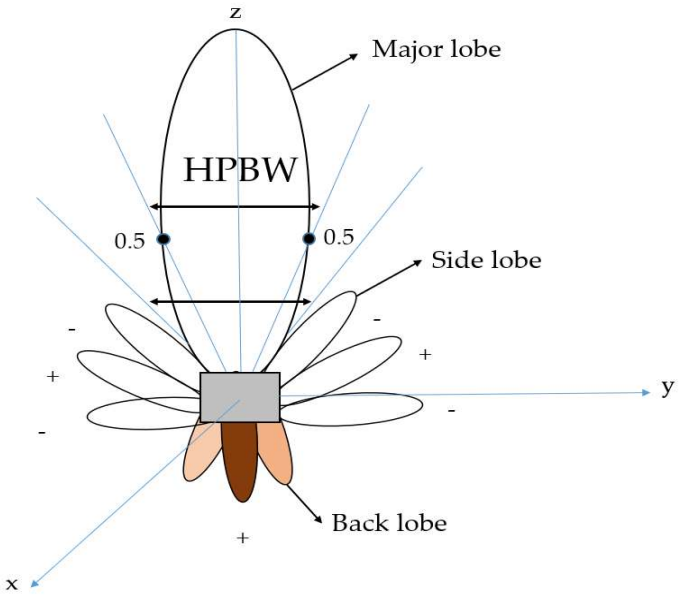

Figure 2.9 A polar representation of antenna vertical pattern including sidelobes and nulls.

An area of the radiation pattern that is bordered by lower-intensity patches is known as a 'radiation lobe'.

- Main lobe
- Minor lobes
- Side lobes
- Back lobes

Radiation from minor lobes often travels in the wrong direction, thus they should be eliminated wherever possible. Among the smaller lobes, the side lobes often stand out as the biggest.

The minor-lobe level, also known as the side-lobe ratio or side-lobe level, is often stated as a ratio of the power density.

Low side lobe ratios (e.g., -30 dB) are critical in most radar systems for reducing the number of misleading target indications caused by the side lobes.

Components in the amplitude pattern

- In principle, there would be three electric-field components (Er, Eϑ, Eϕ) at each observation point on the surface of a sphere with a constant radius.
- In the far field, the radial Er component of any antenna is either zero or vanishingly tiny. This is true for all antennas.
- Some antennas may contain just one, two, or all three components depending on their shape and the distance at which they are seen. This may vary from antenna to antenna.
- In general, the intensity of the whole electric field would be |E| =

$$\sqrt{|E_r|^2 + |E_\vartheta|^2 + |E_\varphi|^2} \qquad (2.1)$$

2.3.3 Beamwidth

An antenna's side lobe level is commonly traded off against its beamwidth, which is a highly significant figure of merit. Similarly, as the beamwidth narrows, the level of side lobe rises. To know how well an antenna can discriminate between two nearby radiating sources or radar targets, the best measure is its beamwidth. The beam width of the antenna determines the directionality of the radiation pattern and can be adjusted to provide coverage in different directions.

Beam width at 50 percent power (HPBW)

The angle between the two directions in which the radiation intensity is half the value of the beam is the plane that contains the direction of the maximum of the beam.

Beamwidth at the first null (FNBW)

Diameter of the gap between the pattern's initial nulls in degrees of angle.

2.3.4 Near and Far-Fields

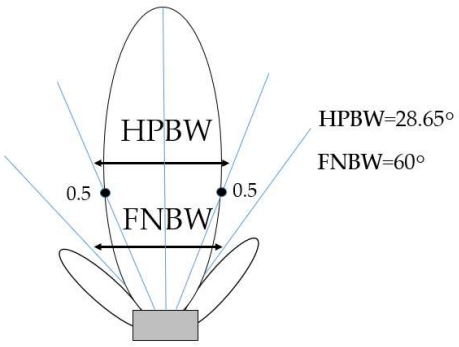

(a)

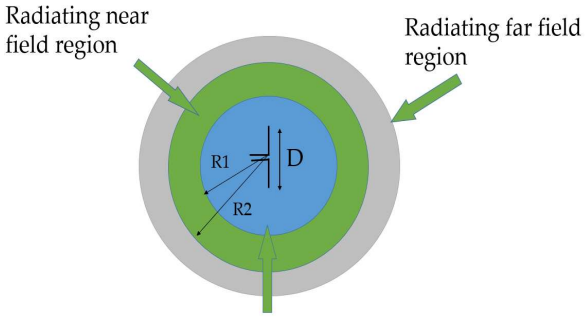

(b)

Figure 2.10 (a) A polar representation of a directional antenna's HPBW & FNBW ratios. (b) Graphical representation of near and far field regions.

D = Largest dimension of the antenna. $R_1 = 0.62\sqrt{D^3/\lambda}$, $R_2 = 2D^2/\lambda$ (2.2)

Reactive Near-Field Region $R < 0.62\sqrt{D^3/\lambda}$

The area of the near-field around the antenna where the non-radiating reactive field predominates.

Radiating Near-Field (Fresnel) Region $0.62\sqrt{D^3/\lambda} \leq R < 2D^2/\lambda$

This area is the part of an antenna's field where radiation fields predominate and the angular field distribution changes with distance, between the reactive near-field and the far-field. This area may not be present if the antenna's largest size is small relative to the wavelength.

Far-Field (Fraunhofer) Region $2D^2/\lambda \geq R$

This is the part of an antenna's field where the distribution of the angular field has little to do with distance.

2.3.5 Gain

The antenna's gain is highly correlated with its directional performance. It not only takes into consideration the antenna's directional capabilities, but also its efficiency. Impedance mismatches (reflection losses) and polarization mismatches (losses) are ignored when calculating gain. Measured in relation to the radiation intensity that would be achieved if the power absorbed by the antenna were emitted isotopically, directional gain describes how strongly a signal travels in a specific direction.

$$\text{Gain} = 4\pi \frac{radiation\ intensity}{total\ input\ accepted\ power} = 4\pi \frac{U\ (\Theta,\Phi)}{P_{in}} \text{ (dimensionless).} \qquad (2.3)$$

Total radiated power (Prad) may be expressed as a function of input power (Pin) in the form of

$$\text{Prad} = \text{ecdPin.} \qquad (2.4)$$

$$\text{G}\ (\theta,\Phi) = \text{ecd}\ \left[4\pi \frac{U(\theta,\Phi)}{P_{rad}} \right. \qquad (2.5)$$

$$\text{G}\ (\theta,\Phi) = \text{ecd D}\ (\theta,\Phi). \qquad (2.6)$$

When the gain is at its highest, the directivity is also at its most focused.

$$\text{G0} = \text{ecdD0.} \qquad (2.7)$$

Absolute Gain

To account for the losses experienced as a result of reflection or mismatch (caused by the antenna element's connection to the transmission line), we may implement a Gabs with absolute gain.

$$G_{\text{abs}} = e_r G(\theta,\phi) = (1-|\Gamma|^2)G(\theta,\phi) = e_r e_{cd} D(\theta,\phi) = e_o D(\theta,\phi).$$

where

$e_r = (1-|\Gamma|^2)$, reflection (mismatch) efficiency,
e_o = overall efficiency.

The two gains are identical (Gabs = G) if the antenna is matched to the transmission line, which occurs when the antenna's input impedance Zin is equal to the characteristic impedance Zc of the line (|Γ| = 0).

To the extent possible, the highest values

G0abs = eoD0. (2.8)

2.3.6 Bandwidth

Broadband antennas have a frequency range from one extreme to the other, and its bandwidth is often stated as a percentage. If the ratio between the highest and lowest frequencies is 10:1, for example, it means the highest frequency is 10 times more prevalent.

The bandwidth of a narrowband antenna is often represented as a fraction of the difference between the higher and lower frequencies relative to the bandwidth's central frequency. A bandwidth of 5%, for instance, means that a frequency difference of 5% of the bandwidth's centre frequency is allowed for operation. While Bandwidth reflection, frequently stated as a reflection coefficient less than -14 dB, is a measure of how effectively an antenna or transmission line transmits energy from one medium to another, such as from a coaxial cable to free space. A reflection coefficient less than -14 dB shows that the bulk of the energy produced is successfully delivered with little reflection back to the source. This provides low signal loss and efficient use of available bandwidth, resulting in improved efficiency and reliability in communication systems.

2.3.7 Beam Squint

Beam squint is the change in beam direction as a function of operating frequency, polarization, or orientation. Beam squint determines the difference between the main beam direction derived from the middle between the 3 dB points of the beam and the mechanical bore-side direction of the antenna.

2.3.8 Cross Polarization Ratio

As polarization diversity is used in base station antenna, most of the base station antennas are dual-polarized antennas, achieved through two orthogonal polarized antennae. The cross-polarization ratio or cross-polar discrimination defines the ratio of the desired part of polarization to the part of orthogonal polarization in a defined polarization system.

2.3.9 Beam Tilt

There are two beam tilts, electrical and mechanical, used to reduce the coverage of a specific antenna. The main lobe can be tilted below the horizon with electrical down tilt, thereby changing the radiation characteristics of the antenna. When an antenna is mechanically tilted, its radiation characteristics do not change. However, the coverage on the ground is affected.

All these parameters are related to the ability of an antenna to focus its radiation in a particular direction. In a base station, these parameters are important for achieving the desired coverage and capacity. Overall, these parameters are important for designing and optimizing base station antennas for maximum performance.

2.4 Today's Trend of Base Station Antenna Systems

The communication system's progression to the fifth generation (5G) calls for immense development of antenna systems to support different standards, and fulfil the demands of high data and capacity. One way is to jump to millimetre wave bands to increase the communication capacity. The mm wave bands are a new covering for BSAs which are executed on different objectives and policies. The mm wave bands create different challenges and design requirements which are not discussed here.

In the last two decades, exciting new developments have occurred in the base station industry. Multi-band antennas are progressively in demand as they significantly decrease the number of required antennas. As towers are occupied by multiple BSAs and other equipment, technologies such as multi-beam, multi-band multi-port are in demand for 5G base station communication. The interest favouring MIMO for wireless communication system has increased to improve the link performance. The introduction of MIMO antenna system has increased link robustness and data capacity by spatial diversity and multiplexing. MIMO antennas with different configurations have been deployed in today's LTE system. MIMO is a fundamental part of today's 4G LTE deployment. It can be realized by 2x2, 4x4 or 8x8 array, with the main purpose being to improve gain, S/N and provide high-quality services. Several topologies are still being investigated for higher order MIMO antenna systems. MIMO has become a progressively important part of mobile network operations with increasing research and development activities in the base station antenna market, specifically involving MIMO technology, as it is a key feature of 5G. This will also help in deploying advanced MIMO for 4G which will prepare the way for the deployment of the next generation of networks.

2.4.1 Challenges in BSA Design and Existing Solutions

Prior to proceeding with details in each challenge area, it is worth providing a general overview of the reported solutions in the literature for each of these challenges. Hence, a summary of available solutions/techniques reported in the literature for some of the key design challenges is provided in Table 2.2. These challenges highlighted in Figure 1.1 are discussed in detail in the following section.

Table 2.2: A summary of available solutions for design challenges in Base Station Antenna design.

Design Challenge	Solutions/Techniques	References
Achieving wide impedance bandwidth	Wideband balun design Modification to radiator shape Use of parasitic element/s to widen bandwidth	[10–13] [17–19] [22–26]
Achieving high isolation levels	Use of differential feed structure Use of decoupling network	[22], [28], [29] [19], [35], [36]
Improving the gain	Modifications to the radiator-addition of notch metal wall	[56]
Minimizing Beam Squint	Enforce symmetric current distribution on the radiating element	[52–54]
Stable HPBW in bandwidth of operation	Cavity shape reflector Convex shaped reflector	[22] [25]
Achieving high Cross polarization discrimination	Modifications to the radiator shape	[55], [56]
Achieving high front-to-back ratio	Modifications to the radiator-Downward sloping dipoles	[50]
Achieving beam steering	Butler matrix Luneburg lens Digital beamforming-integrated RF transceiver	[7] [8] [69]
Achieving compact size designs/cost	Multiband compact radiating element design	[2], [4], [72], [73]

A. Port Measurements: Impedance Bandwidth

One of the key challenges for the modern base station antennas is the bandwidth. While the spectrum is harmonized for certain mobile telecommunication bands, different countries tend to use different portions of the spectrum based on the license given to operators. It is desirable to design base station antennas to cover the entire allocated spectrum, despite operators not having access to full bandwidth, as it allows one antenna design to be used globally instead of variants for different geographic markets. However, it is difficult to design a single base radiating element that operates in all the frequency bands listed in Table 2.1 Hence, it is often best practice to use multiple radiating elements to cover multiple bands.

Impedance bandwidth is an important measure in BSAs as it provides the frequency band in which a minimum return loss level is achieved. Typically this is about 14 dB for BSAs [9]. It can be challenging to achieve the return loss requirements over a wide band. To meet the requirements, this wideband matching needs to be achieved both for radiating elements as well

as for the feed network. Generally, the techniques used to widen the impedance bandwidth can be categorized into three parts. (a) Use of a wideband Balun (b) modifications to radiator, and (c) use of parasitic elements.

(a) Wideband Balun

A generic and the most adopted Balun design is shown in Figure 2.8. The 50 Ω transmission feed is transformed to a balanced feed through an impedance transformer as shown in Figure 2.8 a. This is then fed to the dipole via a series LC resonator. This series LC resonator may be required depending on the impedance presented by the dipole. It is usually not required for a halfwave dipole but is used for longer dipoles. The implementation of the Balun on a microstrip feed or otherwise known as stalk is shown in Figure 2.8 b. The 50 Ω feed is connected at the bottom of the stalk, which is underneath the reflector once mounted on the antenna (Figure 2.8 c). The first transmission line (TL) and Open line (OL) at the input side of the transformer is implemented on the front side of the stalk. The backside balanced Short Line (SL), which is also connected to the reflector ground, acts as the ground for TL and OL microstrip lines printed on the front. The balanced Open Line (OL) then has a provision to include two inductors. The dipoles are soldered to one side of the capacitor on the top. The area of the parallel printed metals is adjusted to provide the required capacitance. It should be noted that Figure 2.8, shows the feed for one polarization only. Two such stalks can be combined together to feed a dual polar design.

The variations of this generic Balun are often used in many designs to achieve wider impedance bandwidths. Some of the reported works include L-probe feed with impedance bandwidth 54% [10], Y shaped feeding line with impedance bandwidth of 45% [11], T probe line [12] with impedance bandwidth of 71.17%, and shorted stub with impedance bandwidth 27.6% in [13]. In [14], microstrip to slot line balun is used to improve impedance matching with return loss better than 14 dB over the operating band 1710–2170 MHz. Slot line impedance is controlled through slot and ground width. The feed point height adjustment is a common parameter used during the Balun design to achieve a broader bandwidth [15].

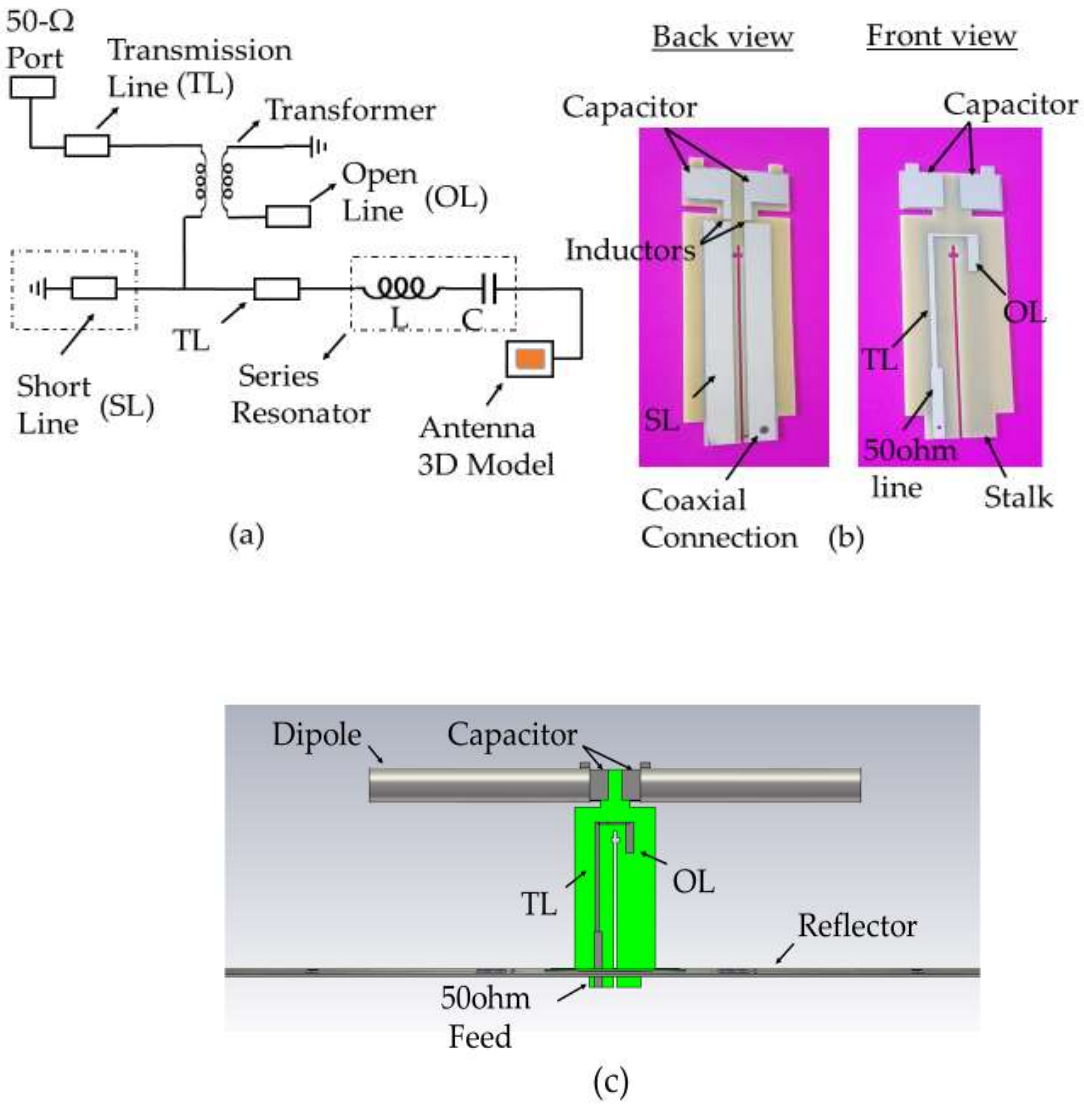

Figure 2.11 (a) Circuit representation of the matching circuit for the feed. (b) Microstrip implementation of the matching circuit (c) Side view of the radiating element.

(b) Modifications to the Radiator

Some of the commonly used techniques include various shapes of dipole [16], multidipole [17], and loop-shaped dipoles [11, 18]; however, some of these techniques result in larger aperture size and limit the design freedom. In [19], a 55% wide impedance bandwidth is achieved from 1.65 to 2.9 GHz by using a fan-shaped etching slot and chamfering quadrants along the diagonal dipole arms. The resulting prototype increased the radiation area and extended the current path to help improve the bandwidth. A bowtie antenna modelled by a Bezier spline was proposed to have a bandwidth of 68% from 1.427–2.9 GHz [20]. The multi-

dipole antenna proposed in [17] achieved wider impedance bandwidth of 60% from 1.55 to 2.87 GHz.

A multimode antenna with an embedded double loop configuration proposed in [18] has an impedance bandwidth of 51% from 1.68 to 2.83 GHz. In this design, a small loop inside an outer loop is added to generate a new resonant mode and hence widen the impedance bandwidth. In [21], a comparison of different patches with and without slots, including shorting strip, is performed to identify the structure that provides the widest impedance match. This comparison shows that the position of the coaxial feed cables, chamfer dimensions, and shape of the slotted patch contributed to 21.7% (0.82–1.02 GHz) and 49.5% (1.64–2.72 GHz) impedance bandwidth.

(c) Use of Parasitic Elements

Another method is to use parasitic elements to improve the impedance bandwidth. An octagonal loop dipole in [11] achieved an impedance bandwidth of 45%. These loop dipoles show wider impedance bandwidths compared to fundamental quarter wave dipoles. When one loop dipole is excited, the other behaves like a parasitic element to improve the bandwidth. The length of the parasitic loop element is optimized in [22] to achieve an impedance bandwidth of 52% from 1.7 to 2.9 GHz.

In [23], an antenna array with a bandwidth of 70% from 1.32–2.74 GHz is designed. The antenna configuration is a U-shaped slot etched on each polarization leaf of the element. A parasitic element with four layers of circular metal disks is introduced to improve the impedance bandwidth. It is found that the number of layers of the parasitic elements directly improves the impedance matching. The operating principle follows the rule that the radiation resistance exhibited in a dipole is proportional to the square of the electrical length of the current path [24]. The addition of a parasitic element makes the reactance of impedance be tuned either capacitive or inductive to achieve the best match. In [25], a parasitic patch was placed above the folded dipole to enhance the bandwidth to 64.7% from 1.4–2.77 GHz. In [26], the antenna showed 63% impedance bandwidth within the 1.68–3.23 GHz range due to the parasitic element. In [27], the resonator-loaded dipole antenna with a U-shaped strip feed widened the bandwidth by moving two resonating modes closer to each other. The length of

the resonator and distance between resonator and dipole is optimized to achieve a 37.5% impedance bandwidth from 0.67 to 0.98 GHz. Although inserting parasitic elements is a unique approach to solve the matching issue, it can adversely impact the radiation pattern performance.

(d) Port Measurements: Port to Port Isolation

The increased use of multiband, multibeam, and dual-polarized base station antennas for cost and space savings leads to challenges in achieving isolation requirements. The port-to-port isolation indicates how well any two RF signals on a multiport or MIMO antenna are decoupled from each other. In general, isolation can be categorized into three main types: intra-band isolation, inter-band isolation, and beam-to-beam isolation.

Intra-band isolation is the coupling between the polarizations of the same/multiple antenna arrays within the same frequency band. This is often referred to as cross-polar isolation when measured within the same array. Figure 2.9 shows a two-port BSA where each port represents two orthogonal polarizations of the same array, while Figure 2.9 b shows a four-port BSA with two antenna arrays of the same band. Ports 1 and 2 feed orthogonal polarizations of array 1, while ports 3 and 4 feed the two polarizations of array 2. The isolation between any of the ports 1 to 4 represents intra-band isolation. Generally, the intra-band isolations are required to be greater than 25 dB or 30 dB [9], depending on the frequency range of operation and operator requirements.

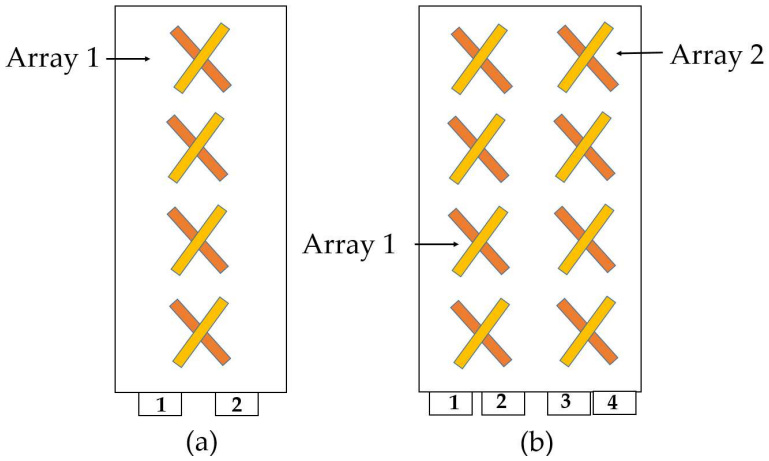

Figure 2.12. (a) Two-port single band antenna. (b) Four-port single band antenna.

Inter-band isolation denotes the coupling between the arrays of different bands. In Figure 2.10, a dual-band antenna example is given, in which ports 1 and 2 represent feeds for Band 1, and ports 3 and 4 represent feeds for Band 2. The |S13|, |S14|, |S23|, and |S24| represent the inter-band isolation between ports of high and low band elements. In multiband antennas, the isolation is measured in all frequency bands of operations, and typically these levels need to be above 30 dB or higher.

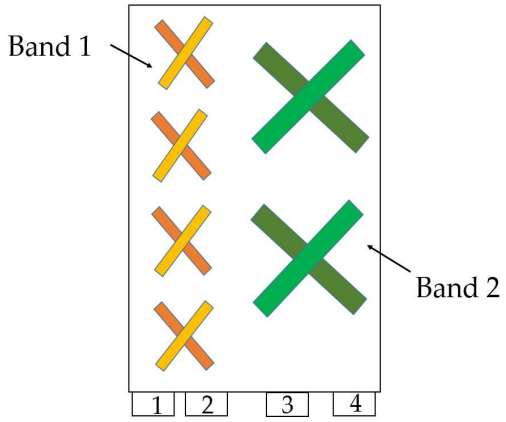

Figure 2.13. A dual-band antenna.

The higher the number of arrays in the antenna, the higher the port-to-port isolation combinations. Table 3 shows all possible port-to-port isolation combinations for a single-beam multiband antenna shown in Figure 2.5. The row entries in Table 2.3 are depicted as transmitting arrays, while the column entries are depicted as receiving arrays, to make it simpler to distinguish the coupled band of interest. For example, $HB1_{tx}$-LB_{rx} indicate the HB array 1 coupling to LB array at High Band frequencies, while LB_{tx}-$HB1_{rx}$ indicate the LB array to HB array 1 coupling at Low Band frequencies. All diagonal entries in the table represent cross-polar isolations within the same band. All non-diagonal entries represent coupling between different arrays of the same band or a different band. It should also be noted that all non-diagonal entries can be further divided into four entries since the arrays are dual polarized. For example, LB_{tx} -$HB1_{rx}$ comprises LB_{+45}-HB_{+45}, LB_{+45}-HB_{-45}, LB_{-45}-HB_{+45}, and LB_{-45}-HB_{-45}, where subscripts +45 and −45 represent two slant polarizations. Usually, the isolation between orthogonal polarizations is always better compared to the same polarization.

Beam-to-beam isolation is a special case applied for multibeam antennas representing the coupling between each beam in the array. Typically, the beam-to-beam isolation needs to be 20 dB or higher.

Table 2.3: Port-to-port isolation combinations for the multiband antenna depicted in Figure 2.5.

Transmitter/ Receiver	**LB Array$_{rx}$**	**HB Array 1$_{rx}$**	**HB Array 2$_{rx}$**	**HB Array 3$_{rx}$**	**HB Array 4$_{rx}$**
LB Array$_{tx}$	Cross polar isolation (LB)	LB$_{tx}$-HB1$_{rx}$	LB$_{tx}$-HB2$_{rx}$	LB$_{tx}$-HB3$_{rx}$	LB$_{tx}$-HB4$_{rx}$
HB Array 1$_{tx}$	HB1$_{tx}$-LB$_{rx}$	Cross polar Isolation (HB)	HB1$_{tx}$-HB2$_{rx}$	HB1$_{tx}$-HB3$_{rx}$	HB1$_{tx}$-HB4$_{rx}$
HB Array 2$_{tx}$	HB2$_{tx}$-LB$_{rx}$	HB2$_{tx}$-HB1$_{rx}$	Cross polar isolation (HB)	HB2$_{tx}$- HB3$_{rx}$	HB2$_{tx}$-HB4$_{rx}$
HB Array 3$_{tx}$	HB3$_{tx}$-LB$_{rx}$	HB3$_{tx}$-HB1$_{rx}$	HB3$_{tx}$-HB2$_{rx}$	Cross polar isolation (HB)	HB3$_{tx}$-HB4$_{rx}$
HB Array 4$_{tx}$	HB4$_{tx}$-LB$_{rx}$	HB4$_{tx}$-HB1$_{rx}$	HB4$_{tx}$-HB2$_{rx}$	HB4$_{tx}$-HB3$_{rx}$	Cross polar isolation (HB)

The techniques used to improve isolation performance include differential feeding and decoupling network/structures. Differential feed structure, in theory, can provide infinite isolation in a dual-polarized symmetrical feed since an excitation of one port does not induce common mode or different voltage currents in the other port. In practice, intra-band isolation greater than 36 dB [28] and 26 dB [22] were achieved through a differential fed scheme. In [29], folded feeding, lines based on differential feeding techniques are used to achieve intra-band isolation larger than 43 dB.

Decoupling networks are also another technique used to improve port-to-port isolations. A coupled resonator-based decoupling network is deployed in [30] to improve inter-band isolation from 8 to 10 dB. The currents induced by the coupled resonator helps to cancel the strong coupling between antennas operated in two frequency bands. Decoupling and matching

network techniques implemented in [31] achieve inter-band isolation levels over 10 dB in the 1.71 GHz t–1.76 GHz and 2.27 GHz–2.32 GHz bands.

As discussed in Section C and indicated in Figure 2.15 a, the compactness of the BSA design embedded scheme can cause low isolation. Different techniques were tried to improve the isolation in such schemes. In [1], a ring-shaped baffle is placed between the lower band and high band elements to decouple the two bands and achieve port-to-port isolation of 23 dB in the low band (0.77 to 0.98 GHz) and 17.5 dB in the high band (1.65 to 2.9 GHz). In [32], a similar configuration is set up, in which a high band element nested inside a lower band is used. Four arc-shaped baffle plates are used in this work, which results in port isolation greater than 27.3 dB for the lower band 704–960 MHz and 28.3 dB for the high band 1710–2690 MHz. The ±45° dual-polarized antenna with the dielectric cavity achieves cross polar isolation of 40 dB in [33] using two carefully positioned symmetrical shorting pins in the coax feedline. An orthogonal coupled sectorial loop-antennas with a cavity is used to achieve >30 dB intra-band isolation over a 1710–2170 MHz band in [14]. Decoupling networks such as bandgap structure [34], band stop decoupling unit [35], and filtering antenna elements [36] are also some commonly used techniques.

A filtering technique with different configurations is employed to get better isolation. C-shaped filtering stubs as shown in Figure 2.11(a) are introduced in [19] for achieving port-to-port isolation >25. The purpose of the filtering stub is to control the current flow across the feeding line of the relevant port to act as a band stop for the specific band to achieve high isolation. Filtering response through parasitic elements as shown in Figure 2.11 b is realized in [26], resulting in improved isolation of greater than 32 dB. The basic filtering structures include a metasurface structure [37], slot [38], shorting vias [39], and parasitic elements [40], and defected ground structure [41] integrated with the radiator to achieve the filtering response for base station application. Although an extra filtering structure increases insertion loss, the filtering antenna as array elements without the extra decoupling structure has been proposed in [36]. The radiating element realized the filtering response by adding the shorting pins and E-slot to achieve inter-band isolation of 35 dB. Balun design is modified to provide required filtering removing the need to have additional filters in [42]. Intra-band isolation >31 dB is achieved in [43] by carefully designing the dipole to mutual coupling to complement the cross-polar isolation.

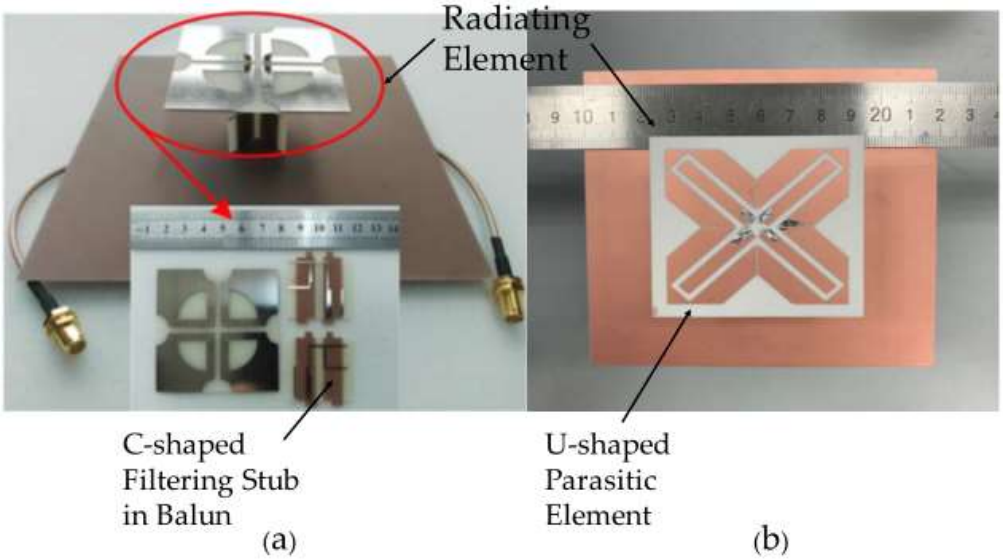

Figure 2.14 (a) Proposed antenna configuration [19]. (b) Parasitic element configuration in proposed antenna [26].

A configuration named lower-band–ground–upper-band (L–G–U), where the high-band antennas are located above the lower-band antenna separated by a low pass surface, is presented in [44]. It demonstrates inter-band isolation better than 30 dB in both working bands. In [45], a frequency selective surface is introduced between the high band and low band elements in the L–G–U configuration to achieve inter-band isolation >25 dB. The frequency-selective surface is optimized to serve as top capacitive loading for low-band 0.69–0.96 GHz and act as a reflector for high-band 3.5–4.9 GHz. In [46], beam-to-beam isolation > 32 dB was achieved through use of a Luneburg lens. This Luneburg lens antenna operates from 1710–2690 MHz, made up of a special periodic structure to become suitable for base station application. In the literature, a Luneburg lens with different materials was designed such as in [47], which is configured with a metamaterial layer to make it compact at lower frequencies (0.8–6 GHz).

B. Radiation Pattern

The far-field radiation patterns are a very important, if not the most important, factor for an operator. Some critical parameters in patterns include 3 dB beamwidth, 10 dB beamwidth, beam squint, front-to-back (F/B) ratio, sidelobe levels, and cross-polarization discrimination (XPD). Some of these parameters are marked in Figure 2.12. The specifications provided by

the operators to antenna designers can slightly change but mostly follow the industry-standard requirements listed in [9].

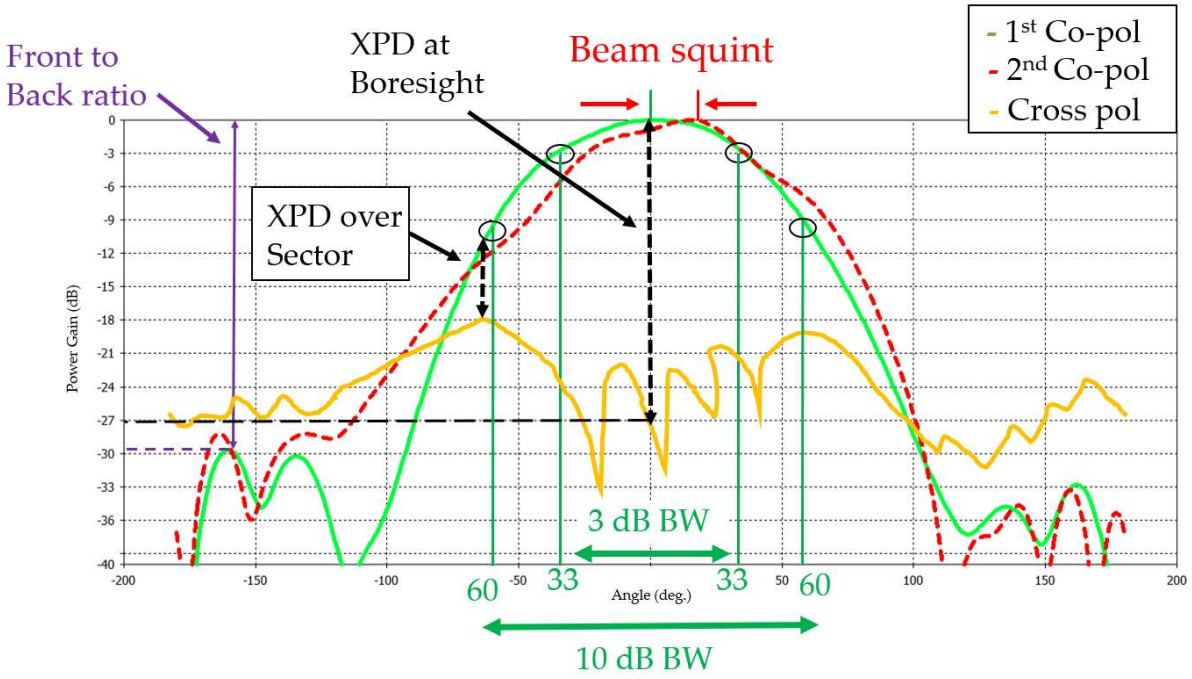

Figure 2.15 Illustration of some critical parameters for antenna radiation pattern.

The beamwidths 3 dB and 10 dB are important in network planning to mark sector footprints. Usually, single beam/sector antennas must have an HPBW requirement of 65° for three sector cell sites and 45° or 33° for six sector sites. The 10-dB beamwidth refers to the angular beamwidth at 10 dB below the peak values. It is desirable to have a 10-dB beamwidth of 120° in a three-sector site which implies that signal strength at the sector edge is 10 dB below the peak in boresight.

The radiation element most often needs modifications in its design to achieve the desired azimuth beamwidth. The important factors that affect the azimuth beamwidth are the length of the radiator and the distance between the radiator and reflector. These parameters are optimized to attain 3 dB beamwidth within the range of 65.7° ± 3.2° [25]. The use of dipole-type radiators is common in the radiating element design. The umbrella-shaped dipoles are configured in [48] to achieve an HPBW (half-power beamwidth) of 63° ± 5° in the H-plane. Another technique to modify the azimuth beamwidth is the use of a cavity-shaped reflector over a planer reflector [49]. Further, rectangular cavity-shaped reflectors in [22] and convex-shaped reflectors in [25]

are used to achieve 3 dB beamwidth around 65° ± 5°. The length and height of the reflector primarily affect the 3-dB beamwidth in the H-plane. This effect is realized in [11] to achieve a 3 dB beamwidth 68° ± 2° at H-plane and V-plane. It is found that increasing the length of the box-shaped reflector narrows the beamwidth in lower frequencies and widens the beamwidth in high frequencies in the band 1.7 to 2.7 GHz.

Another critical parameter in radiation patterns is the front-to-back (F/B) ratio. A higher F/B ratio is desirable to minimize backward radiation that can contribute to co-channel interference. Typical values need to be 25 dB or more in most of the base station antenna designs. Having a large reflector helps improve the F/B ratio. However, most of the BSAs have size constraints in terms of antenna width. Different topologies have been adopted in the literature to achieve the desired F/B ratio. Radiating elements proposed in [50] have downward-sloping dipoles, which improves the F/B ratio. An F/B ratio better than 30 dB and sidelobe levels better than 25 dB were achieved. Placing a large reflector behind BSA can improve F/B; however, it can introduce other intricacies such as increased wind resistance, large antenna size, and antenna loading. An electromagnetic scattering structure applied on the radome is used in [51] to reduce back lobe radiation.

Beam Squint is another critical performance parameter for antenna radiation patterns. The beam squint refers to the deviation of the main beam direction from its boresight in the azimuth plane. The beam squint is measured in ±degrees from the boresight direction. The squint can be measured as a 3-dB beam squint or a 10-dB beam squint, and the aim is to keep the squint as low as possible throughout the entire operating band for all elevation tilts. Generally, the squint gets worse with higher elevation tilts. In [52], a beam squint up to 12° is reported at 10° elevation tilt. Different techniques are followed to minimize the beam squint. In [53], a combination of microstrip and a strip line of PCB's are introduced in the radiation element to minimize the beam squint below 5° for down tilt measured at 7° and 0°. Another technique is to enforce symmetric current distribution on radiating elements to minimize squint. This is achieved in [20] by using the Pawsey stub balun to feed radiating elements and to reduce leaky current distortions to keep the HPBW within 54°–76°. In [54], the beam squint < 4° with a maximum 10° down tilt is achieved through octagon-shape-folded dipoles as shown in Figure 2.13a.

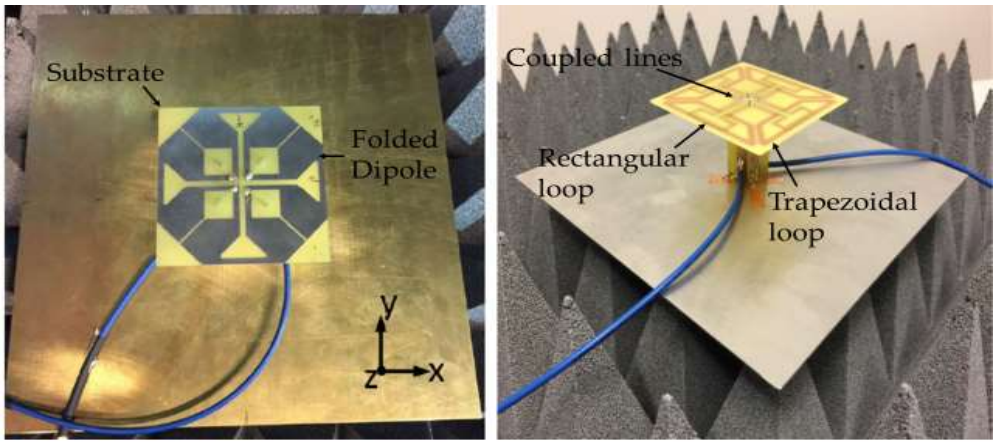

Figure 2.16 (a) Fabricated prototype of folded dipole [54]. (b) Fabricated Prototype of magnetoelectric loop dipole [55].

Cross-polar discrimination (XPD) is another important parameter when looking at radiation pattern performance. In general, the XPD above 10 dB in the sector is recommended for base station application. The magnetoelectric layered loop dipole configuration shown in Figure 2.13 b, is used in [55] to achieve XPD over 20 dB in the boresight direction. Antenna gain is also a vital characteristic in BSA design. Operators prefer a positive gain slope across the band as the higher gain at higher frequencies compensates for the additional free space losses. In the azimuth, the gain in sector edge directions is lower compared to boresight due to gain roll-off. A lower gain roll-off in azimuth patterns is achieved in [56] by introducing a notch metal wall to the radiating element, which enhances the gain by 2 dB at sector edge ± 60° angle.

The previously mentioned radiation pattern-related parameters are applicable for single-band and multiband antennas. However, in multiband antennas, radiation patterns can be severely impacted due to cross-band scattering when interleaved or embedded arrays as shown in Figure 2.15. In a dual-band interspaced array, the high-frequency element patterns are impacted due to scattering from the currents induced in low-frequency elements and vice versa. The impact can be on multiple parameters such as beamwidth, squint, and XPD. Overcoming such impacts can be very difficult. It is often attempted to ensure that each radiating element is transparent to the other in their operating frequency bands, which is a challenging task. In [57], the high-frequency band (HB) pattern distortions caused by the lower frequency band (LB) radiating elements are minimized by introducing chokes into the LB element. These chokes are quarter-wavelength open circuit segments at high band frequencies, and this minimizes scattering. In

[58], the printed dipole is segmented into smaller segments that are not resonant in the higher frequency band region, and each segment is connected to the other by inductive thin lines. This makes the lower band element transparent to the higher band radiating element. In [59], a cloaked antenna system is realized to minimize the scattering of closely located antennas. A dual-polarized mantle cover to cloak the dipole antenna is used in this work, and radiation performance is almost unaffected.

The previously mentioned challenges for patterns are fundamental and equally applicable for single beam, multibeam, or steerable beams in BSAs. When it comes to 5G, there are some additional challenges and complexities associated with the mMIMO and beamforming. As mentioned earlier in Section 2, there are two main beamforming technologies, namely analog and digital, used in BSAs for sub-6 GHz. Although the analog beamforming is not true mMIMO, it is still used in some of the 5G base station antennas to form multiple beams. The true mMIMO in sub-6 GHz is achieved through digital beamforming in 5G BSAs.

The most popular techniques used for analog beamforming are based on either Butler-matrix circuits [60] or Luneburg lenses [61]. Compared to lenses, the Butler-matrix circuit implementations are compact, low-cost, and planar. The designers can incorporate the Butler matrix implementations with the feed distribution network, thereby not necessarily increasing the antenna height. However, there are several challenges associated with the Butler matrix implementation such as dual-band operation, isolation between beams, side-lobe suppression, and wide operating bandwidth [62]. The branch line couplers used in the Butler matrix have inherent bandwidth limitations, and, as a result, they cannot be designed to have multi-band operation. The approach is to have distinct Butler matrices for each band [63] to overcome this limitation. However, this comes with inherent crossband coupling challenges, which were discussed in Section (d). The narrowband challenges were addressed with wideband quadrature couplers and fixed-phase shifters in a Butler matrix [64]. Although there has been some reported literature on high-beam-to-beam isolation [65], it is still an ongoing challenge. One solution to minimize the sidelobes as well as grating lobes is achieved by changing the antenna element arrangement in [60].

In contrast to butler matrices, a careful design of a lens-based beamformer can provide stable radiation patterns, with low sidelobe levels in a wide band [8]. However, the size of the lens in

front of the antenna increases the antenna height as well as weight. Therefore, low profile, low cost, and lightweight lenses remain a potential research topic for analog beamforming in BSAs. The other analog beamforming techniques reported in the literature include the use of metasurfaces [66], parabolic cylindrical reflectors [67], and reconfigurable parasitic radiators [68].

The digital beamforming architecture, which provides true mMIMO capability, has certain challenges as well. One of the key challenges is the design complexity. An example 4 × 4 Tx/Rx dual polar mMIMO configuration for a BSA is shown in Figure 2.14. Each radiating element requires an RFIC to provide amplification and filtering, which is then connected to the digital beamformer. This dual polar Tx/Rx array requires in total 32 RFICs and 8 baseband beamformers. All these components need to be placed closer to the radiating element, making the integration of the antenna element and RF circuitry very complex. Unlike mm-wave designs, the sub-6 GHz designs cannot be realized as an integrated AiP in MMIC technology due to the large size of the antenna element. In addition, the large number of RFICs and digital processing results in high power consumption. Even with the state-of-the-art efficient power amplifiers available in the sub-6 GHz bands, the thermal dissipation from processors and RFICs remains a significant challenge that needs to be addressed in the design. Thermal vias and thermal pads are necessary at the back of the RF and digital electronics to dissipate the heat in these antennas [69]. The increased power consumption results in less value for money for the operators despite the capacity improvement. Some antenna designs have addressed this by limiting the real-time beamforming on the horizontal axis only [61]. The elevation beam tilting in this case is not done electronically and is initially set by the remote electrical tilting mechanism using the legacy phase shifters. Then, the Azimuth beamforming is done using the phase and amplitude control among array columns.

Another challenge with the mMIMO antenna design is the calibration. The phase needs to be calibrated with high accuracy along the entire RF transceiver chain in order to ensure the expected beamforming gains. The amplifiers can have varying phases based on their operating conditions such as bias points, temperature, and frequency of operation, and these variations can lead to deviations from the expected phase distribution at the elements. As a result, the patterns may not form nulls, where it is expected which leads to increased interference with adjacent users. The antenna testing is another challenge for mMIMO as the access to RF inputs

of the antenna is difficult with the other components in the RF transceiver chain. Therefore, instead of doing antenna pattern testing with an RF input, Over-the-Air (OTA) testing is required with the baseband IQ data as the input/output.

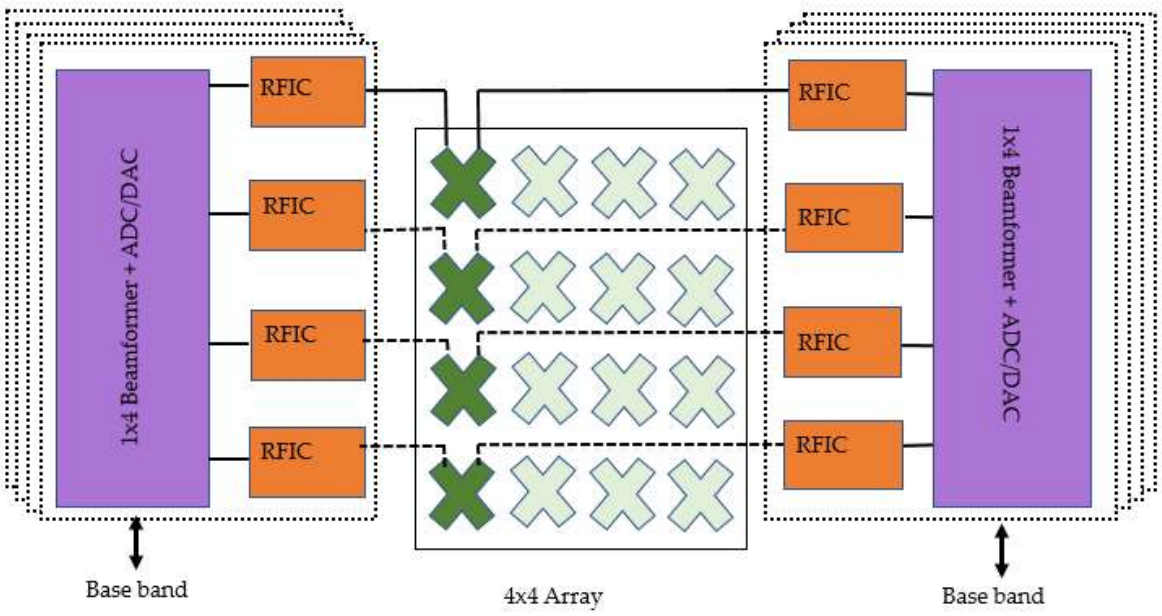

Figure 2.17. Components of a 4 × 4 Tx/Rx dual polar mMIMO configuration.

C. Size and Cost

Operators are keen to maximize the performance per unit area in the tower space. Therefore, they require compact antennas with better overall performance at a low cost. The miniaturizations are often achieved by having interspersed multiband arrays [4]. A comparison of different arrangement schemes for high-frequency elements and low-frequency elements is performed [2]. As shown in Figure 2.15, side-by-side schemes, up-and-down coaxial schemes, and embedded schemes were considered. Although the up-and-down scheme is simpler, cable losses increase due to the increased length of the main feed line. The embedded scheme has the advantage of compactness as two antennas are located within a single band antenna volume. However, embedded schemes exhibit challenges of isolation and pattern distortions. A single radiating element for both the low and high bands is used in [70, 71] to reduce the number of required radiating elements and footprint. However, the required vertical element spacing for optimum elevation patterns is hard to achieve with this approach. Hence, the grating lobe levels

are high. The dual broadband planer BSA configuration is followed in [72], where high band elements are nested inside lower band elements to achieve compactness.

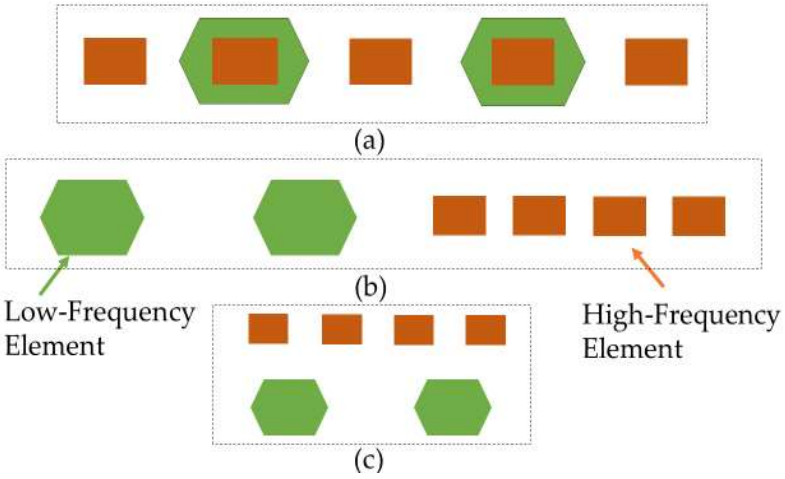

Figure 2.18. (a) Multiband embedded scheme; (b) multi band side-by-side scheme; (c) multiband -up-and-down coaxial scheme [2].

The lower cost in the antenna production is achieved by using low-cost, simple, printed antennas. The printed circuit board technologies reduce antenna assembly times. Another low-cost choice for enabling 5G BSA is 3D printing, which facilitates complex designs. Three-dimensional printing is an effective manufacturing method for designing MIMO antenna prototypes to reduce the cost. In [73], ±45 dual-polarized antenna is fabricated using 3D printing technology while achieving a wide bandwidth. Although printed antennas have a low-cost advantage, they can exhibit higher dielectric losses compared to die-cast radiating elements. Die-casting can be cost-effective if the entire element is made from a cast thereby reducing the assembly time. In addition to the cost incurred on radiating elements, the other RF components, such as phase shifters, may incur higher costs. A wiper phase shifter [74] can be a cost-effective solution as it is very compact but this may have other disadvantages, such as limited control for null-filling in down tilts and the use of a large number of cables. Other types of phase shifters such as [75, 76] can overcome some of these limitations while reducing fabrication costs.

2.5 Base Station Antenna Materials and Mechanical Characteristics

The mechanical characteristics of base station antenna systems are a very important consideration. As base station antennas are mounted on towers they must be capable of withstanding the environmental conditions. The selection of materials that will be used in an antenna or array breaks down to materials for the various components.

- The radiating elements and support members
- Radomes
- Feed harness and connectors
- Hardware and mounting

The choice of material of the above-mentioned components are equally important in the overall consideration of the antenna system as it determines the life and serviceability. The choice is mainly depending on the application but essentially it must be suitable for use in mobile radio communication. Base station antenna's material and mechanical characteristics is a vast field to discuss.

Chapter 3: Cross Band Scattering in Multi-Band Antennas

3.1 Requisite for Scattering Suppression in Multi-Band Base Station Antennas

The growth in connected devices requires high connection density in 5G networks. In fact, requirements specify more than 1 million devices per square kilometre for 5G massive machine-type communication (mMTC), which is a 10-fold increase compared to 4G [1]. This is catered for through small cell densification and improved spectrum utilization, which both require compact multiband antenna systems. The compactness and need for multiband antenna systems presents conflicting demands, since the need for multiple bands requires multiple arrays and thus more space [2,32]. The only way to realize a compact antenna is to interleave these multiband arrays. The main challenge is to then ensure the radiation patterns are not distorted due to scattering from other radiating elements in the vicinity. In a multiband interleaved array, different frequency elements are arranged closely together. This arrangement can cause interference between the high-frequency and low-frequency elements. When the low-frequency elements generate currents, these currents can scatter and affect the patterns of the high-frequency elements. Similarly, the currents induced in the high-frequency elements can interfere with the patterns of the low-frequency elements. Figure 3.1 likely provides a visual representation of this phenomenon, showing how the different frequency elements are together and when one is excited, scattering and interference occurs due to induced current causing the different frequency elements impacting their respective patterns. The impact can be seen on multiple parameters such as beamwidth, squint, and cross-polarization discrimination (XPD). Often, attempts are made to ensure that each radiating element is transparent to each other in their operating frequency bands, which is a challenging task.

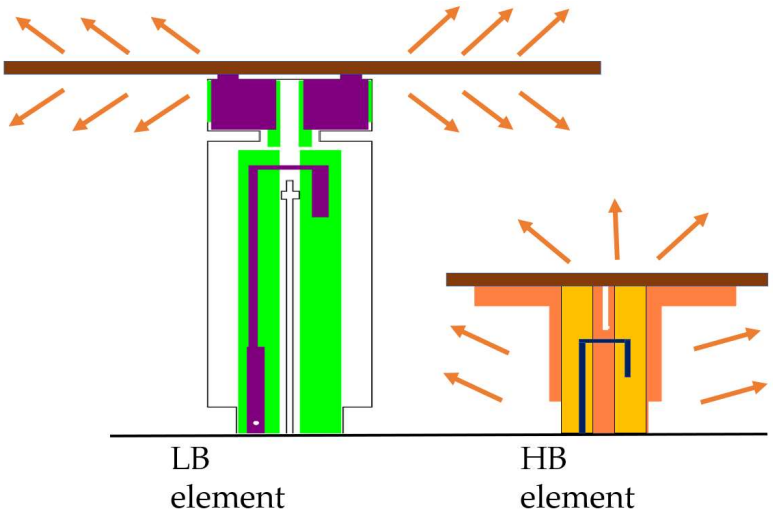

Figure 3.1 Visual representation of radiation when two antenna elements are in the vicinity.

3.2 A Simple and Effective Approach for Scattering Suppression

The high band pattern distortions in an 1810–2690 MHz frequency band, were introduced due to low band radiators working in 690–960 MHz. The common approach to reducing the crossband scattering is to adopt different sizes and shapes of metal cavities or walls [81,14,58,57]. In [83], the high-frequency band (HB) pattern distortions caused by the lower frequency band (LB) radiating elements are minimized by introducing chokes into the LB element. Many techniques have been discussed in chapter 2. Although these techniques suppress the crossband scattering, they do require significant modifications to LB or HB elements which can increase the cost of manufacturing due to added complexity of products.

The novelty in this work is in the simple and effective approach proposed to reduce the crossband scattering at HB by orienting the LB radiating element in horizontal (H) and vertical (V) directions, as shown in Figure 3.2b, in contrast to the conventional slant LB dipole configuration shown in Figure 3.2a. The main challenge then is to generate the slant polarization (±45 degree) from H and V oriented dipoles. This has been overcome by utilizing a 180° hybrid coupler.

3.2.1 Antenna Configuration

The HB and LB elements are interleaved in the current base station antenna (BSA) for space savings. Due to the use of ±45 polarized elements, the dipoles are oriented in a slant configuration, as shown in Figure 3.2a. It should be noted that a full array has multiple such elements arranged vertically, and that only a segment is depicted in this figure for clarity. A fabricated prototype of the antenna is shown in Figure 3.3.

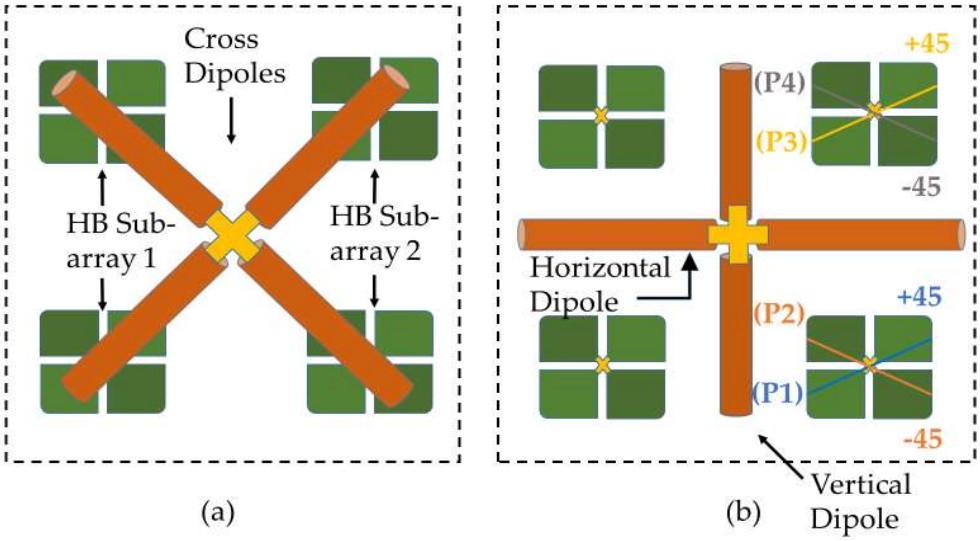

Figure 3.2 (a) Slant dipole configuration used in traditional interleaved scheme for dual-band dual-polarized BSA. (b) The proposed horizontal and vertical LB dipole configuration (LBHV) with HB subarrays. P1 and P3 refer to +45 polarizations; P2 and P4 refer to −45 polarization.

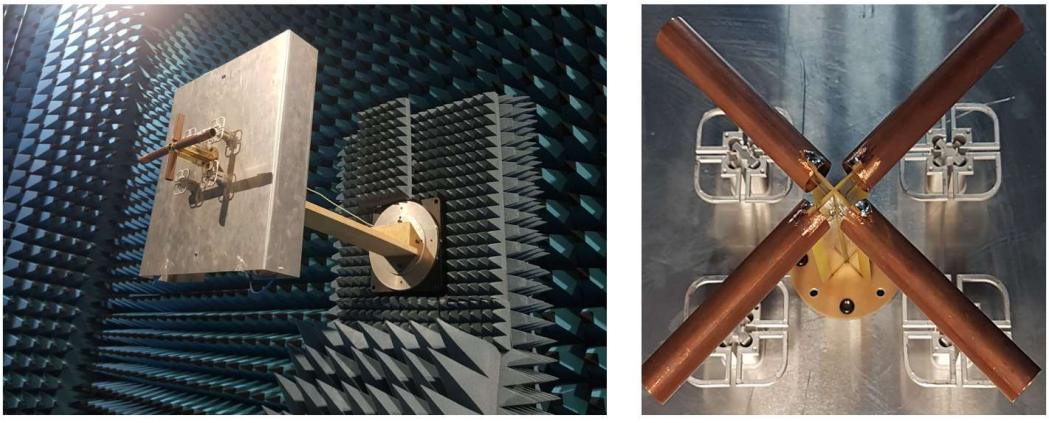

Figure 3.3 Fabricated prototype with (a) LBHV antenna element (b) LB slant element.

3.2.2 Working Principle

The base station antennas require ±45 polarized antenna elements, and the proposed horizontal and vertical dipoles provide only horizontal and vertical polarization. Therefore, a novel technique creates a ±45 polarization virtually from H- and V-oriented dipoles. The 180° hybrid coupler is a common microwave component which can be realized either as a rat-race, ring or magic T-hybrid. The 180° hybrid coupler is commonly used to get in and out of phase signals. Different design approaches have been followed in the literature, just as in [84] where a specialized TL is designed for a compact rat race coupler.

As shown in Figure 3.4a, a 180° hybrid coupler is used between the inputs and the LBHV element. Port 2 feeds the horizontal polarized element, and port 3 of the hybrid provides the vertically polarized dipole.

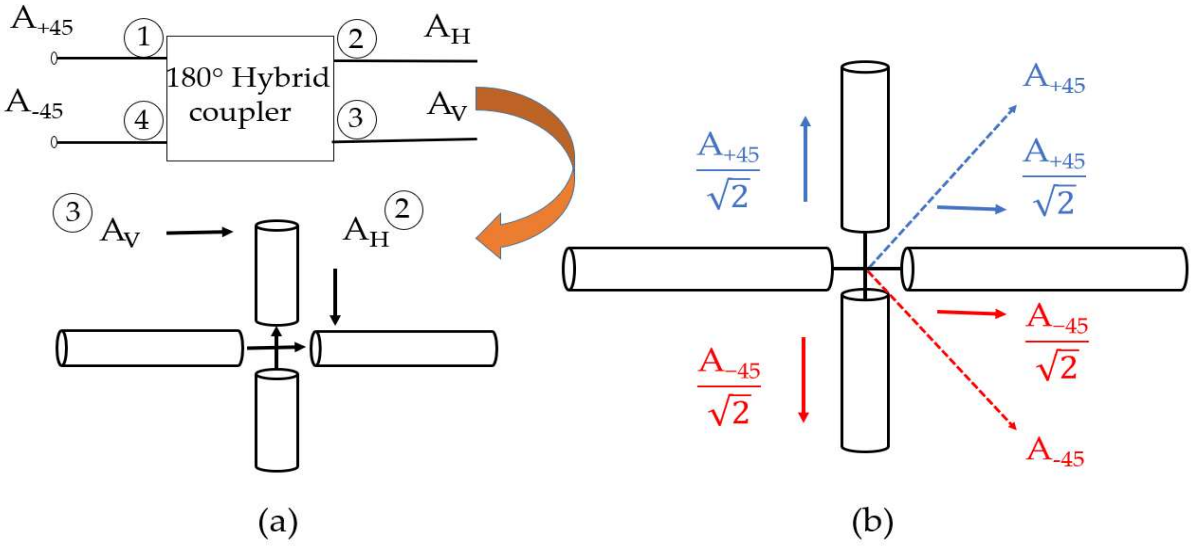

Figure 3.4 (a) Conversion of slant-polarized inputs to H and V polarized inputs, (b) creation of virtual slant polarizations from H and V feed signals.

The AH and AV can be expressed in terms of the +45 and −45 input signals A+45 and A−45 as:

$$\begin{bmatrix} A_H \\ A_V \end{bmatrix} = [S_{180^\circ}] \begin{bmatrix} A_{+45} \angle \quad \theta_{+45} \\ A_{-45} \angle \quad \theta_{-45} \end{bmatrix} \tag{3.1}$$

$$A_H = \frac{1}{\sqrt{2}} [A_{+45} \angle \theta_{+45} + A_{-45} \angle \theta_{-45}] \tag{3.2}$$

$$A_v = \frac{1}{\sqrt{2}}[A_{+45} \angle \theta_{+45} + A_{-45} \angle \theta_{-45} - 180°] \qquad (3.3)$$

The output at port 2, fed to the horizontal-polarized dipole, contains the in-phase components of both the +45 and −45 polarizations, while the output port 3 contains signals of +45 in-phase and a −45 signal with a 180° phase shift. Since the +45 signal is fed in phase to both the H and V polarizations, it virtually creates a sum vector in the +45 direction, as shown in Figure 3.4b. The −45 component fed to the vertically polarized element has a 180-degree phase difference compared to the horizontally polarized dipole. Therefore, it creates a signal polarized in the −45 direction, as shown in Figure 3.4b. By the theory of reciprocity, the received signals at H and V dipoles provide the sum and difference signals, which are +45 and −45 signals, back to the baseband unit.

3.2.3 Feed Network

The LBHV element should have a comparable performance in terms of patterns to a slant dipole, while providing minimum distortions to the HB patterns. The length of the dipoles in the H and V polarizations are optimized to meet these requirements. The optimized values were obtained through a series of parametric studies. It was found that the vertical dipole length presents more resonant behaviour at the high band and needs to be shorter to reduce HB pattern distortions. This can result in a wider 3 dB beamwidth for LB patterns. A longer dipole close to a full wavelength is required in the H orientation to compensate for this.

The LB dipoles need to be impedance-matched for the 690–960 MHz band. The impedance-matching network is based on a feed network design proposed in [83]. A ladder-type band-pass filter using a serial and shunt resonant LC circuit is used for wideband matching. As shown in Figure 3.5, a circuit model contains three tuners, i.e., a series resonator and a shunt resonator used to control/reduce the changing reactance, followed by a quasi-quarter wavelength transmission line (TL2). The optimization and physical realization were conducted in a CST studio to obtain the best match over the required band, as shown in figure 3.6.

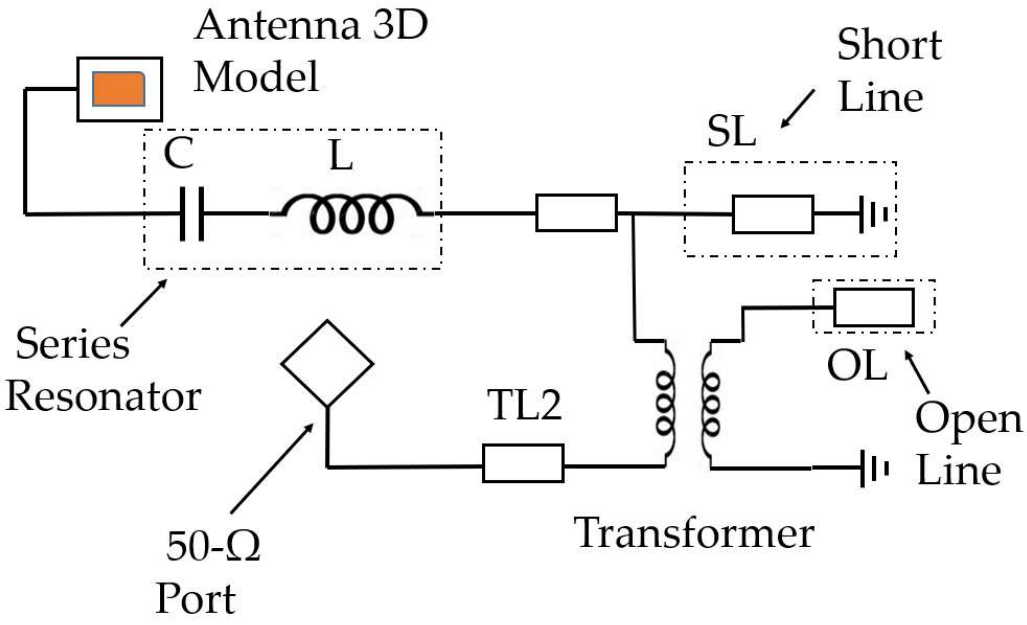

Figure 3.5 Circuit theory model of matching circuit.

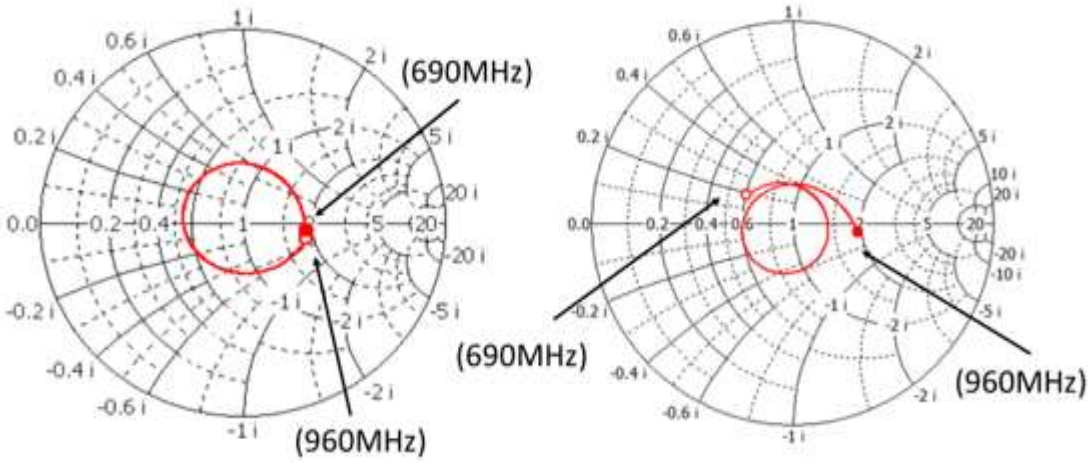

Figure 3.6 Matching over the required band.

The matching circuit was implemented using microstrip technology, as shown in Figure 3.7a. The lines TL (transmission line) and SL (short line) are realized as coupled lines that are printed on the back-conducting layer, while TL1 and OL (open line) are conventional microstrip layers.

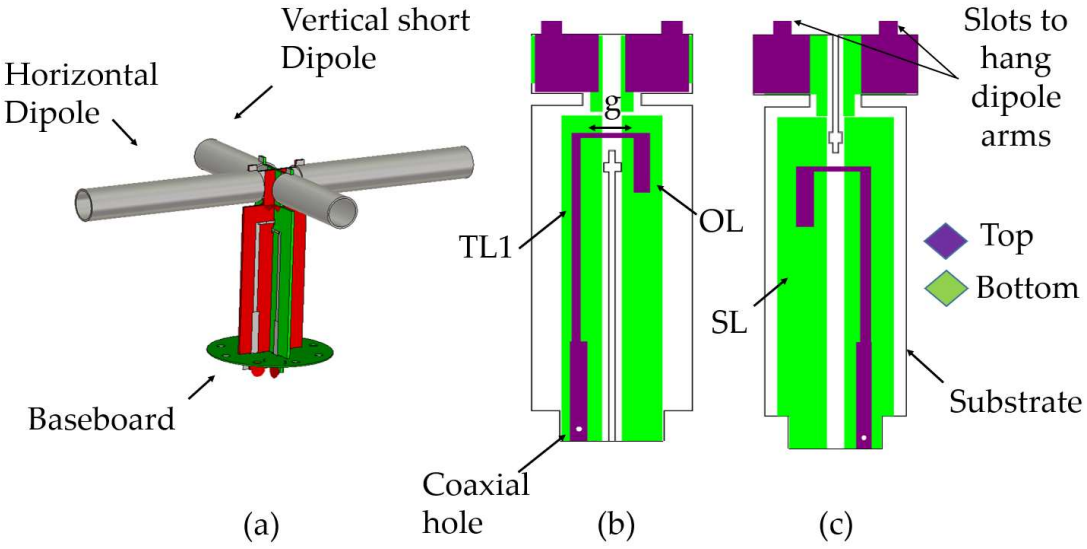

Figure 3.7 (a) Perspective view of the LBHV. The horizontal dipole is 135 mm long, and the vertical dipole is 60 mm long, (b) details of the LB horizontal dipole (LBHD) feed, (c) details of the LB vertical dipole (LBVD) feed.

The configuration of horizontal dipole balun is shown in Figure 3.7b, while short dipole balun is depicted in Figure 3.7c. They are orthogonally arranged to feed the pair of horizontal and vertical LB arms.

3.2.4 Experimental Results

The prototype with a ground plane measuring 500x500 mm^2 was created and subjected to testing. Figure 3.8 represents the experimental setup. In Figure 3.8(b), the details of the back coaxial cables are depicted. In this case, cables are directly inserted into the feed points. The outer conductor of the cable is soldered on SL, while the inner conductor of the cable is soldered on TL. Figure 3.9 depicts an antenna setup where the antenna is suspended within a chamber. To create a resemblance of a tower-like structure, a mounting bracket is utilized. The mounting bracket serves as a support structure for the antenna, allowing it to be securely attached and positioned within the chamber. It has been designed to mimic the shape or form of a tower, providing stability and a realistic visual representation. The mounting bracket is fabricated with the same material as the ground. To facilitate specific testing scenarios, it is attached to the chamber mounting plate.

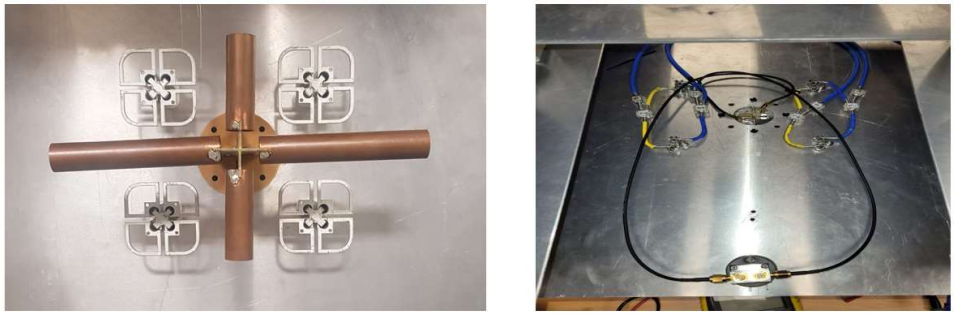

Figure 3.8 Fabricated prototype (a) horizontal and vertical (HV) optimized dipole. (b) Back view of antenna.

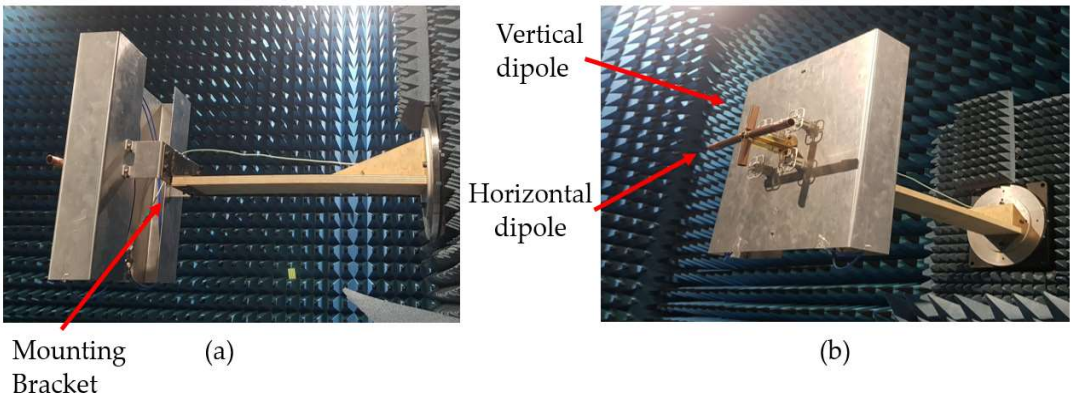

Figure 3.9 (a) Antenna hanging on bracket for tower like elevation. (b) Optimized antenna in chamber for measurement.

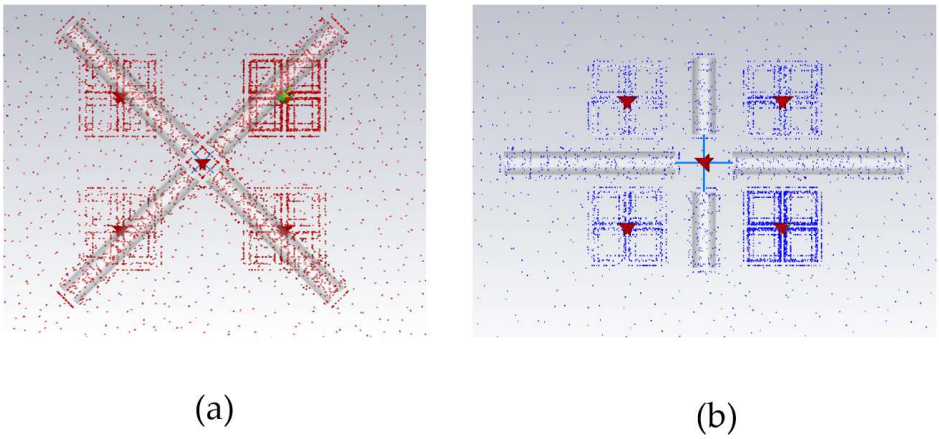

Figure 3.10 surface currents (a) cross dipoles (b) HV dipoles.

A careful observation of the current distribution at HB frequencies revealed that the induced HB currents reduce in magnitude as the LB dipoles are moved away from a slant position to horizontal and vertical positions as illustrated in Figure 3.10. As a result, HB patterns are cleaner, as shown in Figure 3.12. This LB configuration is referred to as Low Band Horizontal–Vertical (LBHV) from here onwards. The measured results show that the pattern performance of HB arrays with LBHV elements is similar to HB-only radiation patterns. The presence of the LB radiator on top of the HB radiators can induce HB currents on the LB dipoles, acting as resonating structures and distorting the patterns. In addition, being directly in front of the HB radiators disrupts the nearfield distribution and scatters the desired HB patterns. This results in undesirable HB patterns, as shown in Figure 3.11.

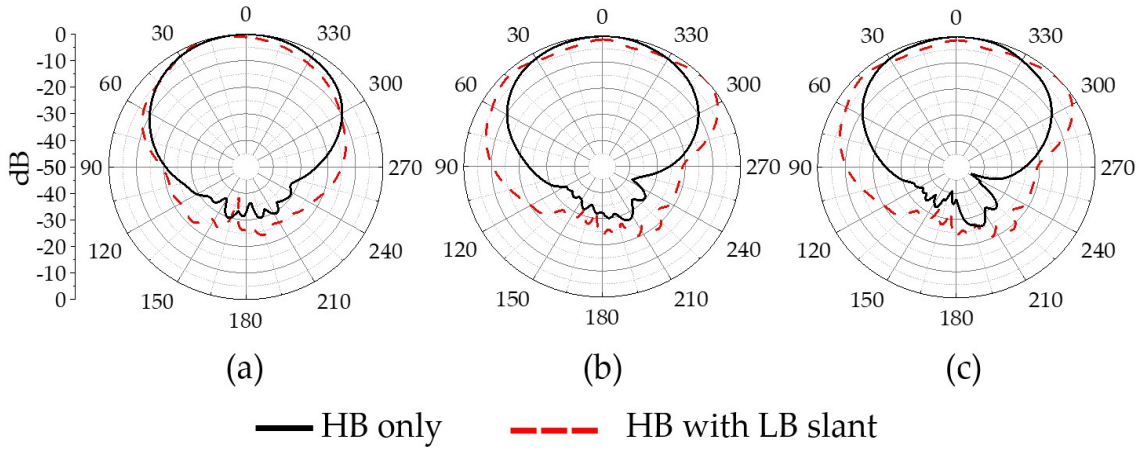

Figure 3.11 High band-only and high band with slant LB antenna-measured azimuth patterns at (a) 1.8 GHz, (b) 2.4 GHz and (c) 2.6 GHz.

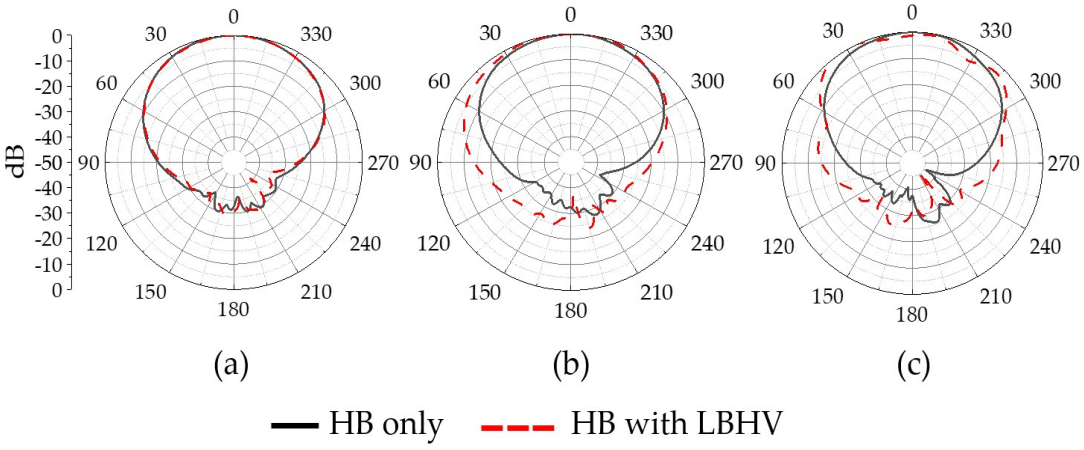

Figure 3.12 High-band measured azimuth radiation patterns with a LBHV element at (a) 1.8 GHz, (b) 2.4 GHz, and (c) 2.6 GHz.

Although matching the short dipole is quite challenging, the antenna is well-matched with a reflection coefficient of better than 12 dB for horizontal polarization, and better than 10 dB for vertical polarization from 690 MHz to 960 MHz, as shown in Figure 3.13. The optimized dimensions of the structure are those listed in Table 3.1 and marked in figure 3.15. Despite this, the achieved HPBW with LBHV configuration is relatively stable, with a reflection coefficient larger than 12 dB. The port-to-port-measured worst-case isolation of LBHV configuration in hybrid mode is 36 dB at 960 MHz and 20 dB at 2 GHz, as shown in Figure 3.14, in the desired whole-band 690–960 MHz and 1810–2690 MHz, respectively.

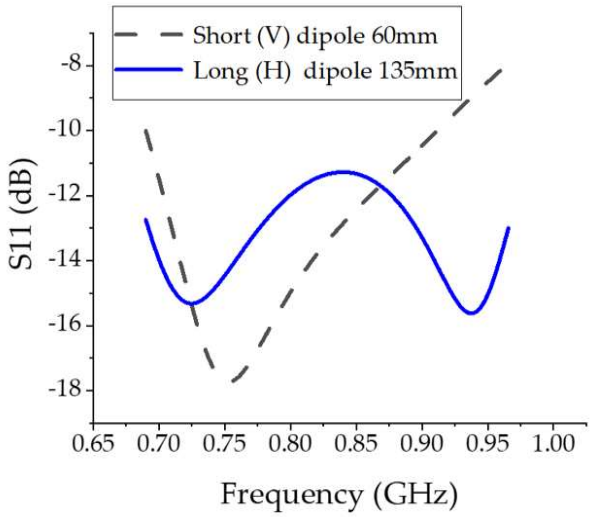

Figure 3.13 Measured results of reflection coefficient.

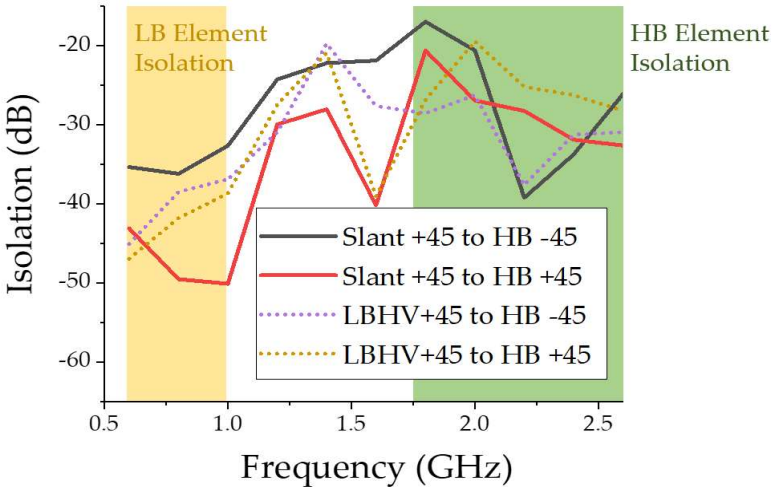

Figure 3.14. Measured isolation of proposed antenna LBHV with slant

Table 3.1: Optimized parameters of the proposed antenna.

Parameters.	Values LB-HD (mm)	Values LB-VD (mm)	Description
W-SL	6.5	10	Width of SL
L-SL	95	95	Length of SL
W-TL1	2	3	Width of TL2
L-TL1	60	50	Length of TL2
W-OL	4	5	Width of OL
L-OL	18	17	Length of OL
g	19	13	Gap between SL

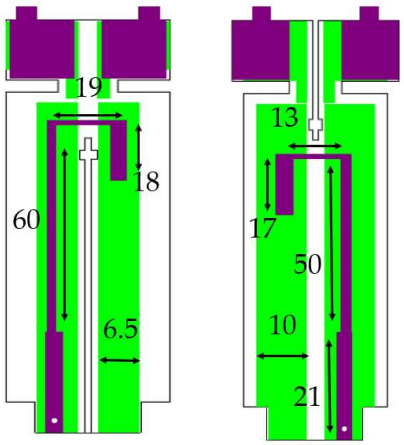

Figure 3.15 Parameters of the proposed design marked on its configuration.

3.2.5 Comparison

It is observed that the main beam shows a significant 3 dB and 10 dB beam squint with the slant dipoles compared to the LBHV, as shown in Figures 3.16a–f. The proposed work is also compared with the recent state-of-the-art works in Table 3.2, which shows isolation performances and the addition of structure type to radiating elements.

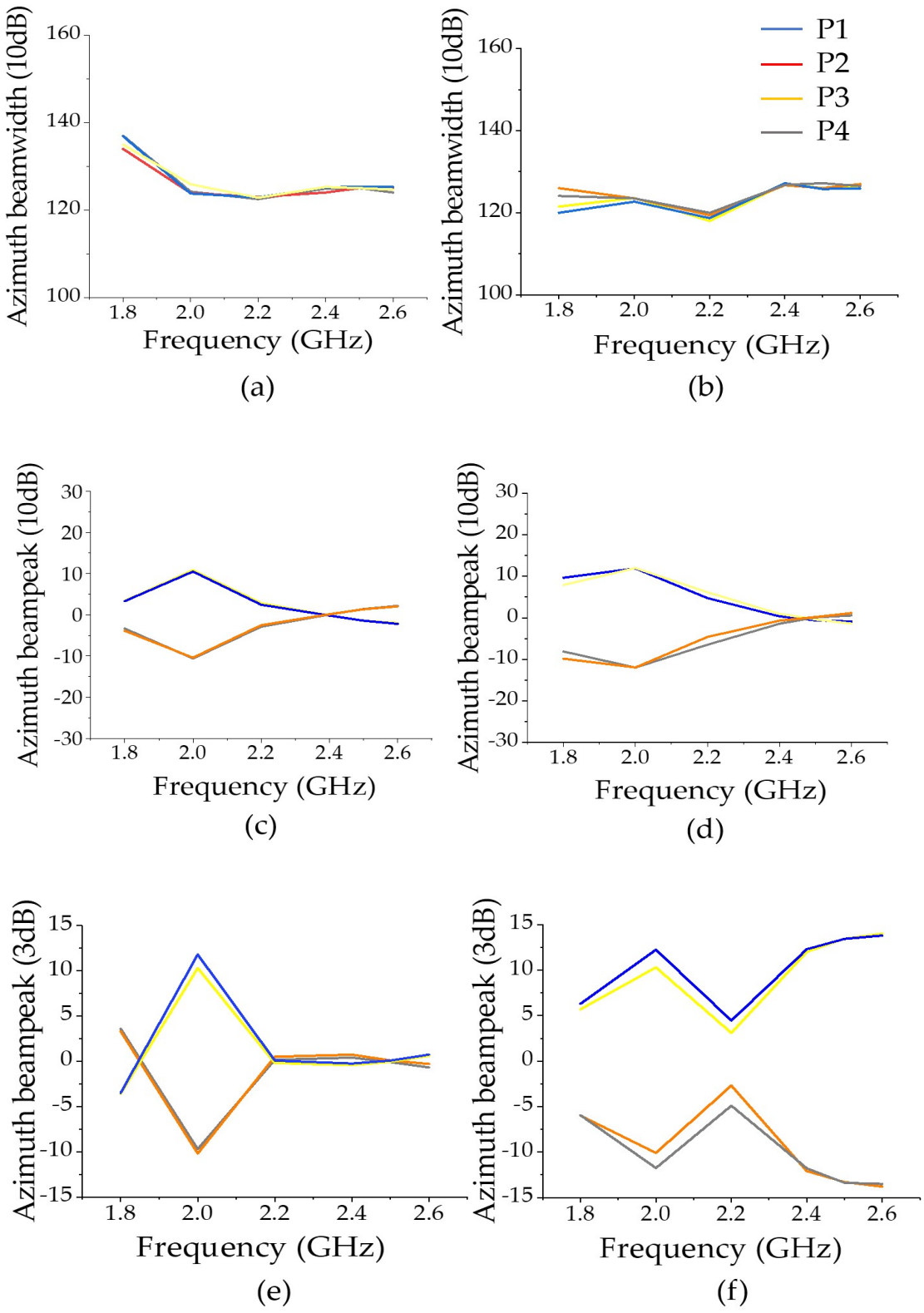

Figure 3.16 Measured 10 dB azimuth beamwidth of HB arrays with (a) LBHV element (b) LB slant element, 10 dB azimuth beam peak of HB arrays with (c) LBHV element (d) LB slant element, 3dB azimuth beam peak of HB arrays with (e) LBHV element (f) LB slant element. The P1, P2, P3, and P4 refer to polarizations indicated in Figure 3.2

Table 3.2: Comparison of recent state-of-the-art works with proposed work.

References	Modification Type to improve isolation	Frequency Band (GHz)	Reflection co-efficient (dB)	Isolation (dB)	HPBW (Measured)
[81]	Metal baffles	0.77–0.98 1.65–2.9	Not Given	>23 17.5	64.5 ± 57.1° 84.4 ± 74.1°
[14]	Arc-shaped baffle plates	0.74–0.96 1.7–2.6	<-14	>27.5	61.5° 90°
[57]	Chokes in LB element	0.82–1 1.71–2.28	<-10	NG	69.5 ± 4° 65 ± 5°
[98]	Filtering antenna elements	1.71–1.88 1.9–2.17	<-12	>30	65 ± 5°
Proposed Antenna	No added structure	0.69–0.96 1.8–2.6	<-12	>36 >20	60 ± 5° 65 ± 11°

3.2.6 Summary

The high band pattern distortions can be reduced by using a horizontal and vertical low band element instead of a conventional slant low band element. The scattering from this low band element is minimized since dipoles are moved away from the high band-radiating elements. This method is simpler compared to other techniques available in the literature that require significant modifications to radiating element design, resulting in an increased cost. The construction of the horizontal low band element is almost similar to a conventional low band element design, and therefore, construction and assembly are simple. The only addition is a 180° hybrid coupler, which is used to generate the slant polarizations. The new low band element is matched over the entire low band frequency range with >12 dB return loss and the low band patterns are identical to conventional slant low band element pattern with 6.2 dBi gain, 60 ± 5° beam width for a single element.

3.3 Novel Cross Interspersed Design of Multi-Band Antennas

3.3.1 Introduction

In this work, a dual-band dual-polarized antenna for 5G base station application is proposed. The proposed antenna avoids using the conventional interspersed technique which cause the cross-band scattering. It consists of a novel cross interspersed configuration and working frequency covers low-band (LB) 690-990MHz and high band (HB) 1810-2690 MHz bands. For demonstration purposes, the prototype of the proposed configuration is fabricated and measured. The dual band prototype features a stable radiation pattern with HPBW 65+5◦ and wideband matching >10dB in the entire frequency bands of interest. Moreover, the experimental results verified a port to port isolation of better than 36dB in the operating band.

There are increasing capacity demands with developing wireless communication system driven by multiband antennas. Although antenna arrays designed with separate apertures can perform as multiband antennas they take up more space and are thus not suitable for size constrained applications such as base stations. Space and weight are key considerations for easy installation and maintenance [85]. Therefore, antenna in multiple interspersed arrays has been deployed to achieve the space and weight savings. In general, interspersed array designed as multiple higher frequency band arrays can be co-located with one low band array.

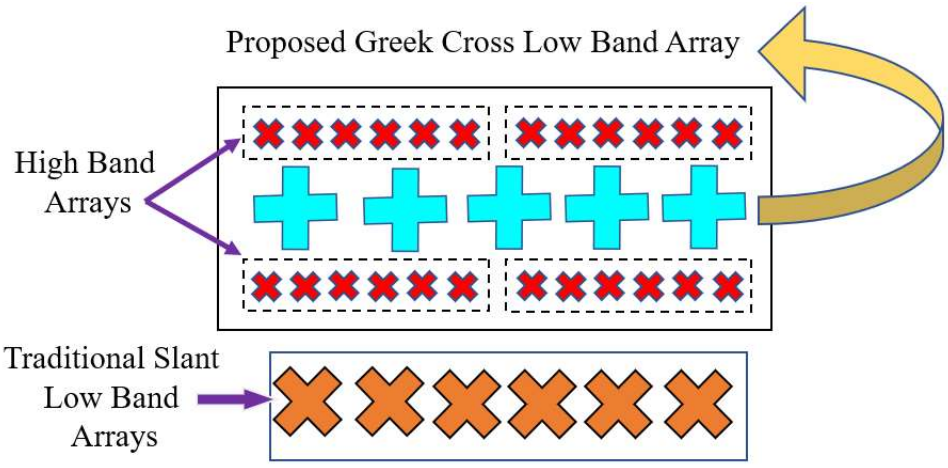

Figure 3.17. Novel low band to high band 1:4 antenna interspersed array configuration.

Interspersed arrays meet the requirement of high density integrated wireless systems. However co-located antennas can cause undesirable effects on each other's radiation performance. Over

the years many efforts have been done to address these challenges. In [59] metasurface cloaks and in [57] scattering cancellation techniques has been deployed. Whilst these approaches help in improving the scattering suppression, the fabrication is complex. Here, we explore an alternative approach to make the radiating element of one band almost invincible from the radiating element of another band. To achieve this, the low band orientation is altered from slant position to a Greek cross position. This direct approach features a cleaner pattern and better isolation.

3.3.2 Antenna Configuration

The analysis in this work has been performed using a simplified configuration. The proposed antenna array configuration is shown in Figure 3.17. It consists of a low band element in the centre of the structure and four high band elements as sub arrays. Figure 3.18 (a) exhibits the structure of the lower band element. The main radiator has two intersecting full-wavelength dipoles perpendicular to each other. To create the ±45 polarization from this Greek cross dipole, a 180-degree hybrid coupler is used between the inputs of the perpendicular dipole.

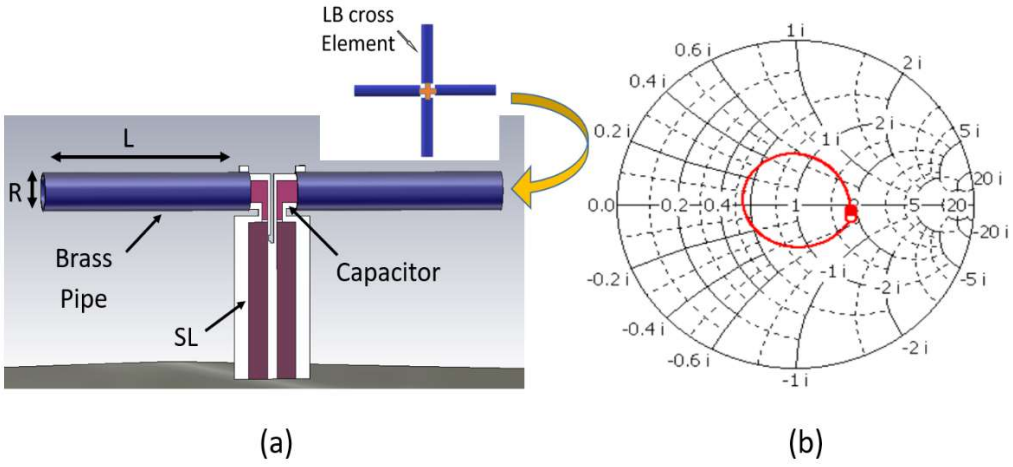

Figure 3.18 (a) A view of low band radiating element. (b) Matching of +45 Polarization (same for -45 due to symmetric of the structure).

Each dipole arm is 110 mm long and made of a copper (brass) material. The vertical feed is made of Fr4 substrate that has a dielectric constant of 4.2, loss tangent of 0.02 and 1.6mm thickness. An impedance matching circuit was designed for realization to get perfect matching as shown in Figure 3.18 (b). The two feeds are mounted between the radiator and reflector.

The matching circuit consists of small portions of transmission lines, short transmission line SL and an open line OL.

In order to demonstrate, here we consider a section, and used 4 HB elements as 2 sub-arrays. A square shape cross the dipole with bends at the outer edges are orthogonal to a realized $\pm$ 45 polarization. The matching network of HB antenna element is based on circuit theory model as discussed in [86], however, balun is fed through a direct coaxial cable Basically, the antenna consists of a pair of dipoles, two feeding line and a reflector whose edges are bent downward to achieve better radiation performance.

3.3.3 Performance Analysis

The analysis is conducted within the base station operational frequency band from 1810-2690 MHz for high band and 690-990MHz for lower band. In order to showcase the operation of the proposed technique, a series of parametric sweeps has been performed. It is investigated through that, the aperture length of the radiator, reflector size, gap between the dipole arms and width of radiator all impact the overall performance of the antenna. Following our design procedure, a proposed antenna prototype was fabricated and radiation performance was obtained. It clearly shows that the proposed alteration technique of LB radiator orientation, makes more room available for an HB element radiation pattern. As it leaves the space over the HB element, compared to the slant interspersed technique, the LB resonating effect is reduced in ratio.

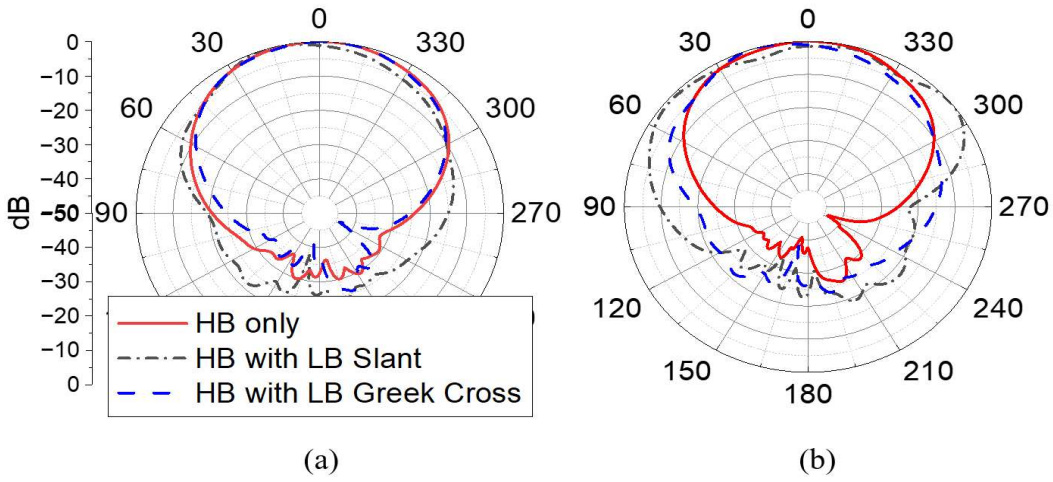

Figure 3.19 HB measured radiation patterns with and without LB element at (a) 1.8GHz, (b) 2.5 GHz.

The performance of our proposed technique in terms of the radiation feature has been tested as shown in Figure 3.19. The figure compares the scenario of interest: HB only (without LB), HB with LB slant element, and Hb with LB Greek Cross element. These measured results show that HB array patterns in presence of LB Greek cross element are quite similar to the HB-only radiation pattern. In slant configuration, close proximity of LB radiating elements on top of HB radiator induce the HB current on LB dipoles, acting as a parasitic structure and distorting the HB patterns. While only changing the orientation of the LB radiator to Greek cross, it would not be directly in front of the HB radiator, hence, there was less nearfield distribution, which reduced the scattering of desired HB patterns.

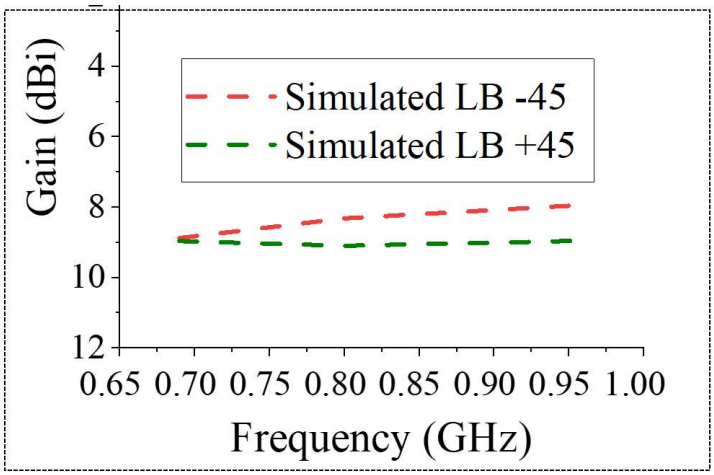

Figure 3.20 Simulated Gain of LB radiating element.

Furthermore, in LB the average antenna gains are 9.4dBi. The simulation curve of the gain in the working frequency band is depicted in Figure 3.20. The fabricated prototype of the proposed antenna is illustrated in Figure 3.21. Most importantly, the advantage of the proposed technique is, that it gives stable HB radiation patterns with almost no impact on the LB element radiation performance, as shown in Figure 3.22.

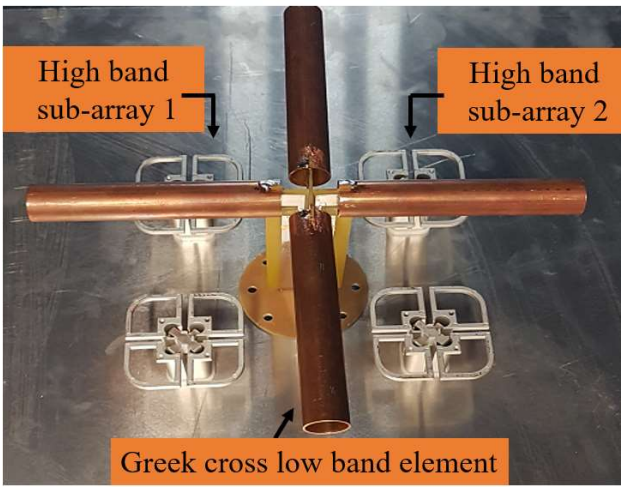

Figure 3.21 (a) Fabricated Prototype of proposed antenna. (b) Gain of LB radiating element.

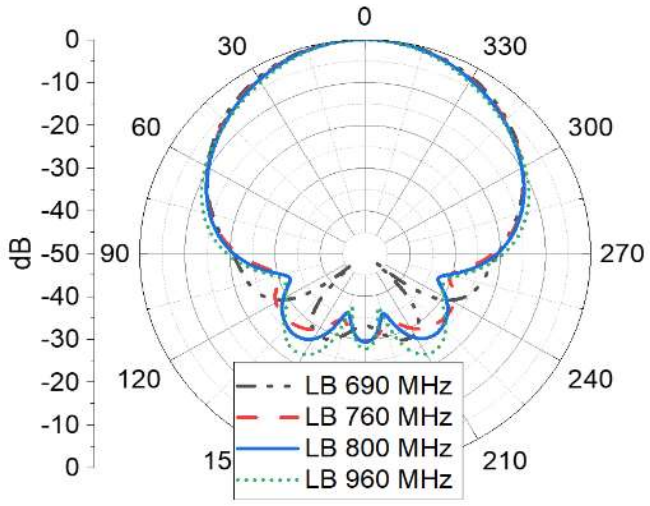

Figure 3.22 LB Greek cross measured +45 azimuth radiation patterns.

3.3.4 Summary

The new low band element orientation is proposed for multiband base station application. The antenna is matched over the entire low band frequency range with >13 dB and >15 dB return loss for HB frequency range. The low band and high band antenna performance is stable with HPBW 65±5°. The technique presented in this work can be implemented in different multi-band systems as more and more antennas require integration on the same platform with less mutual interference.

Chapter 4: Resonance in Multi-Band Antennas

4.1 Introduction

Designed to handle increased traffic demand [87], the 5G access network marks a significant milestone in the evolution of mobile communications. In mobile communication, the antenna plays a vital role in the translation of the analog circuit signals to electromagnetic waves to propagate through air [88]. These antennas in the last access element i.e. gNBs in 5G or NodeBs in 4G are commonly referred to as base station antennas (BSA) [89]. BSAs has evolved from Omni-directional single band antennas from early generations to sectorized multiband multibeam antennas in 5G [90]. To meet the capacity demands for operators, the base station antenna needs to be multiband as this improves the resource utilization. On top, the size of a multiband antenna does not vary a lot compared to a legacy single band antenna. Thus, within the same size constraints a 5G BSA should support multiple frequency bands such as 617 MHz-960 MHz (Low Band),1695 MHz-2180 MHz (High Band 1), 2490 MHz-2690 MHz (High Band 2) and 3300 MHz – 3800 MHz (High Band 3) [91].

Common practice is to have separate antenna arrays to cover each of these bands. In doing so, antenna arrays will be interspersed on the same ground plane. The challenges in such designs include pattern distortions [57] due to scattering from nearby elements. The pattern distortions can be twofold. First is the High Band (HB) pattern distortions due to nearby Low Band (LB) antenna elements. The second is the LB pattern distortions due to HB antenna element radiating in its common mode (CM). In Table 4.1 LB some key patterns performance parameters impacted due to HB element are listed. The first issue is overcome by introducing choking techniques [92], implementation of metal baffles [32,2] and frequency selective surfaces [45,85]. However, the second challenge of HB common mode radiation at LB [93] hasn't been investigated extensively.

The LB pattern distortions due to HB CM is observed through the impacts on 3dB beamwidth and cross-polarization levels. The 3dB beamwidth of LB patterns will exhibit a significant widening and cross-polarization levels can be high due to CM radiation. Often attempts are made to reduce the common mode (CM) resonance by tuning the dimensions of the HB elements. The common approaches are to include capacitive elements in the feed, thus moving

the CM resonance to a higher frequency or out of band [93]. This approach causes broadening of the azimuth beam width at a lower frequency for the commonly used LB radiator.

In this work, we propose a novel approach to reduce the CM resonance by adding a CM suppression circuit. We introduce a CM suppression circuit to the impedance matching network of the HB radiator to minimize the induced CM currents at LB frequencies. This CM suppression circuit is designed to present a high impedance to HB matching circuit to appear as an open circuit.

Table 4.1: LB key patterns performance parameters impacted due to HB element.

Frequency (GHz)	**Beamwidth (Deg.)**	**Squint (Deg.)**
0.66	82.5	-6
0.67	82.1	-5
0.72	86.4	10
0.75	77.7	16
0.77	75	14
0.85	68.8	5
0.90	66.1	2

4.2 A Distinctive Approach for Common Mode Resonance Suppression

5G demands significant increments on a number of connected devices. As a result, gNodeBs are constantly pushed to serve more spectrum and smaller sectors. These increased capacity demands are met by using multiband antennas in base stations. One of the key challenges with multiband antennas is the pattern distortions due to the presence of other surrounding antenna elements structures. This work provides a novel approach to address the challenge of pattern distortion in the lower frequency band 690-960 MHz due to common mode (CM) currents in high frequency band antenna elements operating in the 1810-2690 MHz. A common mode suppression circuit is integrated with the impedance matching network of the high band antenna element to reduce these common mode currents. The experimental results verified that

the common mode suppression circuit reduces the common mode currents at low band frequencies by moving the common mode resonance frequency outside the low frequency band, resulting in cleaner low band patterns meeting pattern specifications.

4.2.1 Antenna Configuration

A typical interspersed HB and LB elements in a modern day multiband BSA is shown in Figure 4.1(a). Due to the use of ±45 polarized elements, the dipoles are oriented in a slant configuration.

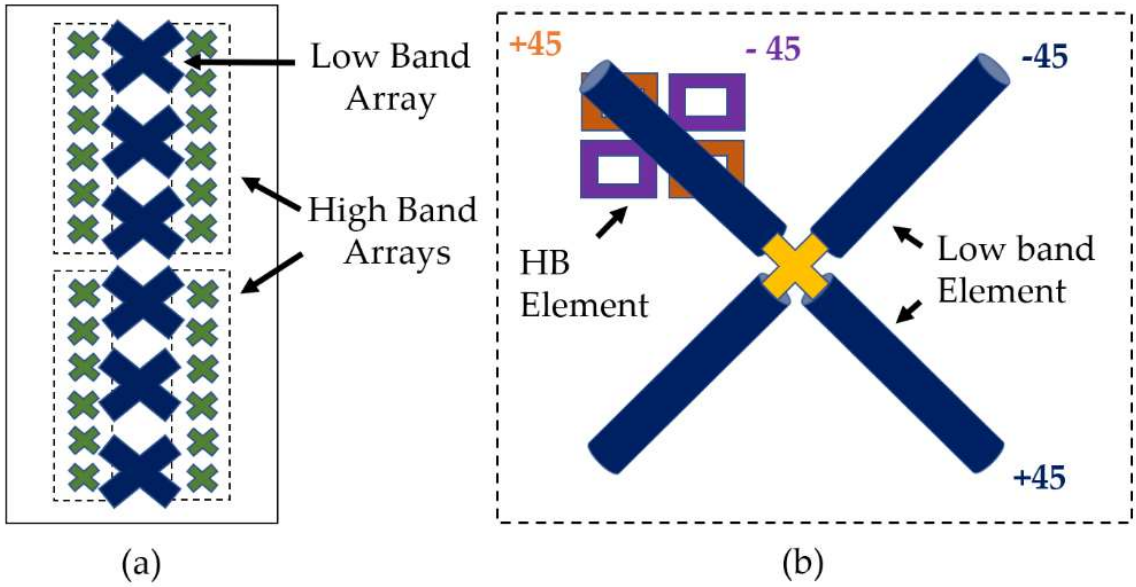

Figure 4.1 (a) Slant dipole configuration used in traditional interspersed scheme for dual-band dual-polarized BSA (b) Schematic of the experimental setup with one LB and HB element.

In such an interspersed arrangement, there are two types of resonances that can cause pattern distortions, namely common mode (CM) resonance and differential mode (DM) resonance. The presence of these resonances is not a problem so long as they occur outside the frequency bands of interest. However, since the total length of the HB feed circuit and the dipoles is approximately one quarter wavelength of LB, when LB radiates it can induce strong common mode currents on HB elements as shown in Figure 4.2. Due to these high CM currents the HB dipole operates as a quarter wave monopole at LB frequencies. This monopole like radiation pattern from HB elements at LB frequencies distorts the LB radiation patterns. Here to clearly present the impact of the HB element on performance of the LB element, a parametric study is

performed whose results are listed in Table 1. The LB element patterns in the absence of the HB element have a half power beam width (HPBW) around 65+5° as shown in Figure 4.3a. However, with the CM resonance caused by the HB element, the HPBW broadens to 75°- 85° as indicated in Figure 4.3(a-b).

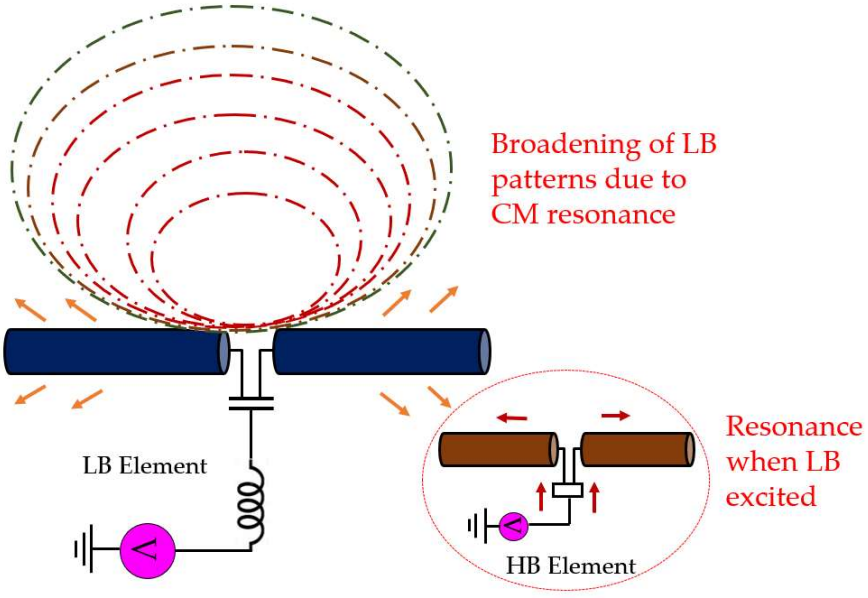

Figure 4.2 Artistic impression of the Resonance induced in High Band (HB) elements when two antenna elements are in the vicinity impacting the LB patterns.

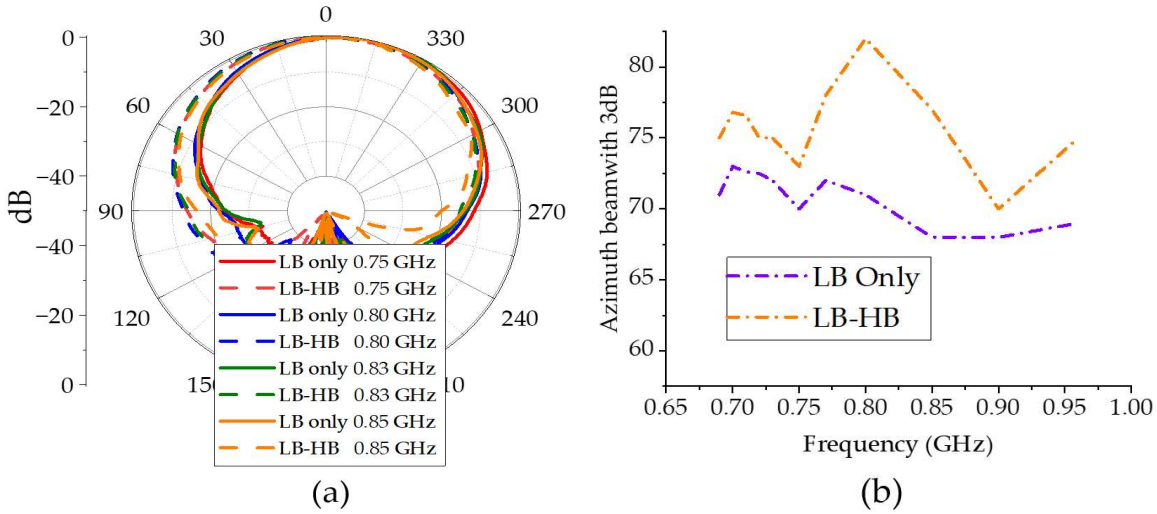

Figure 4.3 (a) Low band only (LB only) and low band with a HB antenna element (LB-HB) azimuth +45 co-pol patterns. (b) Measured 3dB azimuth beamwidth of LB element.

4.2.2 Antenna Model Description

In order to demonstrate the effect of CM resonance, a simpler dual band antenna setup is constructed. A schematic representation of this antenna setup is shown in Figure 4.4. Only one LB element and an HB element is used from the interspersed array to keep the simulation setup simpler. The LB antenna is a rod dipole antenna while, for HB, the antenna configuration is simplified and consists of two identical sub-dipoles positioned perpendicular to each other. The analysis conducted in this study focuses on a cross-dipole antenna, which is depicted in Figure 4.4 (b). To enhance the performance of the antenna in terms of bandwidth and gain, square-looped dipole arms are employed. These square-looped arms provide a larger aperture for improved performance. The traces forming the square-looped arms have a length denoted as L and a width denoted as W. The square-looped arms are placed in close proximity to each other, with a small separation distance denoted as g. This arrangement promotes strong coupling between the elements, which can have a positive impact on the antenna's performance.

To achieve a cross-dipole system that meets the design specifications, it is crucial to understand how each parameter affects the overall performance. In this work, various parameter sweeps were conducted to investigate this relationship. During each sweep, only one design parameter was allowed to vary while the others were kept fixed at the values listed in Table 4.2. These dimensions in the table represent the optimized values obtained through an exhaustive set of simulations, and they were used for fabricating the prototype antenna. The dipoles are printed on a substrate made of Rogers 4550B material. The relative permittivity (dielectric constant) and permeability of the substrate are 3.55 and 1.0, respectively. The substrate also has a loss tangent of 0.0027 and a thickness of 1.6 mm. The traces connecting the square loops have a width of 0.3 mm. As demonstrated later, the CM effects are observed even with only one HB element.

Table 4.2: Simulated LB bandwidth comparison with and without CMSC.

Freq. points (GHz)	LB only (Deg.)	LB with HB (Deg.)	LB-HB with CMSC (Deg.)
0.69	71	75	70
0.7	73	76.8	70.5
0.71	72.6	76.6	72.5
0.72	72.5	75	72
0.73	72	75	72
0.75	70	73	69
0.77	72	78	70
0.8	71	82	69
0.83	68	77	66
0.85	68	70	66
0.9	68	77	67
0.96	69	75	67

A conventional slant LB dipole [94] was used as the LB element. For the LB element, the parameters and dimensions of a full-wavelength dipole antenna intended for cellular base station applications are in the frequency range of 698 to 960 MHz. The dipole arms are constructed using brass tubes. Each tube has a diameter (D) of 12.7 mm and a thickness (t) of 0.3 mm. The arms have an equal length (L) of 110 mm and are separated by a distance (s) of 15 mm. The dipole is positioned 90 mm above a conductive ground plane, which is approximately $\lambda_{0/4}$, where λ_0 represents the wavelength at the center frequency (818 MHz) of the target band in free space. The dipole and matching circuit are supported by a Rogers 5880 substrate. The substrate has a dielectric constant (εr) of 2.2, a loss tangent ($\tan \delta$) of 0.0009, and a thickness (h_sub) of 1.6 mm.

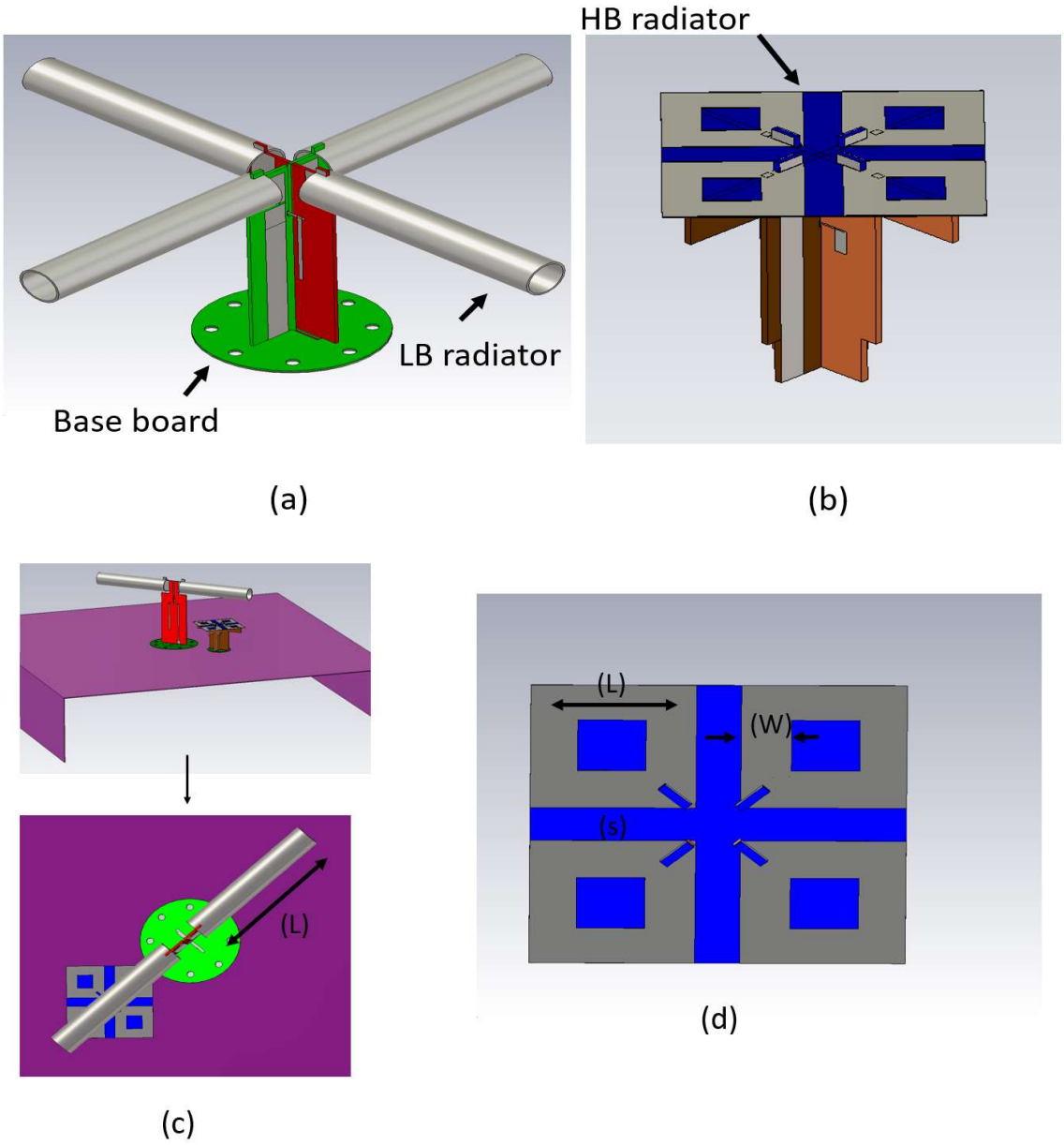

Figure 4.4(a) LB geometry (b) HB geometry (c) dual band antenna setup with reflector (d) cross dipole geometry.

4.2.3 Matching of LB and HB Elements

In the simulation process of the simplified cross-dipole antenna, a step-by-step design procedure was followed. Initially, the basic structure of the antenna was designed and its radiation performance was evaluated through simulations or theoretical analysis. After obtaining the initial design and understanding its radiation characteristics, a matching circuit was designed. The purpose of the matching circuit is to ensure efficient power transfer between

the antenna and the transmission line or feed system. It helps to match the impedance of the antenna to the impedance of the transmission line, maximizing power transfer and minimizing reflections. Once the matching circuit was designed, the combined system of the antenna and matching circuit was optimized together. This optimization process involved adjusting various parameters and configurations to achieve the desired performance goals. Parameters that may have been optimized include the dimensions and characteristics of the antenna elements, as well as the components and topology of the matching circuit. The combined antenna and matching circuit were iteratively optimized to achieve the final prototype design. This optimization process aimed to improve the antenna's performance, such as radiation efficiency, bandwidth, and impedance matching, while considering the practical constraints of fabrication and realization.

The dual-polarized cross-FWD (full wave length dipoles) consists of two sub-FWDs, each having a standard configuration with two straight copper tubes serving as the dipole arms and used as the LB element, as shown in Figure 4.4 (c). A conventional slant LB dipole was used as the LB element. The LB dipole impedance matching from 690-960MHz is based on a feed network design that includes series, shunt resonators and a quasi-quarter wavelength transmission line (TL2). A circuit theory model of matching circuit and implementation is proposed in [95].

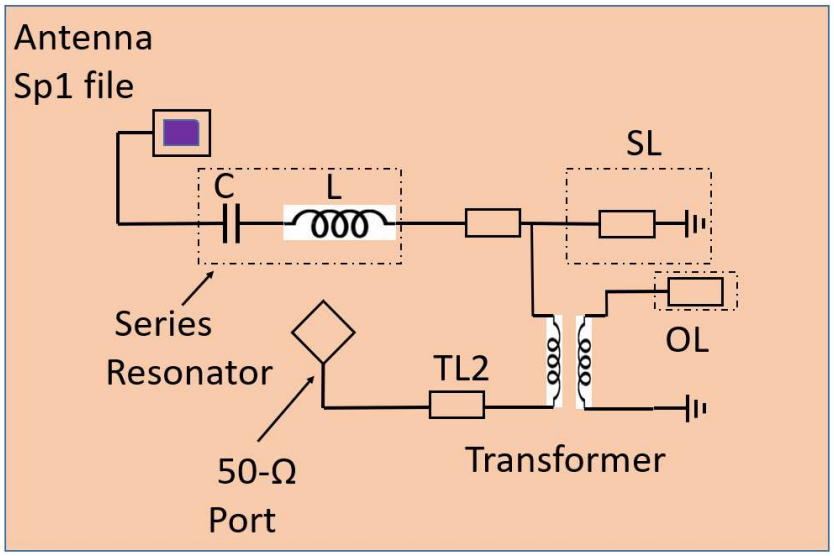

(a)

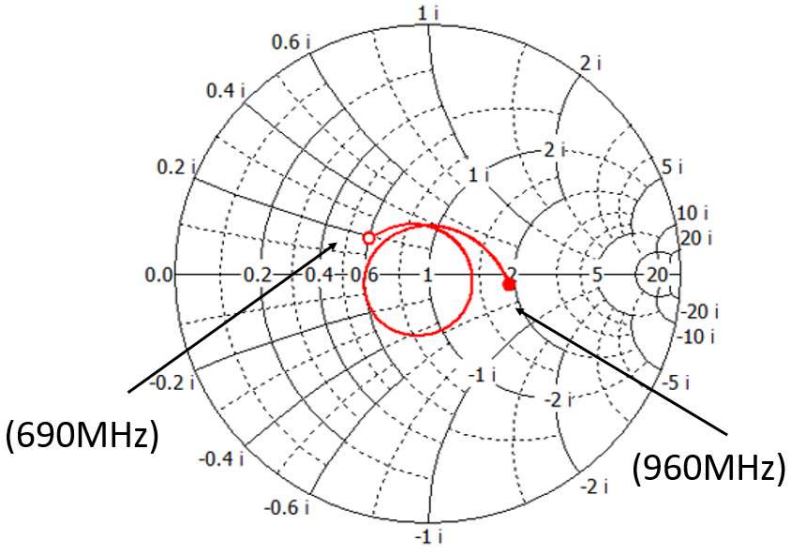

(b)

Figure 4.5 (a) Configuration of the matching circuit for the full-wavelength dipole,

(b) Matching of dipole 1(pol 1)

A hybrid triple-tuned matching circuit is implemented for LB matching with an integrated balun. It is a type of impedance matching network used for anti-resonant full-wavelength dipoles. This circuit is designed to ensure efficient power transfer between the transmission line and the antenna, maximizing the antenna's radiation efficiency. The circuit incorporates three tuning elements to achieve impedance matching as shown in figure 4.5. These tuning elements are capacitors and inductors arranged in a specific configuration. By adjusting the values of these components, the circuit can provide impedance matching at multiple points within the frequency band of interest. A balun, short for balanced-to-unbalanced, is an essential component in balanced antenna systems. It converts the balanced signal (differential mode) of the antenna to an unbalanced signal (common mode) suitable for transmission over a coaxial cable or other unbalanced transmission lines. The integrated balun within the matching circuit ensures that the dipole's balanced signal is properly converted for transmission.

The optimization process for the matching circuit of the full-wavelength dipole was conducted using an HFFS circuit. During the optimization process in the HFSS circuit, all the components used in the matching circuit, including capacitors, inductors, and the transformer, were tuned

and adjusted to achieve the desired impedance matching performance. As a result of the optimization process, the full-wavelength dipole was successfully matched across the target frequency range of interest, which was previously mentioned as 698 to 960 MHz for cellular base station applications shown in Figure 4.5b.

A typical HB antenna feed with the dipole is shown in Figure 4.9a. The feed point of the HB antenna is at the bottom of the TL (transmission line) below the ground plane. The TL and OL (open line) act as an impedance transformer from the unbalanced to balance feed, the balanced SL (short line) and TL1(transmission line 1) printed at the back of the substrate. Further details on this Balun design can be found in [86] which is based on the circuit theory model. The configuration of the network model with the matching is shown in figure 4.6.

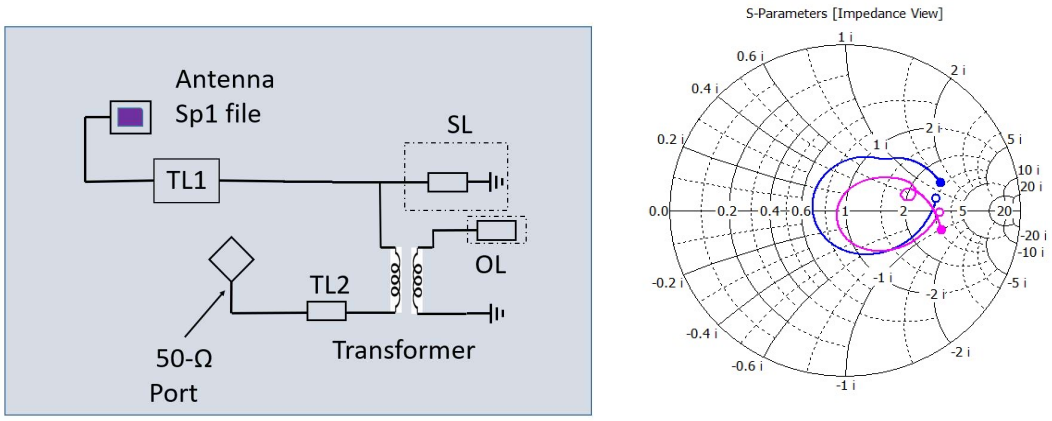

(a) (b)

Figure 4.6 (a) Configuration of the matching circuit for the full-wavelength dipole (b) Matching of pol 1 and pol 2.

4.2.4 Working Principle

A careful observation of the current distribution on the HB dipole shows that the currents on the feed board (stalk) and dipoles travel in the same direction mimicking the current distribution of a monopole as shown in Figure 4.7(a-b) when LB patterns are distorted. Only the current distribution at 0.69GHz and 0.75 GHz on a HB antenna is shown in the Figure 4.7,4.8(a-b). The currents on HB elements show similar behaviour for other frequencies where LB patterns are distorted. An LB antenna element is located near the HB antenna element in

this simulation setup and is differentially excited. In order to minimize this CM resonance, the effective resonance length of the HB antenna element at the LB frequencies needs to be altered. Currently the length of the HB dipole and the height of the stalk is 35mm, which is λglb/4 at LB frequencies where λglb/4 is the guided wavelength at low band mid frequency.

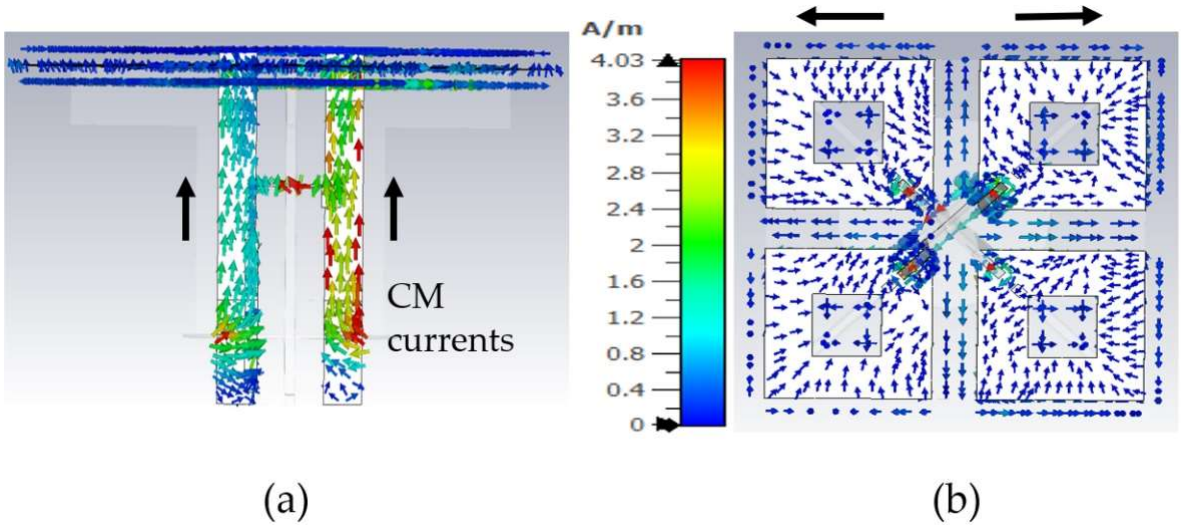

Figure 4.7 Currents on high band antenna element at LB frequency 0.69GHz (a) side view (b) top view showing the HB dipole.

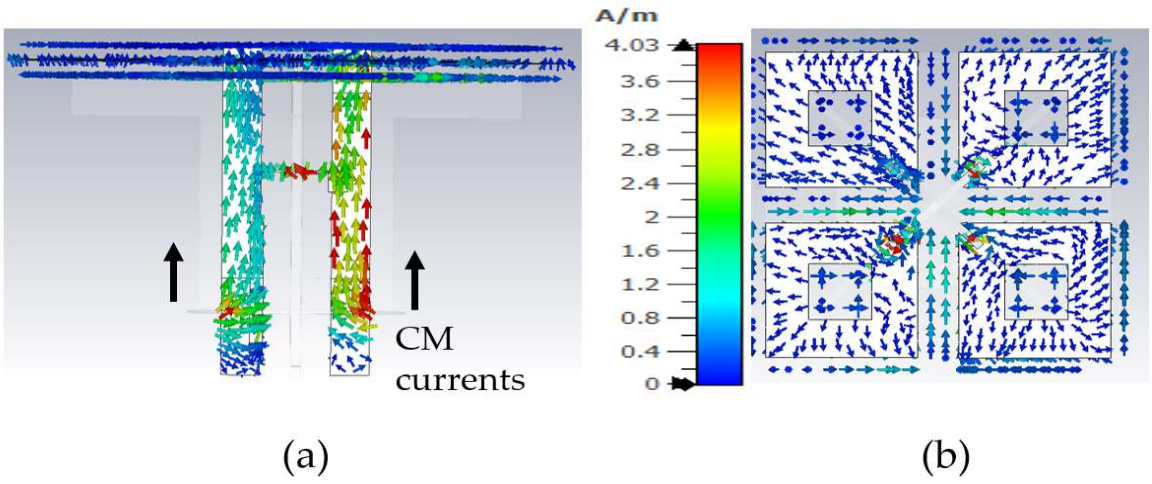

Figure 4.8 Currents on high band antenna element at LB frequency 0.75GHz (a) side view (b) top view showing the HB dipole.

In order to avoid LB currents in the HB stalk we introduce a common mode suppression circuit (CMSC) between the dipoles and the balanced feed as shown in Figure 4.9b. Effectively the CM suppression circuit should allow all the HB currents to flow as usual while the LB currents

are bypassed. The introduction of C1 in the CMSC provides a high series impedance to the LB currents forcing them to flow to ground via the series transmission line L2. Just having a C1 is not sufficient to avoid common mode currents at LB for this dipole. Therefore, providing a shorting path for LB currents through L2 is necessary. The L2 length is selected such that it is approximately λgHB/4 at HB, where λgHB is the guided wavelength at HB. Since one end of this L2 is shorted to the ground it presents an open circuit to HB currents, forcing them to go through C1. The value of the C1 is tuned in CST such that it provides low impedance at HB frequencies and high impedance at LB frequencies. This will ensure that the HB feed circuit operates as a conventional HB feed without a CMSC.

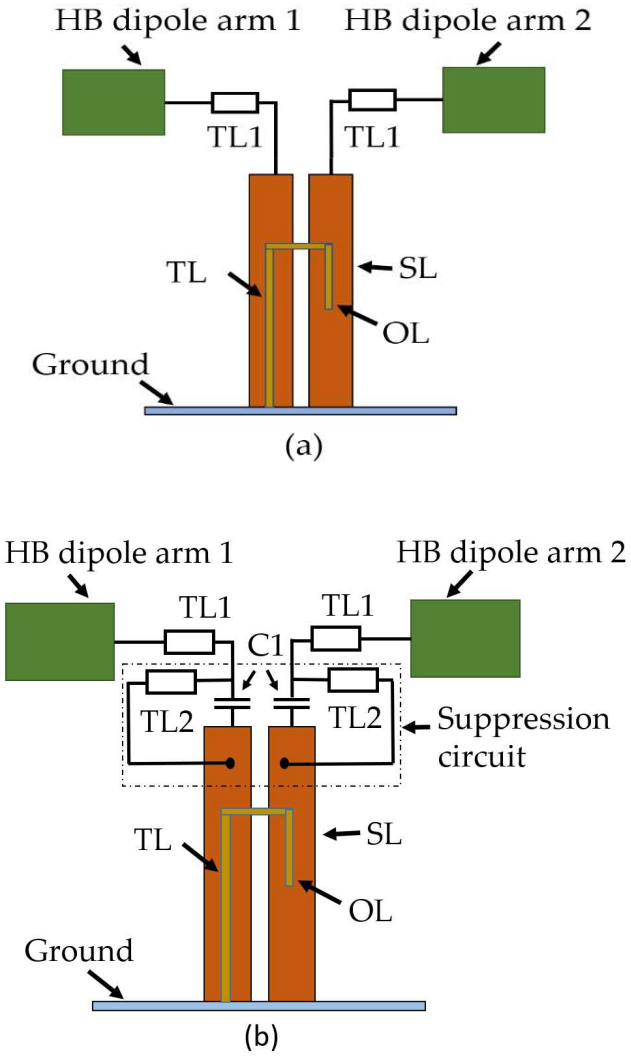

Figure 4.9 Schematic diagram of (a) typical HB antenna feed with the dipoles, (b) modified HB antenna feed with the CM suppression circuit. The TL refers to (transmission line), OL (open line) and SL (short line).

4.2.5 HB Feed Network Realization

A conventional HB antenna element feed without the CMSC is shown in Figure 4.10. Implementing C1 on the feed board can be done either as a printed capacitor or an external lumped capacitor while the latter is undesirable due to cost and additional effort for assembly. Implementing the C1 as a parallel plate capacitor using PCB technology is in fact cost effective and requires no additional effort during the assembly process. The C1 is therefore printed as a parallel plate capacitor as shown in Figure 4.11.

The realized capacitance of the C1 is 0.58pF. The capacitance C1 and length of the L2 transmission line was tuned during the simulation to minimize CM LB currents while observing pattern performance during the parametric study. The LB CM currents on the HB antenna element is not visible anymore with the CMSC as shown in Figure 4.13, only differential currents are observed on the HB antenna element which does not radiate effectively due to the mismatch. It will not even impact the matching of both polarizations as shown in figure 4.12.

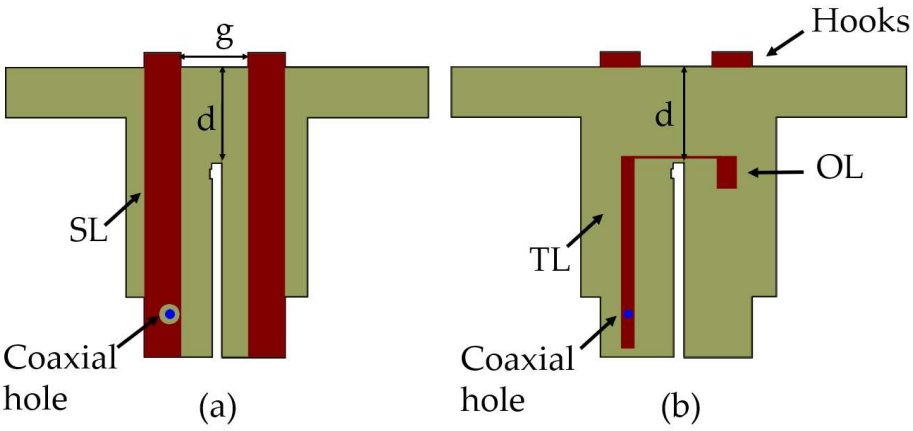

Figure 4.10 Schematic representation of a typical HB antenna element with impedance matching circuit.

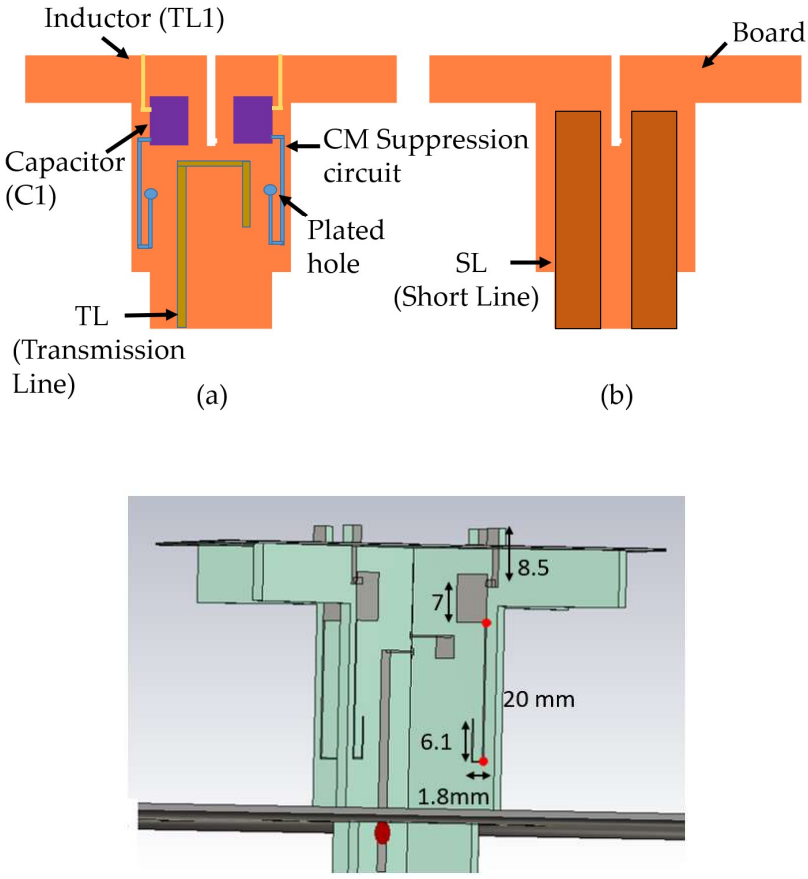

Figure 4.11 Schematic representation of HB antenna element stalk with CMSC(a) front view (b) back view (c) Parameters of the proposed design marked on its configuration.

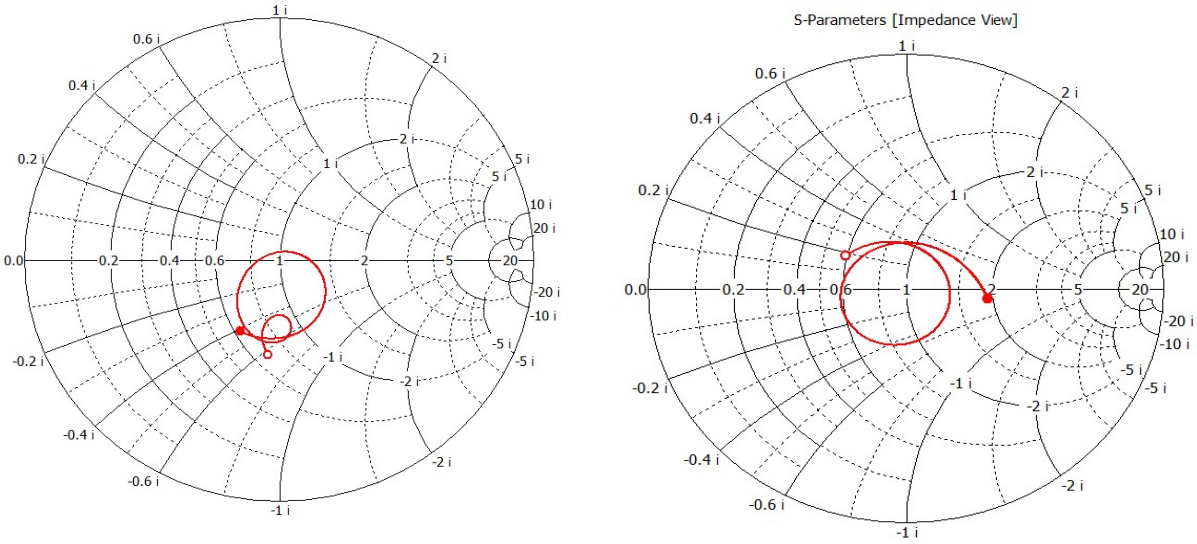

Figure 4.12 After CMSC return loss for both polarizations.

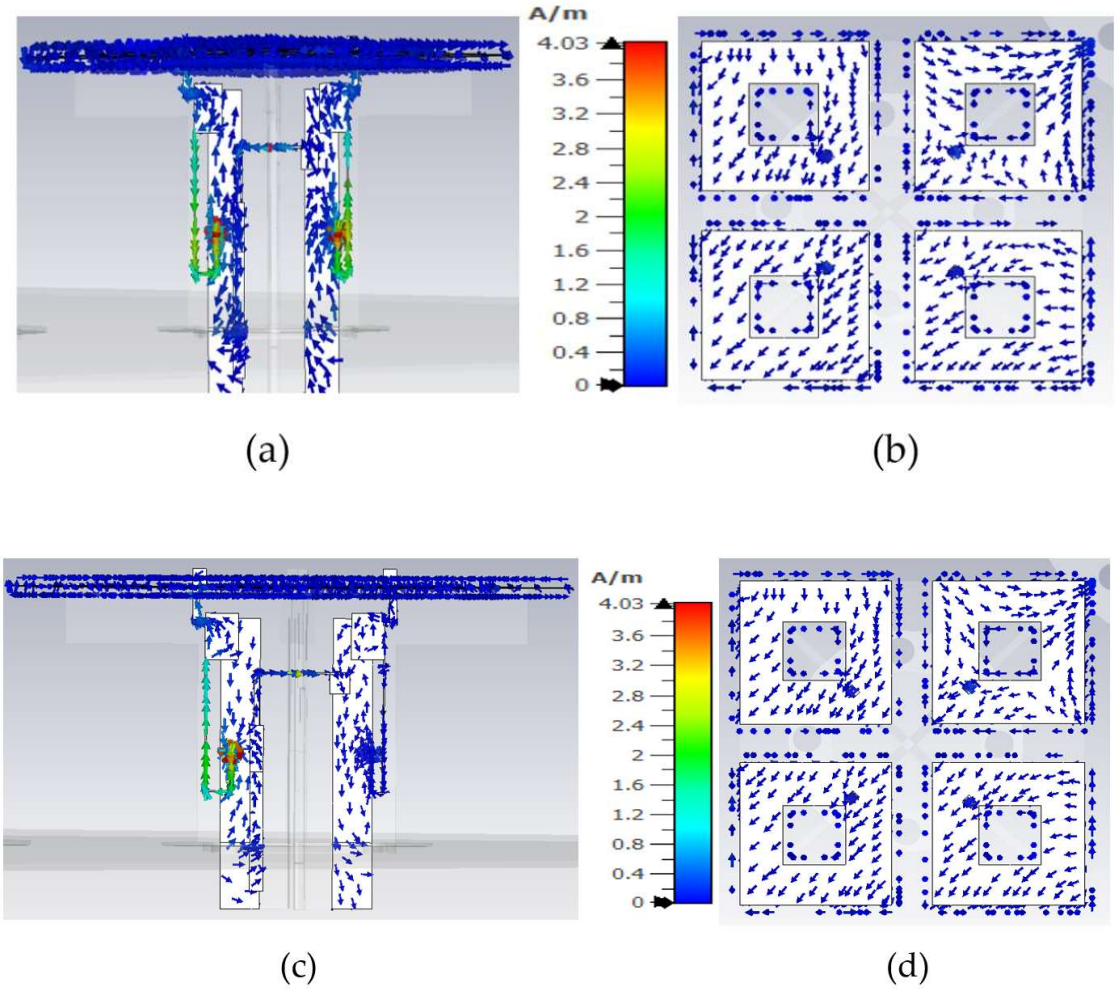

Figure 4.13 Currents on high band antenna element with CMSC at LB frequency 0.69GHz (a) side view (b) top view showing the HB dipole.

4.2.6 Experimental Results

The experimental setup consists of one LB element and one HB element as shown in Figure 4.14a. Based on simulations it was found even one HB element near the LB element was sufficient to cause pattern distortions. The antenna was fabricated and tested. The prototype with a 500x500 mm2 ground plane was fabricated and tested, as shown in Figure 4.14 (a) while figure 4.14 (b) shows the pictures of the HB antenna prototype after the addition of CMSC.

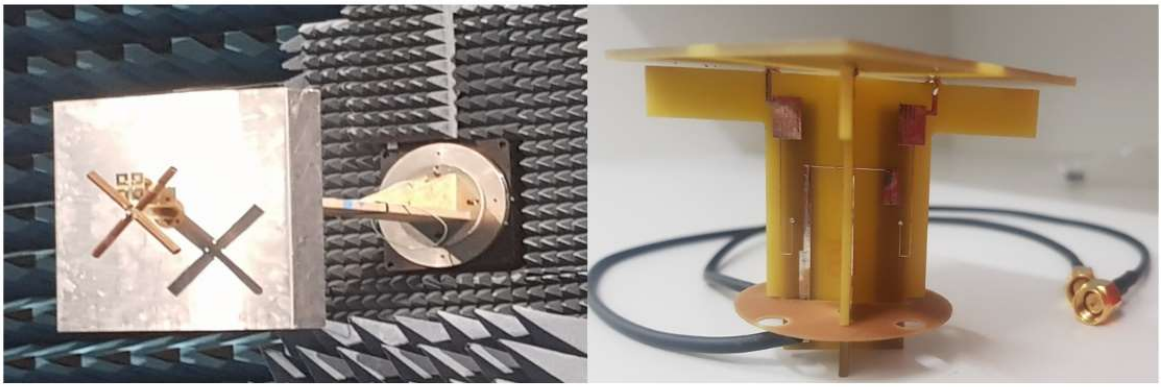

Figure 4.14 (a) The experimental setup consisting of one LB element and one HB element (b) fabricated HB antenna element containing CMSC.

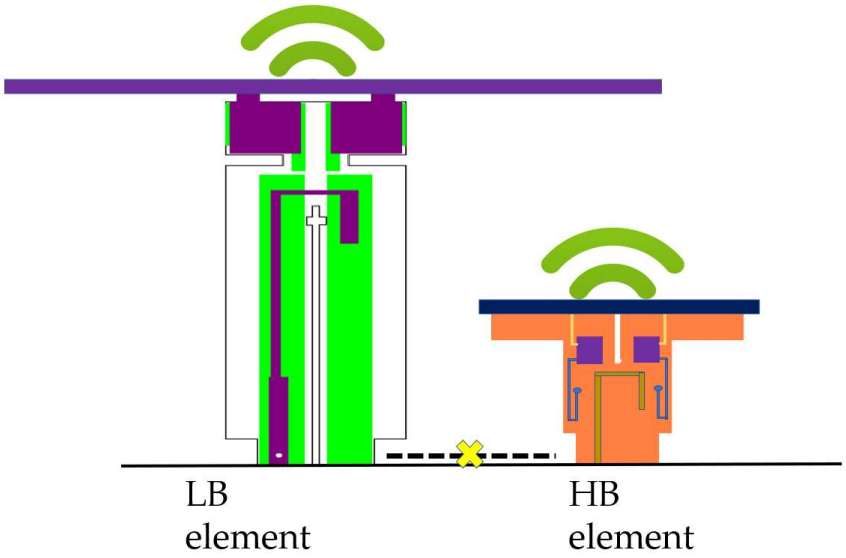

Figure 4.15 Artistic impression after CMSC insertion in High Band (HB) elements impacting the LB patterns.

The optimized radiator in the antenna design is powered by traditional baluns that have been specifically designed following the guidelines outlined in section 4.2.3. These baluns serve two purposes: providing balanced feeds to the dipoles and transforming the impedance of the dipoles to match the desired specifications. An artistic impression after CMSC insertion is represented in figure 4.15 to show how CMSC helps to reduce CM resonance and increased isolation between two radiating elements. The specific configurations of the two baluns, as well as the final configuration of the antenna, are depicted in Figure 4.16 for the B element, and Figure 4.17 for the LB element. In order to prevent overlapping with each other, the feed

lines are arranged in slightly different positions. These figures provide a detailed representation of the feed structure employed in the antenna design. To establish the connections, the cables are directly inserted into the feed points, with the outer conductor being soldered onto SL while the inner conductor is soldered onto TL. By employing these baluns and configuring the feed structure as shown, the antenna design ensures proper balance in the feed and impedance transformation, which are crucial for achieving optimal performance and efficient transmission or reception of signals. The performance characteristics of the antenna were measured. Both the HB and LB antenna element achieved fulfill the minimum design requirements for impedance matching across the frequency band of interest as shown in Figure 4.18. The optimized dimensions of the structure are provided in Table 4.3.

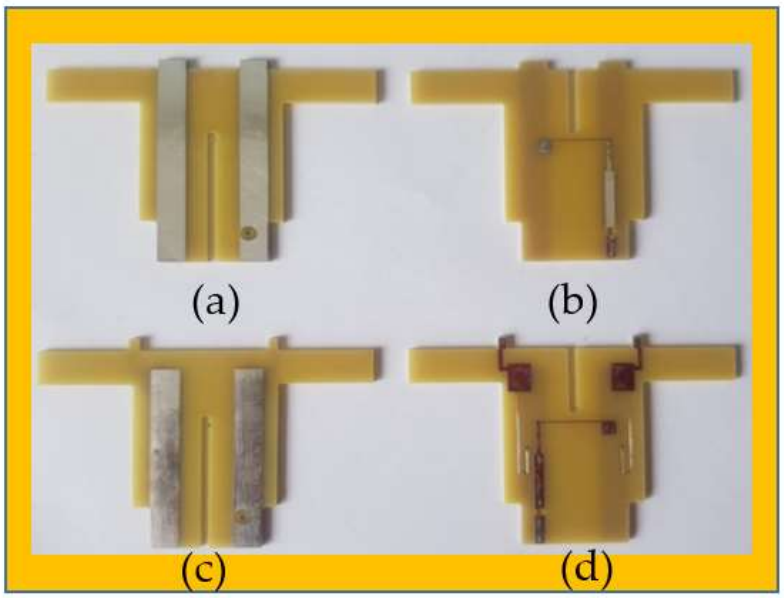

Figure 4.16 Perspective view of the HB antenna balun 1(a&b) front and back view of HB only (c&d) front and back view of HB with CMSC.

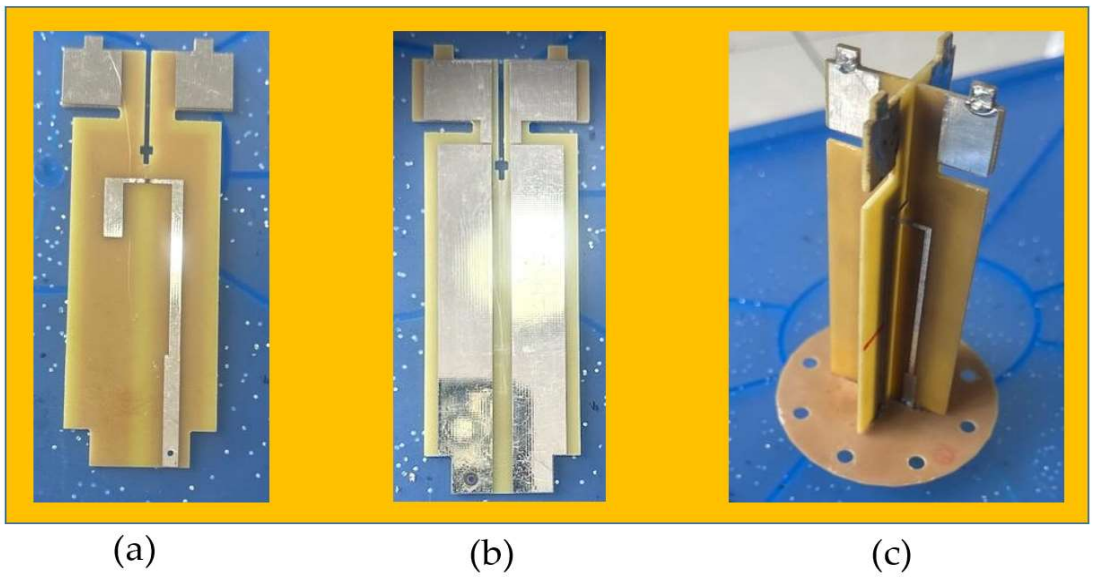

Figure 4.17 Perspective view of the LB antenna baluns.

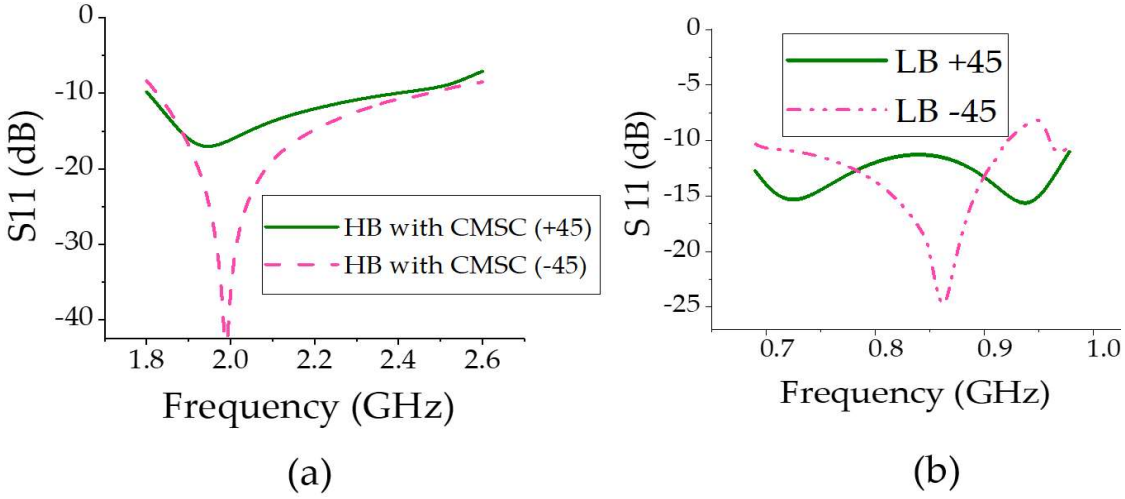

Figure 4.18 The measured reflection coefficient of the (a) HB element (b) LB element.

Table 4.3: Optimized parameters of the proposed antenna.

Parameters	Values HB (mm)	Description
W-SL	6	Width of SL
L-SL	43	Length of SL
W-TL	1.3	Width of TL
L-TL	15	Length of TL
W-TL1	1	Width of TL1
L-TL1	5.5	Length of TL1
W-TL2	0.2	Width of TL2
L-TL2	20	Length of TL2
W-OL	2.8	Width of OL
L-OL	6	Length of OL
g	11	Gap between SL

The symmetric arrangement of the radiators in the antenna design has resulted in radiation patterns that are very similar for both polarizations. This means that the antenna exhibits consistent radiation characteristics regardless of the polarization of the signals. Since the radiation patterns of the two polarizations are similar, it is common practice to present the results for one polarization, often referred to as the "port 1" excitation. This simplifies the presentation of the results without sacrificing important information. The agreement between the simulated and measured patterns is a positive outcome, indicating that the antenna's performance as predicted by simulations aligns closely with the actual measurements. This agreement validates the accuracy of the simulation models and provides confidence in the antenna's expected performance.

Figure 4.19 (a) shows the measured far field patterns at LB. With the inclusion of CMSC in HB elements, the LB co- and cross-polarization radiation patterns in Figure 4.19 (a,c) shows a significant improvement compared to patterns in Figure 4.3a. As indicated in Figure 4.19 (b) the 3dB beamwidth is very close to a 3dB beamwidth of the LB element alone thereby completely removing the broadening effect due to common mode currents. The HB patterns with and without the CMSC is shown in Figure 4.20 where the HB patterns are almost identical

and showing no impact due to the CMSC. The stable radiation patterns across wide operating bandwidths indicate that the antenna's performance remains consistent over a broad range of frequencies. This is valuable as it ensures reliable communication and consistent signal quality across the entire operating bandwidth.

The interband isolation between the LB and HB elements are measured as shown in Figure 4.21. For clarity, the isolation between HB +45 polarization with the LB polarizations are shown. Without the CMSC both LB +45 and -45 slant polarizations have high coupling at the bottom of the low band frequencies. With the CMSC, the coupling is reduced by over 10dB for the same polarization while it is more than 20dB for opposite polarizations. This significant decoupling also provides an indication of the transparency of the HB antenna element to LB frequencies. The simulated values also agree very closely with the measurements from the experimental setup.

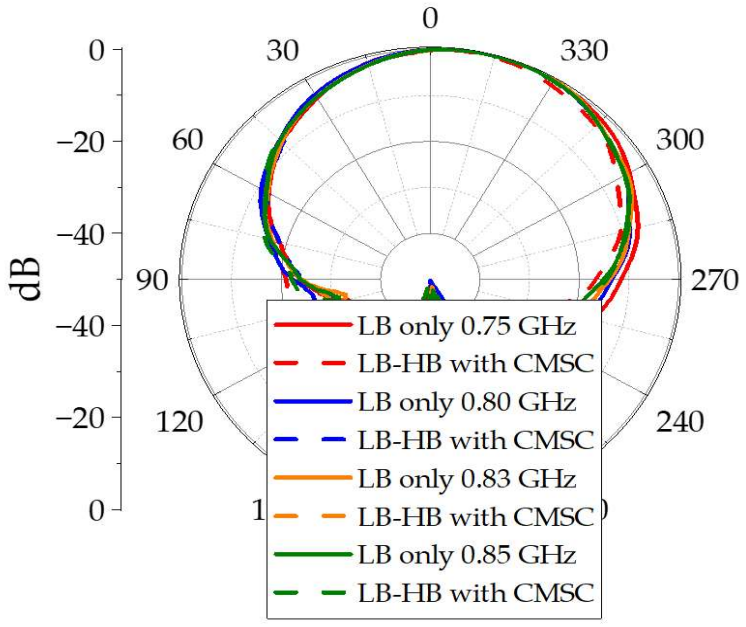

(a)

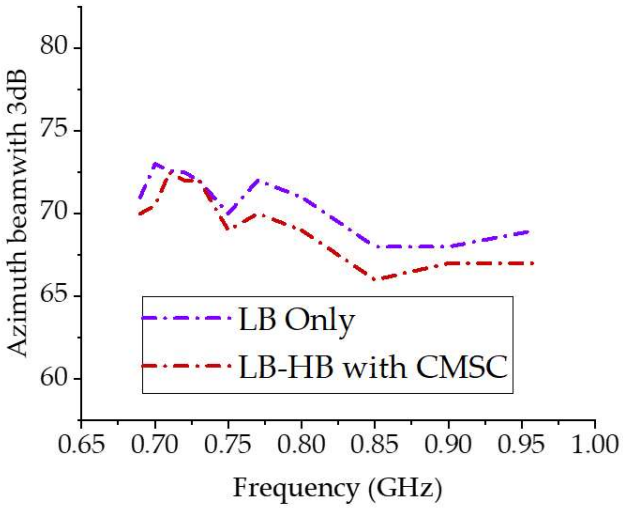

(b)

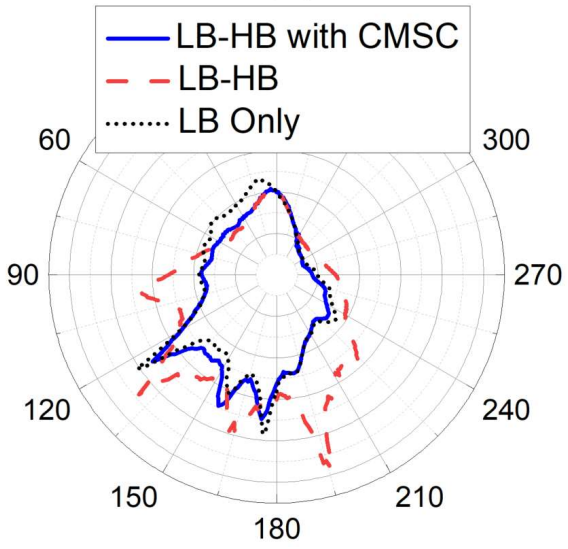

(c)

Figure 4.19 (a) Low band only (LB only) and low band with HB antenna element containing CMSC (LB-HB with CMSC) azimuth +45 co-pol patterns. (b) Measured 3dB azimuth beamwidth of LB patterns(c) Cross pol. Patterns at 0.8GHz.

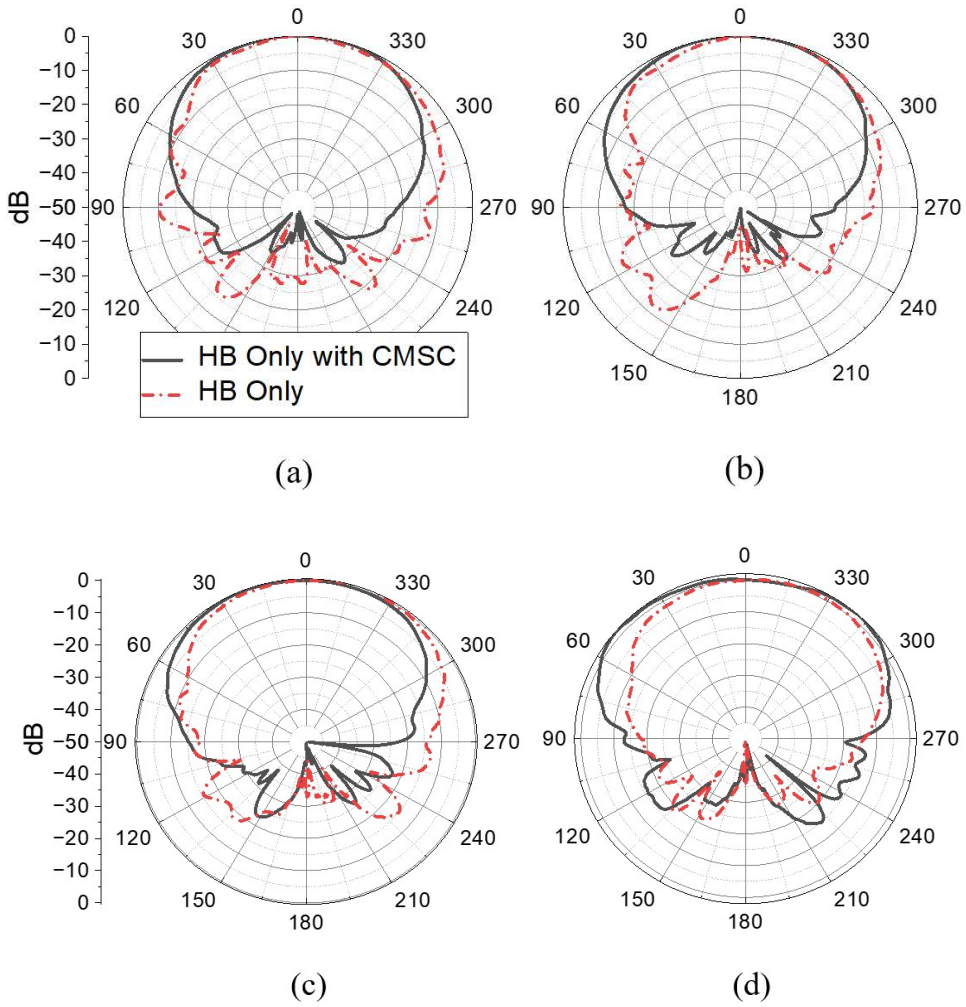

Figure 4.20 High band only antenna element azimuth co-pol patterns (a) 1.8 GHz, (b) 2 GHz and (c) 2.2 GHz (d) 2.4 GHz.

The suppression of CM resonance indicates that the antenna is effective in reducing unwanted interference between different frequency bands. This is particularly important when multiple antennas or systems are operating in close proximity, as it ensures that each antenna can function without negatively impacting the others. Whilst guaranteeing the co-existence of antennas for different services, these techniques enable efficient and reliable communication across a wide range of frequencies. This is crucial in today's rapidly evolving communication landscape, where different services and standards coexist and interact. It allows for smoother

transitions and upgrades in communication technologies without significant interference or compatibility issues.

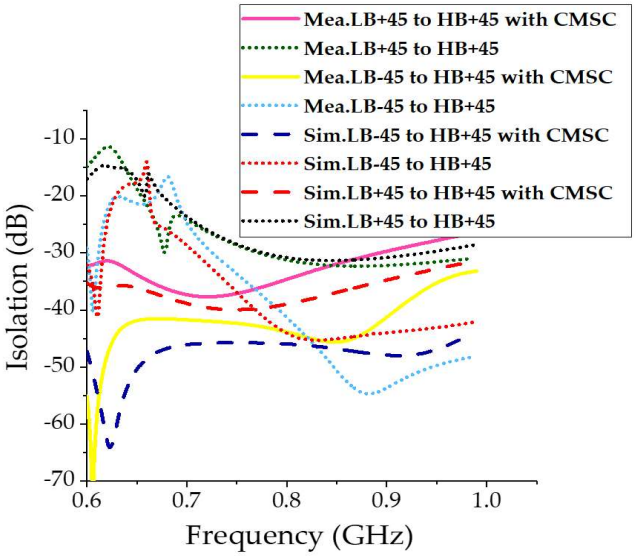

(a)

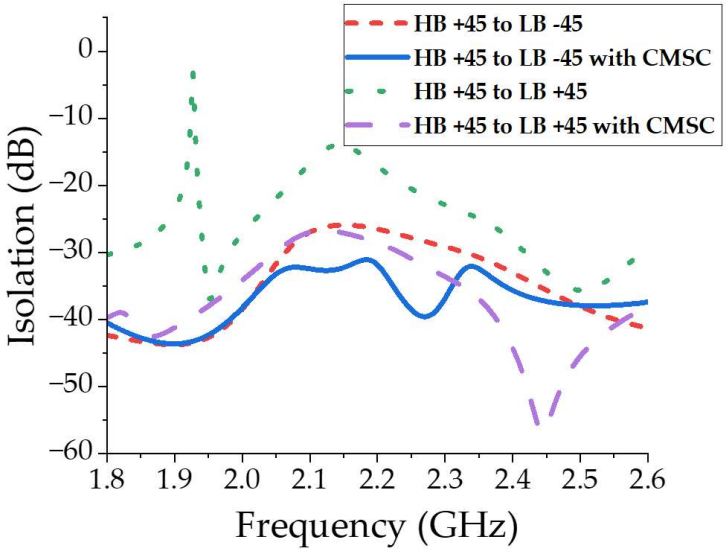

(b)

Figure 4.21 Interband isolation between LB and HB at (a) LB frequencies (b) HB frequencies.

4.3 Comparison

To have a side by side comparison of HPBW, the LB azimuth co-pol calculated patterns are plotted in Figure 4.22. They are presented as three cases (i) LB only

without any HB element (ii) LB with HB without CMSC and (iii) LB with HB with CMSC. This comparison indicates that CMSC contribution to the radiation patterns. The proposed antenna can be simplified to a dual -array however, future research can be done on multiple bands. To address the advantages of the proposed design, a comparison of results with the previous work on mutual coupling suppression techniques is tabulated in Table 4.

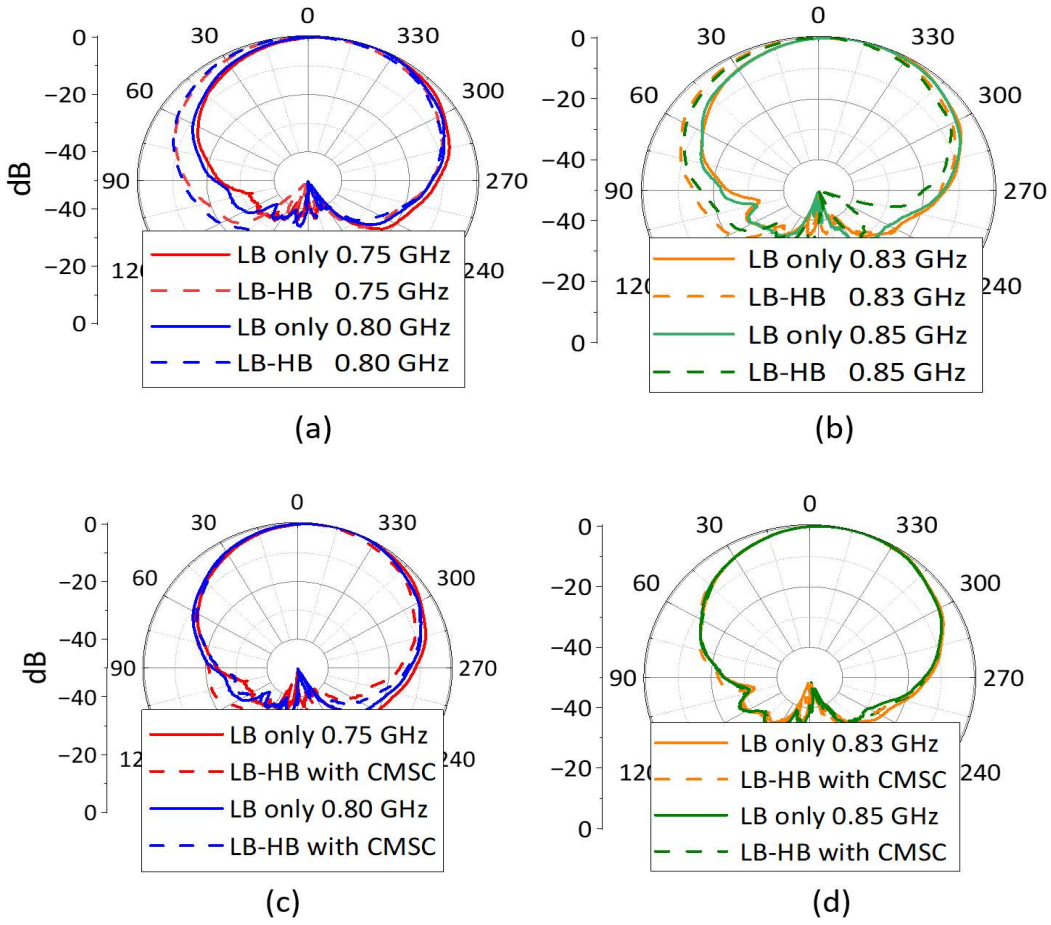

Figure 4.22 Comparison of LB azimuth co-pol pattern.

Table 4.4: Comparison of the proposed antenna with recent state of art works.

References	Mutual coupling suppression Techniques	Frequency Band (GHz)	Isolation (dB)	HPBW (Measured)
[88]	Passive dipoles + baffles	0.69- 0.96 1.7-2.7	27 22	72° ±2° 65°±5°
[45]	Frequency selective surface	0.69-0.96 3.5-4.9	<28 <25	60° 75°
[85]	Frequency selective surface	2.3-2.7 3.3-3.8	<25 23.5	44°-48° 66°-69°
[93]	Capacitance -loading technique/chokes	0.70-0.96 1.7-2.2	<20	75°+5° 64°+5°
[36]	Filtering antenna elements	1.71-1.88 1.9-2.17	<30	 65°±5°
[96]	Decoupling network	2.3-2.4 2.4-2.483	>25	60°± 5° 65°±5°
[1]	Metal baffles	0.77-0.98 1.65 -2.9	<23 17.5	64.5°- 57.1° 84.4° - 74.1°
[97]	Capacitance -loaded HB element	0.69-0.96 1.7-2.2	<20	75°+ 5° 64°+ 5°
Proposed Work	Common mode suppression circuit	0.69- 0.96 1.8-2.6	<30 <25	65°+ 5° 65°± 5°

4.4 Summary

The LB pattern distortions in multiband antennas occurs due to common mode resonance currents induced in HB antenna elements. This causes significant distortions in LB radiation patterns. This is very undesirable for the network performance as it leads to inter-cell interference in adjacent sectors due to coverage overlaps resulting in degradation of network quality. The common mode is suppressed by introducing a capacitor with a quarter wavelength short line at LB frequencies to the HB feed network. This suppresses the LB currents at resonance frequencies without significantly changing the HB current distribution at HB frequencies. As a result, CM resonance behaviour of the HB dipole is no longer visible resulting in cleaner patterns at low band frequencies. The 3dB beamwidth variation is 65°+5°. The HB patterns are not affected and the HB element impedance matching below 10dB can be obtained.

Chapter 5: Compactness in Multi-Band Antennas

Traditional base-station antennas have generally been dipole-type or patch-type antennas, and there hasn't been much study on how to build wideband multiband antenna's directivity while taking size constraints into account.

In recent years, the usage of mobile communication systems has grown in popularity, resulting in the establishment of a variety of commercial mobile services that operate on multiple frequency bands. As a result, multiband antennas have received more attention. These antennas must have the appropriate directivity across all frequency bands, implying a sector beam with a high front-to-back (F/B) ratio. However, in order to decrease expenses and wind pressure, base-station antennas must likewise be small in size. It is difficult to design multiband base-station antennas with the necessary directivity since the directivity is greatly dependent on the antenna's relative size to the wavelength.

Several approaches have been proposed in the past to obtain the requisite directivity in multiband/wideband antennas for base-station use including the stacked patch antenna, which has exhibited a half-power beamwidth at specified frequency bands, and the magnetoelectric dipole, which has proved a stable half-power beamwidth within a defined frequency range. However, at lower frequencies, the F/B ratio of these antennas degrades.

5.1 Compact ± 45 Dual Polarized Antennae for Triple Band Cellular Communication

5.1.1 Introduction

Due to its capacity to lessen multipath fading, dual-polarized antennas have attracted a lot of interest in modern communication systems. There has been a lot of dual-polarized antenna research. The IMT-2020 standard has been accepted by several nations for their 5G networks and services. A number of frequency bands,

including 3.4 GHz to 3.8 GHz in Europe and 3.3-3.6 GHz and 4.8-5.0 GHz in China, have been licenced for 5G. In several nations, the 5G band N78 (3.3-3.8 GHz) has been assigned. Broadband multiple-input multiple-output (MIMO) antennas with large impedance bandwidths have emerged as a feasible option to fulfil the demands of 5G. The dual-polarized printed dipole antenna with a 52% impedance bandwidth shown in [99] is one illustration.

A triple band antenna (TBA) covering 2160 MHz-2690 MHz (High Band 1), 3300 -3800 MHz (High Band 2), and 4800-5000 MHz (High Band 3), intended for base stations, is implemented in this part. It is demonstrated that by loading two dipoles with two pairs of circular slits, a TBA with the necessary half power beam width (HPBW) and front to back ratio at the frequency bands could be created. The addition of circular slits resulted in an acceptable beam width with a high F/B ratio throughout all three frequency bands. The intended TBA had an 8dBi gain over three frequency bands. Figure 5.1 depicts the suggested antenna prototype.

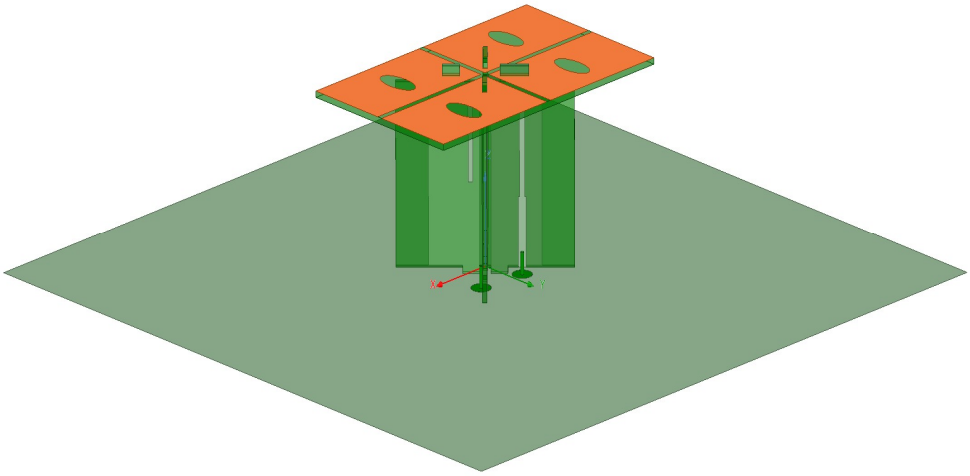

Figure 5.1 Prototype of proposed antenna.

5.1.2 Antenna Configurations & Matching Network

The proposed antenna aims to provide a low-cost and low-profile solution for wireless 5G cellular communication. The antenna design follows a step-by-step approach to achieve the desired characteristics. In the first step, an un-slotted printed dipole antenna with a ±45° cross-pair arrangement is designed. This

configuration allows for dual polarization, which is beneficial in mitigating multipath fading and improving signal quality. The ±45° arrangement ensures that the antenna can transmit and receive signals with both polarizations. In the subsequent steps, slots with diameter of wp are introduced, (as illustrated in figure 5.2), in the centre of each quadrant patch whose width and length are (Wd x Ld). These slots serve to further enhance the antenna's performance and optimize its characteristics. To increase the band of patch antennas typically adopted in base stations, a comprehensive literature in section 2.4.1 can be used as starting point. For instance, in [122] bandwidth is improved up to 40% by increasing dielectric thickness and by adopting different methods. The 5G research work is mostly for beam forming [123], MIMO antenna selections [124, 32], milli-meter wave bands [125, 126] and antenna designs for base station 5G applications [127–116]. The massive MIMO antennas with larger bandwidths have become a good solution to meet 5G demanding requirements. There are plenty of 5G antenna designs that have been proposed. The base station antennas must have stable radiation pattern with S11 smaller than - 10 dB, high port isolation, front to back ratio (FBR) smaller than - 25 dB, XPD level less than - 20 dB for $\theta = 0°$ and - 10 dB for less than 60°. A printed dipole antenna with dual-polarization and impedance bandwidth over 52% is proposed in [128]. In [129], the impedance bandwidth is observed 51% with S11//-15 dB. The broadband antennas are proposed for 2G, 3G and 4G base stations in [1, 23,32].

As we know that the slots are always introduced on the patch for bandwidth enhancement and multi-band feature. It can be seen in Figure 5.6(a) that the simple patch configuration gives a single band with reference to both 10 dB reference line in the return loss. From the detailed literature review it can be deduced that the addition of inductance may increase the bandwidth and resonance. For instance, in [113] an E-shaped patch configuration has been realized for band enhancement. Similarly, 4 chamfering quadrants (half circle slots) are added with fan-shaped etching slots in [19] for band enhancement. The addition of slotted E-shaped and fan-shaped etching slots (similar to our quarter-circles) change resonant feature with the additional inductance introduced. During the flow of current to the antenna

patch, it has to flow around the slots that increase the length of current path. So, this becomes the source of additional inductance for the antenna patch. The same topology is adopted by the authors in the proposed antenna configuration. In the end, we reached the desired 2.1-2.6 GHz, 3.3-3.8 GHz, and 4.8-5 GHz working bands. To reach this goal, once each single antenna element has been studied, numerical simulations and optimizations of the proposed antenna have been performed in Ansoft HFSS. Authors got the idea of a radiator and balun structure from the following reference [19,116] and performed numerical analysis and optimization on ANSYS HFSS 18.2 with random structural change of all parameters to get better gain, bands, isolation, XPD and HPBW. Furthermore, the radiator has been redesigned to get better results than [19]. The micro strip patch dimensions were calculated with the formulae from [121].

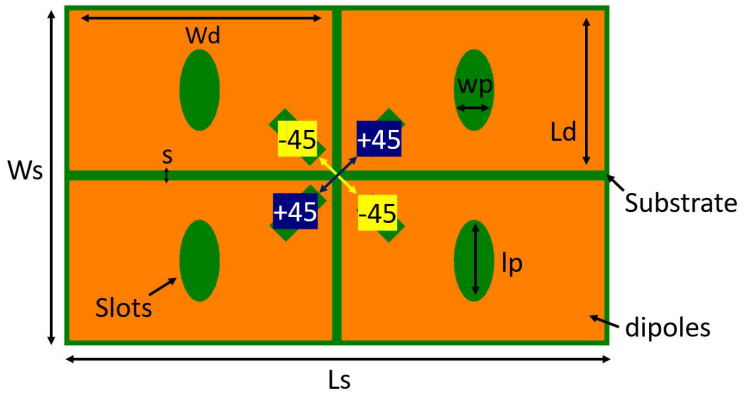

Figure 5.2 Prototype of proposed antenna.

Throughout the electromagnetic analysis, radiation patterns and reflection coefficients are carefully observed at each stage of the antenna design process. This analysis helps in assessing the antenna's performance and determining the optimal structure. By noting the radiation patterns and reflection coefficients, the designers can fine-tune the antenna's geometry and dimensions to achieve the desired triple-band operation and ±45° dual polarization. The goal of this proposed design is to create a cost-effective and compact antenna solution capable of operating in multiple frequency bands, suitable for 5G applications. The step-by-step approach and iterative analysis allow for the optimization of the antenna's performance

parameters to meet the requirements of the intended wireless communication system.

The antenna configuration, Figure 5.2, depicts the antenna setup. It is made up of various parts, including a primary radiator, two baluns (balun 1 and balun 2) that serve as feeding structures, and a reflector. The radiator is printed on top of a second RT-3880 substrate that is 0.7 mm thick. Both baluns are built on a FR4 substrate that is 0.8 mm thick and has a dielectric constant of 4.4 and a loss tangent of 0.02. They're positioned between the radiator and the reflector. The primary radiator is produced on a 32x37 mm substrate. It is split into four equal sections by two 1-mm-thick centreline slots, with each component representing one dipole arm. Each dipole arm has a surface area of 15.5x18.5 mm. The two pairs of dipole arms are parallel to the diagonals corresponding to two orthogonal dipoles, linearly polarized at ±45°, respectively.

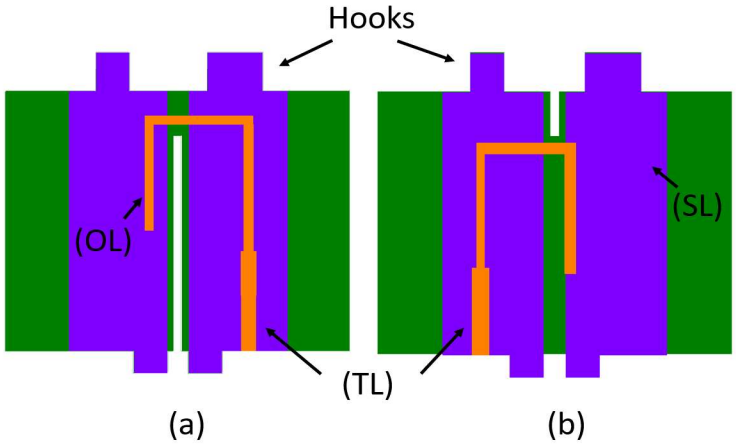

Figure 5.3 Prototype of proposed antenna.

Each dipole arm is meticulously designed to accomplish the necessary triple-band functioning. There are two major components to the tuning process. To begin, each dipole arm has an oval-shaped slit in the centre. This slot, seen in the centre, allows for the insertion of an inductive effect, resulting in the generation of a second resonant mode. Rectangular microstrip antennas, as well as slotted variations, have evolved from standard rectangular patches and display increased performance by modulating the parallel slots to create extra resonances.

Table 5.1: Optimized parameters of the proposed antenna.

Parameters	Values (mm)	Description
W-SL	6.36	Width of SL
L-SL	23.5	Length of SL
wd	15.5	Width of patch
Ld	25.5	Length of patch
Ws	32	Width of substrate
Ls	52	Length of substrate
s	1	Gap
wp	2	Diameter of slot
W-TL	0.6	Width of TL
L-TL	12.3	Length of TL
W-OL	0.5	Width of OL
L-OL	10.4	Length of OL

Once the structure of each arm of the dipoles and the cross-polarized dipoles has been identified, the antenna's feeding network is discussed. Figure 5.3 depicts the feeding network, which consists of two baluns that comply with multiple tasks. Two Γ -shaped transmission lines printed on FR4 substrates are used to implement the baluns. These transmission lines are specially designed to be joined in a cross 45° configuration, as seen in Figure 5.4. The transmission wires' centre grooves aid in alignment and establishing a connection.

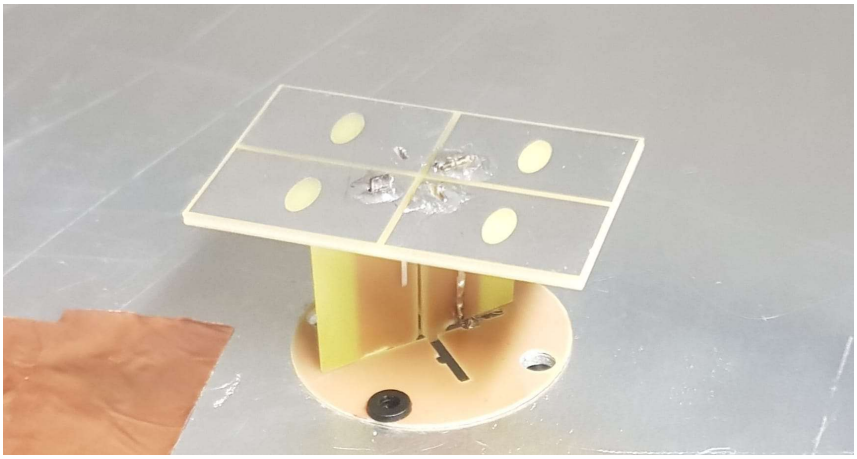

Figure 5.4 Prototype of proposed antenna.

Furthermore, as seen in Figure 5.3, the baluns have upper and lower bumps. These bumps provide structural as well as electromagnetic functions. They're made to fit into particular grooves on the radiator element and the reflector. After the soldering procedure, this configuration assures structural stiffness and offers an electrical connection between the components. Moreover, the size of the baluns is set to maintain a specific distance between the radiator and reflector, which, in the suggested design is optimised to be 23.8 mm. This spacing optimisation aids in optimising the radiation parameters of the antenna, such as radiation pattern and efficiency. Figure 5.5 shows a constructed prospective view of the radiator and baluns, as well as the supporting base board.

5.1.3 Experimental Results

The suggested antenna element was optimised and numerically simulated using ANSYS 18.2 HFSS. To accomplish the specified performance and frequency ranges, the antenna was designed in many phases. The proposed antenna's reflection coefficient and directivity were examined to ensure its performance. For ideal antenna characteristics, the diameters of the two pairs of slots and reflectors were optimised. The final dimensions were given in Table 5.1. Figure 5.6 depicts the proposed antenna's reflection coefficient. When the two pairs of slots are not loaded, the antenna's bandwidth gets somewhat narrower. Even with the slots, the antenna's reflection coefficient remains less than 10 dB throughout the three frequency bands. This implies that the antenna maintains a broadband impedance-matching performance.

However, the disparity between simulated and measured results in the third band (HB3) underscores the impact of environmental factors, size variations, and soldering techniques, necessitating the identification of crucial solutions to rectify this discrepancy. Environmental factors and fluctuations in dimensions and soldering methods have been identified as key contributors to this inconsistency. Nevertheless, precise soldering practices offer a potential avenue to mitigate these challenges and augment overall performance.

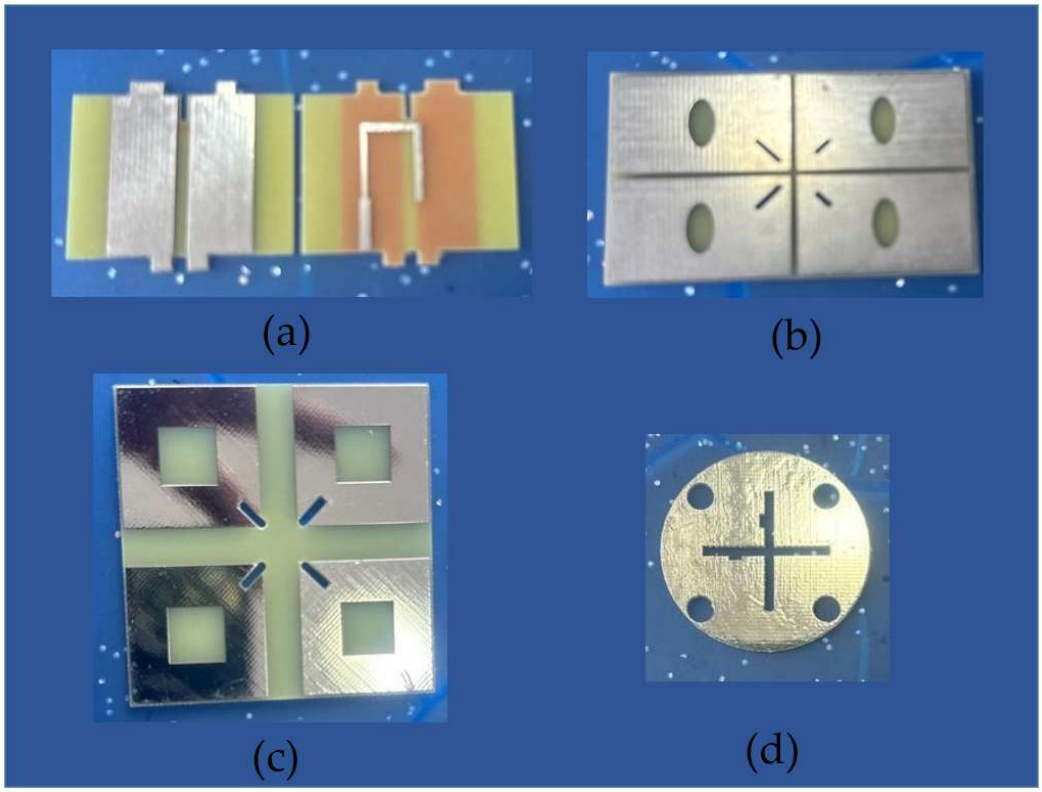

Figure 5.5 Perspective view of the antenna balun 1(a, b) front and back view (c) Radiator for proposed antenna (d) base board for holding balun.

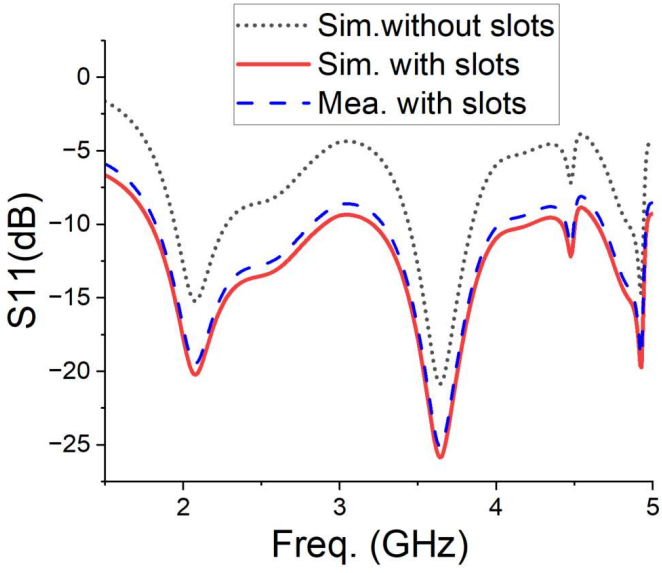

(a)

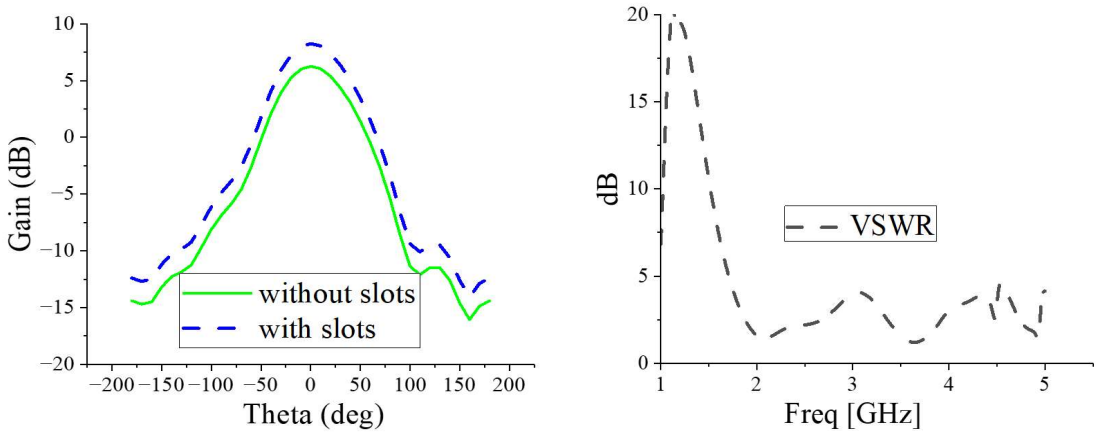

(b) (c)

Figure 5.6 Measures results of proposed antenna (a) Reflection coefficient (b) gain (c) VSWR.

The radiation patterns of the suggested antenna were simulated and measured at the design frequency of 3.6 GHz, and the results are presented in Figure 5.7. The simulated and observed normalised radiation patterns accord and are consistent. Due to geometric symmetry, the radiation pattern for the -45° polarisation is not displayed because it is comparable to that of the +45° polarisation.

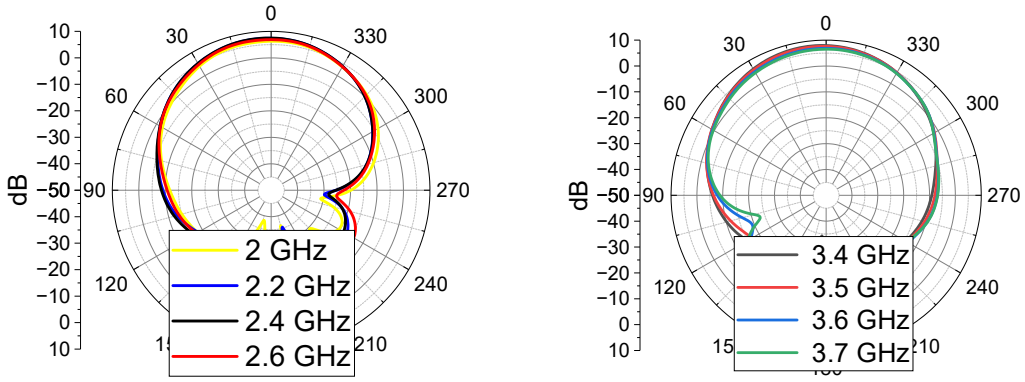

Figure 5.7 Radiation pattern of proposed antenna.

5.1.4 Summary

To demonstrate its performance, the suggested dual-polarized triple band antenna with a 45° cross pair dipole structure was built and measured. A vector network analyser was used to conduct the experiments in an anechoic room. The observed

antenna characteristics are shown in Figure 5.6, which displays the S-parameter reflection coefficients, isolation of the two ports, and VSWR. The antenna obtained a -10dB reflection coefficient with bandwidths of 2160 MHz-2690 MHz (High Band 1), 3300 -3800 MHz (High Band 2), and 4800-5000 MHz (High Band 3). These bandwidths correspond to the desired triple band operation for sub-6 GHz. Figure 5.7 depicts the directivity of the proposed antenna for frequencies of 2 GHz, 2.6 GHz, and 3.4-3.7 GHz. The directivity represents the ability of the antenna to concentrate radiation in a specific direction. The graph in Figure 5.7 illustrates how the directivity varies with frequency, providing an insight into the antenna's radiation characteristics. The antenna gain has been calculated to be 8.12 0.4 dBi, which is consistent with the simulated gain. The minor difference is due to variables such as coaxial cables and insertion loss. The half-power beam width (HPBW) of the antenna is measured to be 70° ± 3° over the entire bandwidth, indicating a wide coverage angle.

Overall, the reflection coefficient of the antenna remains low over the frequency bands of interest, indicating good impedance matching, while the directivity provides information about the antenna's radiation concentration at different frequencies.

5.2 Array Design of Multi-Band Compact +45 Dipole Antenna

The deployment of 5G networks is indeed expanding worldwide, and the sub-6 GHz frequency bands, including the 3.3-3.8 GHz band (known as N78), are an essential part of the 5G spectrum. Many countries have already assigned this frequency band for 5G use. Base station antennas operating in the sub-6 GHz bands are critical for 5G networks because they enable signal transmission and reception at these frequencies. These antennas are intended to meet the specific requirements of 5G technology, which include greater data speeds, lower latency, and improved capacity above previous generations of wireless networks. 5G networks can provide larger coverage and improved penetration through barriers such as

buildings by using the sub-6 GHz band. This is particularly important for delivering reliable and high-speed connectivity in urban areas where buildings and structures can impede signal propagation. Overall, base station antennas operating in the sub-6 GHz bands are a vital component of 5G infrastructure, enabling the deployment and expansion of 5G networks around the world.

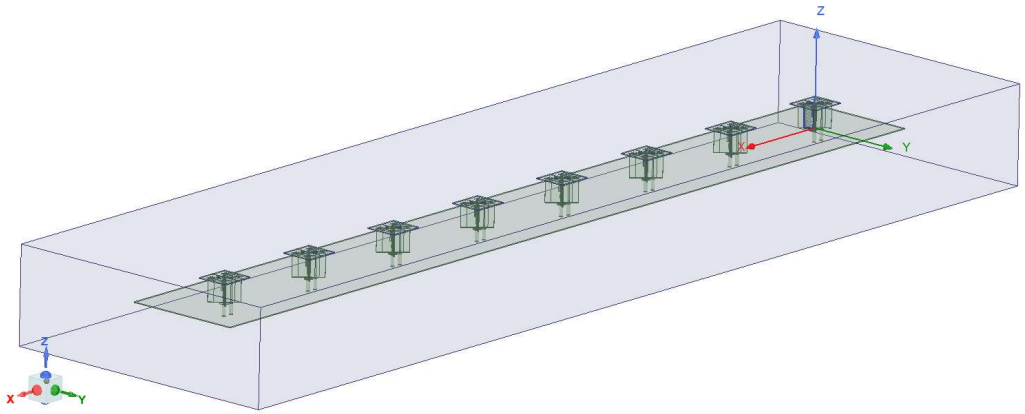

Figure 5.8 Triple band antenna proposed array.

This work describes the design of a small, low-cost, low-profile triple-band 45° dual-polarized 1x8 dipole antenna array shown in Figure 5.8 for 5G base station applications. This antenna array is an expansion of a single antenna unit originally created for sub-6 GHz cellular applications in section 5.1, and it provides better performance and coverage for 5G frequency bands. The antenna array has an impedance bandwidth of, 3.3-3.85 GHz, and 4.7-5 GHz, with return loss values less than -15 dB. These bandwidths align with the frequency ranges commonly used for 5G communication.

5.2.1 Array Design

A multi-band compact antenna technology is used to design the antenna array. With the help of this technology, various frequency bands may be combined into one small design, making better use of the available space and costing less money. The antenna array is flexible and adaptable for a variety of communication scenarios

thanks to the +45° dual-polarized arrangement, which ensures that the antenna array can broadcast and receive signals with both polarisations.

To achieve the required performance, the array design requires the positioning of many antenna components in a certain arrangement. Techniques for electromagnetic (EM) analysis are used to model and improve the radiation properties of the antenna array, including gain, impedance matching, and pattern diversity. The design and analytical findings demonstrate that the suggested antenna array satisfies the criteria for 5G applications. A high degree of performance and compatibility for 5G communication in the designated frequency bands are shown by the achieved gain and impedance bandwidths.

By leveraging the multi-band compact antenna technology, this antenna array provides an efficient and cost-effective solution for 5G deployments. Its low-profile design allows for easy integration into various base station setups, while the triple-band coverage ensures compatibility with different 5G frequency allocations.

5.2.2 Realization of Array

The layout and dimensions of the single antenna element shown in Figure 5.2 are followed in the design of the 1x8 antenna array for 5G base station applications. The radiator and balun configurations of each antenna element in the array are identical to those of the single element. The total reflector size of the array is 130 × 960 × 0.7 mm^3, with a ground patch located at the bottom. The inter-element spacing between adjacent antenna elements is λ, which is determined by the desired operational frequency and the wavelength associated with it. When elements are spaced at a distance of one wavelength or greater, it helps to minimize mutual coupling effects between adjacent elements, which can lead to improved radiation patterns and reduced sidelobe levels. Often, high directivity of planar array is accomplished by inserting more elements within a fixed size. The total size of the array includes number of elements and spacing. For planar array, when the inter element spacing (d) is equal or greater than half of the wavelength (λ/2), multiple side lobes other than the main lobe will be formed. Furthermore, HPBW is

compromised with the increment of element spacings, [130]. For the purpose, 0.25 λ, 0.50 λ, 0. λ and 1 λ inter-element spacing were simulated to get an optimum result of gain, HPBW and impedance bandwidths.

Therefore, while a space separation of one wavelength may offer advantages in terms of minimizing mutual coupling, it is essential for the designer to carefully consider the trade-offs between array size, element spacing, and sidelobe levels.

At each antenna reflector, the cross-coupled dipoles are shorted with the ground through baluns. This arrangement ensures proper functioning and impedance matching of the antenna elements shown in Figure 5.9.

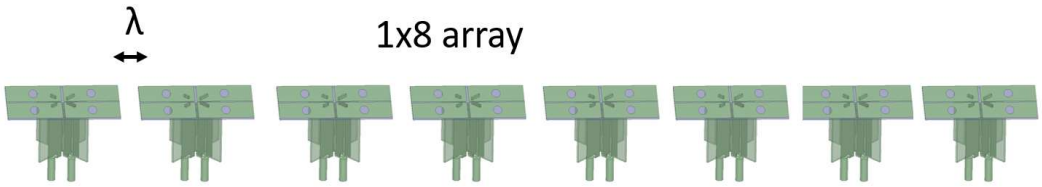

Figure 5.9 1x8 antenna array prototype.

To facilitate measurements and testing of the proposed antenna array, a single signal source can be used to excite the array. This is achieved using a Wilkinson power divider. The Wilkinson power divider is a specific type of power divider that is widely used in RF and microwave applications. It provides good isolation between the output ports and maintains well-matched impedance conditions. By utilizing the Wilkinson power divider, the single signal source can be split into multiple equal-power signals, which are then fed into each port of the antenna array. This allows for simultaneous excitation of all the antenna elements in the array, ensuring consistent and synchronized operation. The Wilkinson power divider achieves good isolation among the output ports, which means that the signals fed into each antenna element remain independent and do not interfere with each other. This is crucial for accurate measurements and testing, as it helps isolate

the performance characteristics of each individual antenna element and ensures reliable data acquisition.

5.2.3 Results and Discussion

Each antenna element in the array is made to have both of its +45degree polarised dipoles linked via a shorted ground to the outer conductor of a coaxial cable. Each balun has a microstrip feed line that is attached to the coaxial cable's inner conductor and is formed like a Γ (Gamma). This arrangement enables each antenna element's +45° dual-polarized radiation pattern. There are sixteen ports in the proposed antenna array, and each antenna element has two coaxial wires flowing out of it, as shown in Figure 5.9. Overall, this design approach ensures that the 1×8 antenna array maintains the desired ±45° dual-polarized radiation pattern for 5G applications. The symmetric arrangement and inter-element spacing contribute to the optimal performance of the array, providing efficient coverage and connectivity for the intended 5G communication purposes.

Figure 5.10 (a) illustrated the proposed antenna covers n78 (3.42-3.5 GHz). Additionally, it covers two full (3.5-3.6 GHz and 4.8-4.9 GHz) and one partial frequency. The band moved to a higher frequency, as a result of the array, but it still covers three relevant bands of interest. Figure 5.10(b) displays the proposed antenna array's simulated gain curve. The antenna array is seen to have a constant gain of 16.65+ 0.4 dBi across all of the suggested frequencies. Figure 5.11 shows the co-polarized radiation patterns in the H-plane at 3.4 GHz, 3.5 GHz, 3.6 GHz, and 4.8 GHz throughout the proposed bands. The HPBW for the whole band is 69 +5◦.

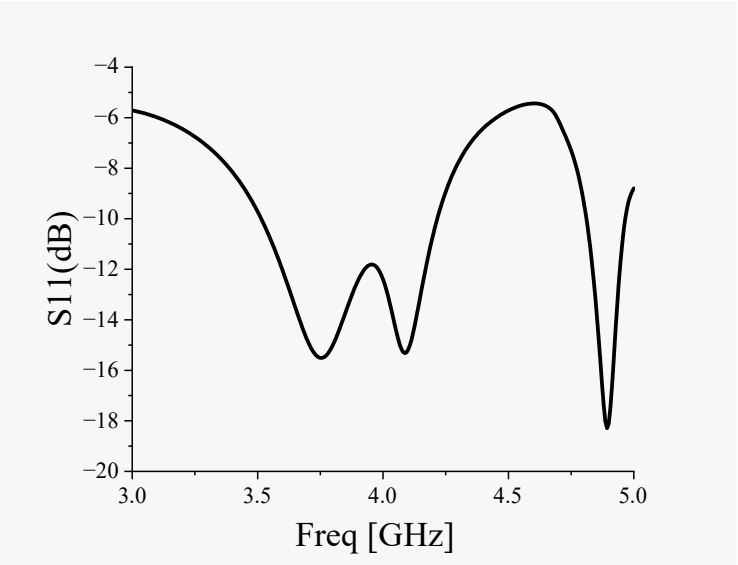

(a)

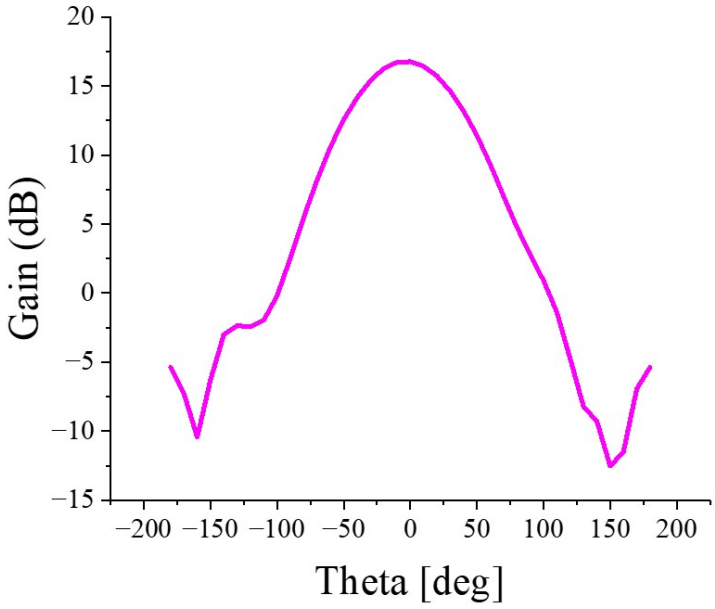

(b)

Figure 5.10 Sim. results of proposed antenna array (a) return loss, (b) gain.

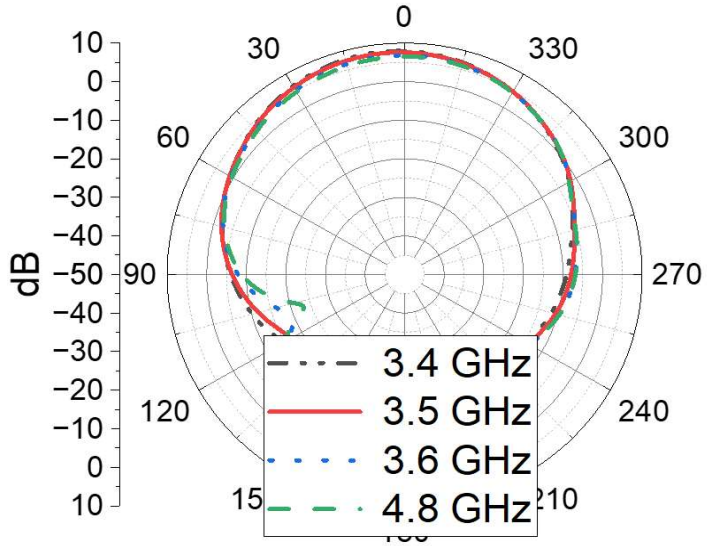

Figure 5.11 Radiation pattern of proposed antenna.

Table 5.2: Comparison of the proposed antenna with recent state of art works.

Reference	Frequency/Band (GHz)	XPD (dB)	Isolation (dB)	FBR (dB	Height (mm)
[117]	3.65–3.81	< - 23	< - 31	< - 15	3
[118]	3.3–3.6	< - 24.5	< - 28.8	< - 29	18.8
[119]	3.45–3.55	–	< - 15	–	1.5
[120]	3.3–3.8	< - 22	< - 25	–	12.2
[29]	3.14–3.8	< - 30	< - 43	–	11.8
[33]	3.2–3.9	< - 28	< - 40	< - 31	14
This work	3.43–3.75, 4.13–4.30, 4.80–4.95	<- 35	<- 47	<- 37	24.3

5.3 Compact Multi-Band Triangular Patch Antenna for 5G WLAN Applications

This work proposed a compact antenna of size 23.7mm x 25.2 mm. The comparison of two triangular split ring resonators (TSRR) with altering characteristics of

defected ground structures (DGS) and nature inspired TSRR has also been performed. A coplanar waveguide (CPW) feed mechanism is implemented to achieve the desired impedance matching for both designs in a step by step process. The nature inspired antenna has an ultrawide bandwidth from 1.6 GHz to 7.5 GHz as compared to a simple triangular antenna with a bandwidth of 1.6GHz-2.8 GHz. The proposed antenna covers most of the 3G, 4G, WLAN and future expected 5G band (S&C band). Both these low-profile antennas are suitable for Internet of Things (IoT), smart homes and radio frequency (RF) energy harvesting applications. The gain of the nature inspired antenna and simple DGS antenna is 5.3 dB and 3.9 dB respectively.

5.3.1 Introduction

This is an age of internet and with enhanced hunger of data, everyone is looking for fast and reliable data sources. Advantages of mobility and cost savings has given wireless LANs some noteworthy benefits over traditional LANs. An access point (AP) is being used to act as a bridge between wireless and wired media [99]. The wired network is connected to AP which is further equipped with an antenna to provide wireless connectivity to nearby devices. In order to get a good signal strength for end users in a network, directivity and gain of the antenna have become crucial design quantities [100]. WLAN communication is mostly carried out in two bands, which are 2.4 GHz and 5 GHz. To achieve effective communication in these bands, planar monopole patch antennas have become a good option due to their compact and simple structure, ease of fabrication and wide impedance bandwidth [101,102]. For indoor applications like trains, shopping malls and hospitals, the omni-directional radiation pattern of monopole antennas make them more suitable. In the recent era, researchers have developed different techniques like electromagnetic band-gap structure [103], artificial magnetic conductor [104] and split ring resonators [105] to improve performance of planar monopole patch antennas.

Split ring resonators are supposed to give desired susceptibility or magnetic response in order to achieve a strong magnetic coupling for an applied

electromagnetic field [106]. Split-ring structures were initially used as fundamental blocks for metamaterials due to parameter dependent permeability of the structures [107]. Later, these elements become famous in different filter applications [108,109]. Recently, a loaded split-ring antenna was introduced for a dual-band WLAN configuration [110]. In this work we will introduce a novel monopole triangular split ring antenna which will be used in WLAN applications. In this letter we have implemented the concepts of defected ground structures (DGS) and a split ring resonator (SRR) to better achieve the desired characteristics of wideband, and an omnidirectional like radiation pattern with acceptable gain parameters. Antenna impedance is perfectly matched to 50 Ω. In the second section of this work design analysis is discussed in detail. Afterwards, results are analyzed and compared for two novel designs. Return loss, current distributions, input impedance, radiation pattern and antenna gain are discussed with their respective pros and cons.

5.3.2 Design Analysis and Results

In this design, the basic building block of the split ring resonator has been implemented to achieve negative permittivity/permeability properties. Electromagnetic properties of the antenna have been optimized to attain the miniaturized size and wide bandwidth at 2.45 GHz band. Initially a simple design is implemented and then the tree-like structure is added to further enhance the antenna bandwidth with effective impedance matching. The complementary split ring resonator implemented in [77] exhibits wideband for the Wi-Fi/WiMAX frequency band, and the compact design implemented in [78] performed well for overall radiation characteristics. Several radiators have been proposed in the literature covering Wi-Fi band and some covering multiband without using complementary split ring resonators (CSRR) [79, 80], however these antennas require a large area for implementation which is a huge limitation in specific scenarios. The antenna structure is based on the RLC design combination. The capacitance of the triangular split ring resonator is calculated from the following expression.

$$C = \varepsilon_o \varepsilon_r \frac{A}{d} (F) \tag{5.1}$$

Here, "ε_0" is free space permittivity, "ε_r" is relative permittivity," ***A***" is cross-sectional area between triangular loop and tree shape element and "***d***" is the gap length. The inductance of this antenna is calculated from equation (2) below,

$$L \approx \frac{3l\mu_o\mu_r}{2\pi}\left[\ln\left(\frac{1}{\rho}\right) - 1.4056\right](H) \tag{5.2}$$

In the above equation, "l" is the length of one side of the structure and "*p*" is the radius of the loop. The design is tuned using the above equations and resonant frequencies are calculated using equation (3).

$$f_r = \frac{1}{2\pi\sqrt{LC}} \tag{5.3}$$

Fringing field effects are considered when tuning the final design as EM waves tend to travel outside the substrate dimensions in a porous fashion around the edges. The geometry of both simulated designs is shown in the Figure 5.12 (a), (b).

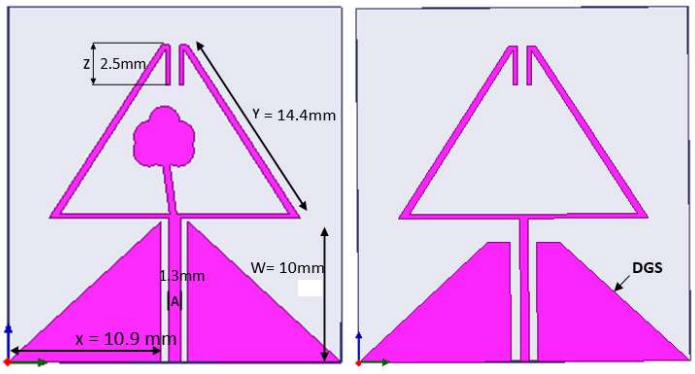

(a) (b)

Figure 5.12: (a): Natured inspired triangular split ring antenna, (b): Simple triangular DGS antenna.

The optimized values of major design parameters are “W= 10 mm”, “X=10.9 mm”,” Y=14.4 mm”, “Z=2.5 mm” and feed width “A” is 1.3 mm. The substrate has compact dimensions of 25.2 mm x 23.7 mm. Ground structures have been modified to a trapezoidal shape from conventional rectangular shapes. The reflection coefficient for both the triangle-based design and nature-inspired design is compared in Figure 5.13. The triangle-based design has a bandwidth from 1.6 GHz to 2.8 GHz which fulfills the general requirement for 2.45 GHz WLAN band and design included with tree shape which has an even super wide bandwidth from 1.6 GHz to 7.5 GHz below the threshold value of -3dB. The lateral design exhibits dual-band characteristics and the second resonance band is measured at 4.5 GHz which is useful for multiband operation of rectenna. During the design process, it is noted that the length of the upper patch has a significant effect on the resonance frequency as does the increase in size of triangle length, resonance frequency decreases and vice versa. The maximum reflection coefficient for the tree-based antenna is calculated to be -39.2 dB at 2.45 GHz, clearly visible in the following plot.

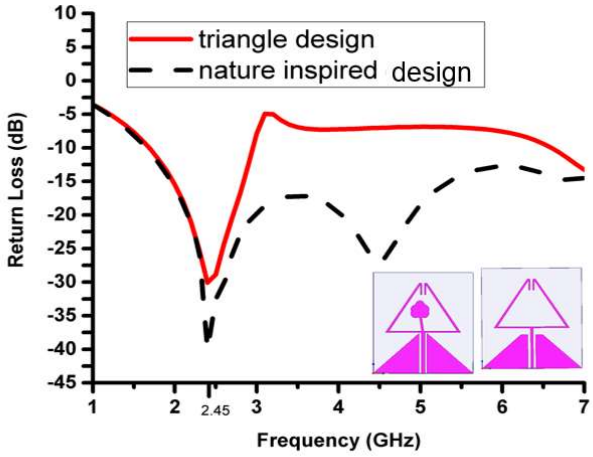

Figure 5.13: Reflection coefficient comparison of nature-inspired antenna and simple DGS design

To gauge the overall performance of both simulated antennas, surface current densities have been plotted in Figure 5.14. Maximum 9.0154 A/m^2 is calculated in case of the nature-inspired antenna and 8.8087 A/m^2 for the simple triangle

antenna. In the simple design more current is incident at the feed line and at the bottom of the radiating patch while, in the nature-inspired antenna, the maximum current density is shifted to the top left strip of the triangle due to the presence of the tree-shaped element. Stable radiation patterns for both designs is observed due to the capacitive and inductive balance created by triangle topology.

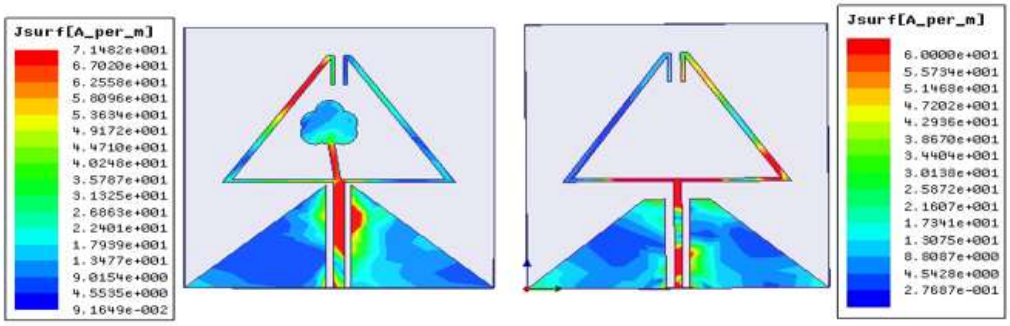

Figure 5.14: Surface current density of nature-inspired design and simple triangular DGS antenna.

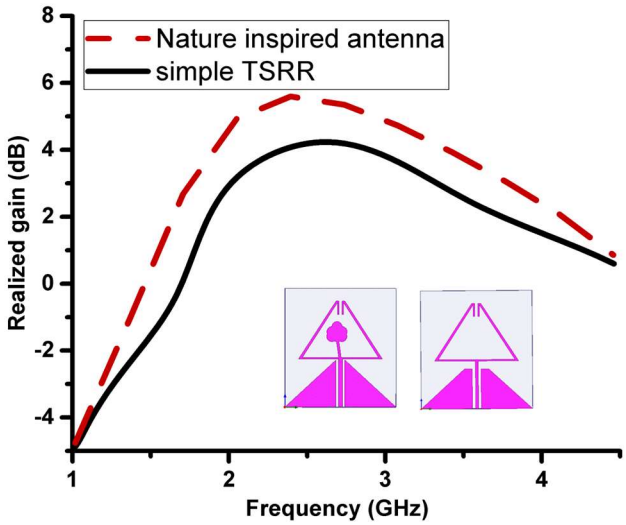

Figure 5.15: Antenna gain comparison of both novel triangular designs.

The simulated gain for the nature-inspired antenna is better than the simple triangle antenna as shown in Figure 5.16. Gain values are calculated to be 5.3 dB and 3.9 dB for tree-shaped and simple designs respectively. For WLAN applications it is desirable to have a high gain antenna but at the same time, some negative gain antennas are also useful in certain scenarios. For example, most mobile phone

antennas operate at negative gain due to compact dimensions and presence of cross interference from the metal surfaces in the confined area. Gain is related to the directivity of the antenna and at which angle we measure the gain of the specific device. The gain of any radiator may be different at different angles. But for antennas with an omnidirectional radiation pattern, gain does not change drastically. Radiation efficiency of the antenna at certain resonance frequencies may be different with respect to other frequency bands, therefore, overall radiation efficiency also plays an important part in the evaluation of gain at designated frequencies. In conclusion, both designs have good RF performance characteristics that are suitable for RF energy scavenging.

5.3.3 Summary

A novel ultrawideband TSRR antenna is designed and analysed having compact size, broad impedance bandwidth and constant gain. Extensive investigations have been carried out to attain optimum characteristics of wide bandwidth using defected ground structure (DGS) and split ring resonator (SRR) techniques. Nature inspired antenna shows promising results for second band at 4.5 GHz which can easily be tuned for future expected 5G applications. Maximum 9.0154 A/m2is achieved for the proposed design with the incursion of tree like structure in the antenna which better conserves the electromagnetic waves when compared to simple TSRR. All these features make a proposed antenna a potential candidate for emerging UWB and IoT/cellular applications.

Chapter 6: Millimetre Wave Antennas

6.1 Introduction

The word mmWave alludes to a region of the electromagnetic spectrum with a relatively small wavelength, roughly around 20 GHz, as well as 100 GHz. Because this spectrum portion is underutilized, mmWave control over information significantly enhances the bandwidth accessible to communications networks. For transmitting data to a large number of recipients, an access point antenna is employed. This sort of antenna acts as a hub for wireless access networking and may absorb and broadcast signals. It connects with the many nodes while also receiving signals from a large number of people. Several types of MmW antennas have been used in the base stations such as: -

- Multiband
- Omnidirectional
- Beamforming
- Sector
- Small cell
- Stadium
- TRi-sector

There are three different kinds of antennas - omnidirectional, semi-directional, and directional for 5G mmWave. This is a technological innovation that repositions millimetre wavelength as a solution for providing wide-area 5G connectivity. This breakthrough increases mmWave penetration from a few hundred meters to approximately 7 kilobits thereby lowering the expense of fixed wireless modem services in metropolitan & rural locations. 5G mmWave is now available in certain cell phones and gadgets powered by Qualcomm's Snapdragons Mobile Application, thanks to breakthroughs in wireless & antenna technology. It offers

the fastest 5G bandwidth available, up to and including faster than household fibre - as well as extraordinary bandwidth and super-low latency.

6.1.1 Importance of mmW Antenna for 5G Technologies

Wearable gadgets are becoming a more appealing option for a variety of uses that range from the battlefield to health to consumer technology. They will indeed play an important part in the next penultimate networks, which have been predicted to function at greater bandwidths and with fewer outages in smaller cellular antennas and Pico cells encompassing larger regions, than penultimate (4G) or earlier capabilities. Moreover, beam transfer function and spatial multiplexing are projected to improve spectrum & energy efficiency at the smartphone and access point levels. The additional characteristics and capacity envisaged for 5G Mobile communications would significantly revolutionize operations in mobility, healthcare, and education, building automation as well as wireless robotics, among a number of other fields, by surpassing the constraints of present 4G technologies. This accomplishment sparked a slew of ground-breaking smartphone designs as well as the announcement of novel mobile hotspots, creating the macrocycle of cellular advancements and developments in mobile sensing technologies. These ever-increasing needs, propelled by explosive growth in mobile internet consumption throughout the world, have coincided with important technological achievements by the antennae creative community.

6.2 mmW Antennas for Base Station

5G ranges from 24.25 GHz to 29.5 GHz, whereas the upper band ranges from 37 GHz to 40 GHz. For all communication to be effective, the realized gain stays steady between 5 and 6 dBi. In all wavelength ranges examined, the separation among ports and bridge discriminate remains superior above 20 dB. In combination with superfast speeds and enormous capacity, 5G digital cellular technologies provide capabilities such as accommodating many simultaneous users and ultra-low latencies. With the rise of teleworking and online education, 5G is gaining

traction as the infrastructural development of the future demands for high-speed, consistent connections. Multi-antennas with several antenna components are crucial in tiny cell core networks for 5G mobile connectivity.

6.2.1 Deployment of mmW Base Station Antenna

The need for mmWave base station antennas arises from the specific frequency range, shorter range/high path loss characteristics, the potential for high data rates and capacity, beamforming requirements, and the deployment of small cells to cater to densely populated areas. These antennas play a crucial role in enabling the deployment of mmWave wireless communication systems and realizing the benefits of this technology [111].

The deployment of millimetre-wave (mm Wave) base station antennas is essential for the implementation of mmWave wireless communication systems. mmWave technology operates at higher frequency bands and offers the potential for significantly increased data rates and capacity when compared to lower frequency bands used in traditional cellular networks. Here are some key factors regarding the need for mmWave base station antennas. In Figure 6.1 Demand and access of mmW base station are listed.

A. Small Cell Deployment

Since mmWave signals have a limited range, they are often installed as tiny cells in heavily populated regions. In areas with high demand, such as cities, stadiums, and event sites, these tiny cells assist improve coverage and capacity.

B. Beamforming and Antenna Arrays

Beamforming methods are often used at mmWave frequency due to the significant path loss and probable signal obstruction. Beamforming enhances signal strength and coverage by allowing the antenna to direct the broadcast signal towards the targeted user or location. Phased array antenna systems, which combine several

antenna components to form and steer beams in various directions, are frequently used in mmWave base station antennas.

C. Higher Data Rates and Capacity

mmWave technology offers the potential for extremely high data rates and increased capacity due to the availability of wider bandwidths. To fully leverage these advantages, mmWave base station antennas are designed to handle high-speed data transmission and support multiple simultaneous connections.

D. Range

Although particular frequency bands may vary depending on the location and regulatory authorities, mmWave frequencies are commonly assigned in the range of 24 GHz to 100 GHz. Dedicated mmWave base station antennas are needed to send and receive communications at these frequencies.

E. Shorter Range and High Path Loss

mmWave signals have shorter wavelengths, which result in higher path loss when compared to lower frequency signals. This means that mmWave signals can cover shorter distances before experiencing significant attenuation. To compensate for the shorter range, mmWave base station antennas need to be deployed in closer proximity to provide adequate coverage and capacity.

Figure 6.1 List of demand & access of mmW base station.

6.2.2 Challenges in mmW Base Station Antenna Design

There are various difficulties in designing base station mmWave antennas for wireless communication systems. Advanced antenna design methods, signal processing algorithms, and system-level optimisations are needed to address these issues. To allow the wide-scale deployment of mmWave base station antennas in 5G and beyond, ongoing research and development activities are concentrated on removing these barriers.

Path loss and Signal Blockage: Compared to signals at lower frequencies, mmWave transmissions have increased path loss due to their shorter wavelengths. In addition, objects like trees, buildings, and even people might interfere with mmWave communications. An important factor to consider when designing mmWave base station antennas is how to get around these obstacles while still offering enough coverage and signal strength.

Narrow Beamwidth: As mmWave antennas operate at shorter wavelengths, their beamwidths are often restricted. The base station and user equipment must be precisely aligned for this to be beneficial for focused signal transmission and reception. Signal quality might be lowered by any misalignment. A problem in

mmWave antenna design is achieving perfect beam alignment and keeping it when users move within the service region.

Antenna Size and Form Factor: Due to their shorter wavelengths, mmWave antennas are often smaller in size. It can however be difficult to create small antennas with enough gain and performance. Base station antenna's form factor and aesthetics must also be carefully considered to guarantee a seamless connection with the infrastructure and surroundings.

Interference and Co-Channel Contention: Neighbouring cells may cause interference and co-channel congestion for mmWave base stations operating in heavily populated regions. The network's functionality and capacity may be impacted by this interference. Beamforming, interference cancellation, and spatial filtering are a few approaches that should be considered while designing antennas that address these issues and maintain effective coexistence with nearby cells.

Thermal Management: Antennas for mmWave base stations can produce a lot of heat, especially in high-power applications. To preserve antenna performance and avoid overheating, proper thermal management is essential. The antenna design must contain effective heat dissipation methods, such as cutting-edge materials and cooling systems.

Cost and design Manufacturing Complexity: mmWave antenna design and production might be more expensive and complex than it is for lower frequency antennas. Costs increase due to the use of more expensive materials, precise production techniques, and sophisticated beamforming systems. A problem in mmWave antenna design is striking a balance between performance, affordability, and manufacturability.

6.3 A Millimetre Printed Wideband Slotted Antenna for 5G Broadcast Applications

mmWave antennas are of paramount importance in 5G broadcast applications due to their ability to support high data rates, increased capacity, short-range coverage, directionality, and the availability of spectrum. These antennas enable efficient and reliable delivery of broadcast content to users, enhancing the overall multimedia experience in 5G networks. To ensure effective wireless broadband communication, it is generally desirable to use a broader bandwidth that encompasses the relevant frequencies of interest. This allows for efficient power amplification and reduces the impact of channel loss. However, the specific bandwidth requirements depend on various factors, including the application, regulatory constraints, and available frequency resources.

The purpose of this work is to combine the properties of two types of antennas, namely omnidirectional and isotropic antennas, using a horn antenna. The objective is to enable the horn antenna to have directional high gain and a wide bandwidth, while also obtaining uniform radiation patterns akin to an isotropic antenna. By striking a balance between these two different antenna characteristics, a medium antenna with useful properties for broadcast applications can be created. The goal of this effort is to overcome some mmW antenna design challenges mentioned in section 6.2.2.

6.3.1 Introduction

This research introduces a novel antenna element that addresses the limitations of the millimeter-wave (mmWave) spectrum by utilizing high antenna gain. Unlike conventional stepped antenna elements, this design allows for lower transmission supply voltages while maintaining high practical isotropic transmitted power and gain. Instead of using multiple antenna elements like dipole or microstrip patch antennas, this design simplifies the structure by using a single antenna with a large radiating aperture. For millimetre wave communication, a substrate-integrated H-plane horn antenna is chosen for its ease of fabrication. However, a major concern

with substrate-integrated horn arrays is the presence of side lobes. Designing a wideband horn with high gain becomes a challenging task that has received limited investigation.

To overcome this challenge, the research presents a novel millimetre-wave antenna structure based on multilayered substrate and patch topology. The antenna offers a large bandwidth and high gain, making it suitable for 5G broadband and mmWave wireless applications. The proposed antenna demonstrates an impedance bandwidth from 24-40 GHz, with S11 (return loss) below 12 dB, and a gain of 8.1$\pm$ 0.8 dBi at the design frequency of 28 GHz.

The antennas operating in mm-wave frequency range give high data rate feature in communication systems [131]. Directional antennas are an excellent choice in high frequency range path loss exponent, Doppler shift spread and delay spread [132-133]. In past, various techniques have been used to improve bandwidth e.g. slotted patches [134-113], multi-layered strip lines [113], stacked patches [135-136] and substrate integrated patches. A substrate integrated waveguide (SIW) feed-network technique is used in [137-138] for large impedance bandwidth with high gain. In substrate-integrated horn antennas, the gain is enhanced with different structures like metal vias [139], horn walls [114] and SIW gap mechanism [140]. A hypothesis is traced from the above-mentioned papers to get broadband feature with high gain radiation pattern. Previously, substrate integrated waveguide (SIW) feed networks and slotted patches are used to increase bandwidth but in [139] the same topology was used additionally with a horn patch drawn with the metallic vias. The topology of SIW substrate structure by using two substrates supported with metallic vias has been adopted However, a complete horn-shaped patch is used on the upper substrate. The challenge of optimized calculation of horn-patch dimension was solved by taking the one-face dimensions of a WR-28 horn antenna. For the purpose, firstly full wave horn antenna at 28 GHz using WR-28 waveguide designed and dimensions are optimized by using following horn-antenna equations.

$$\left(\sqrt{2x}-\frac{b}{\lambda}\right)^2(2x-1)=\left(\frac{G_\circ}{2\pi}\sqrt{\frac{3}{2\pi}}\ \frac{1}{\sqrt{x}}-\frac{ba}{\lambda}\right)^2\ \ \left(\frac{G_\circ}{6\pi^3}\ \frac{1}{x}-1\right) \quad 6.1$$

$$\frac{\rho_e}{\lambda}=\ x \quad 6.2$$

$$\frac{\rho_e}{\lambda}=\ \frac{G_\circ^2}{8\pi^3}\left(\frac{1}{x}\right) \quad 6.3$$

$$x_{trial}=x_1=\ \frac{G_\circ}{2\pi\sqrt{2\pi}} \quad 6.4$$

$$a_1=\sqrt{3\lambda\ \rho_2}=\sqrt{3\lambda\ \rho_h}=\frac{G_\circ}{2\pi}\ \sqrt{\frac{2\pi}{2\pi x}} \quad 6.5$$

$$b_1=\sqrt{3\lambda\ \rho_1}=\sqrt{2\lambda\ \rho_e}=\sqrt{2x\lambda} \quad 6.6$$

In the 2nd step picked the H-plane view of the horn antenna (from the calculated dimensions using above equations) for the proposed dimensions to draw a horn patch on the substrate. In the next step, from the calculated dimensions of horn antenna, authors draw a patch on the upper substrate of the proposed antenna by taking the one-face (H-plane) dimensions of a WR-28 horn antenna.

6.3.2 Antenna Configuration

The antenna in this design covers the millimetre wave band 20-45 GHz for wireless application. The centre frequency of the proposed antenna's design is 28 GHz. To start with, a single substrate horn patch is printed with the rule of a sectoral H-plane horn antenna, where a1 and b1 are dimensions of aperture and a & b are the distance from horn throat to wave guide, as illustrated in Figure 6.2. The proposed antenna element is composed of major horn structure with width D and length L. The width and length are extracted through the theory model described in the [112]. The printed horn's aperture has been optimised using the fullwave simulator (HFSS), and the improved design parameters are displayed in Table 6.1. It is observed that the gain of the antenna is 5dBi and impedance bandwidth is 25-30GHz.

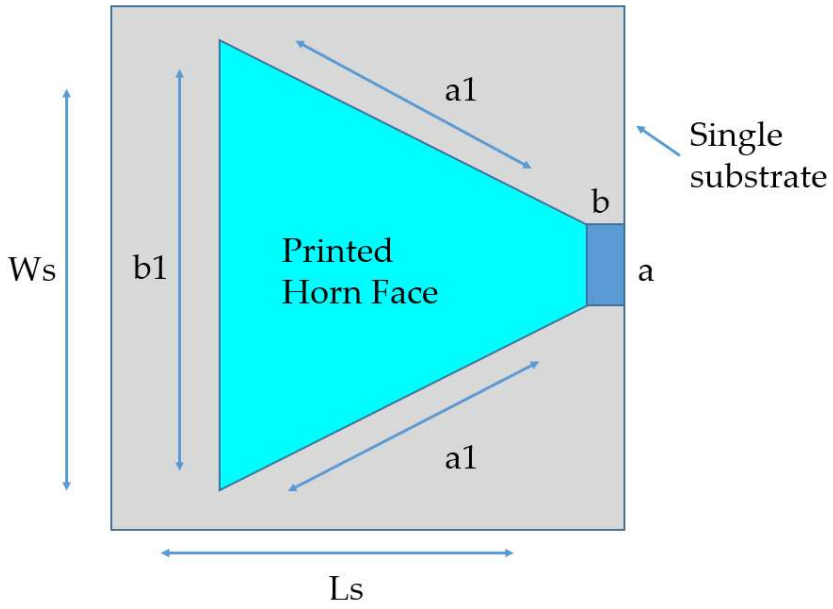

Figure 6.2 Horn prototype for proposed antenna.

(a) *Substrate Layering and Patch Topology*

The design of mmW antenna is based on a multilayered substrate structure. The antenna geometry with the layered substrate is illustrated in Figure 6.3. To increase the gain and bandwidth, multilayered topology with slots is implemented in the printed aperture horn antenna. The substrate of the same dimension and material as the base antenna, is lodged beneath the first substrate, to make a sandwich structure. The antenna is designed on a double-sided sandwich substrate made up of Roger RO3003 which has a thickness of H and a relative dielectric constant of εr = 2.2. Two substrates made a sandwich structure which are supported through steel cylinders. The slotted patches are introduced on the printed horn face to increase the gain. The slotted patches are an inspired form of a square shape resonator. In the centre of the printed horn, slotted resonating patches are etched. The horn-shaped patch serves as the primary radiator, with these square-shaped slits engraved on the top surface as illustrated in Figure 6.4.

Table 6.1: Optimized parameters of the proposed antenna.

Parameters	Values HB (mm)	Description
Ws	55	Width of substrate
Ls	65	Length of substrate
Hs	0.5	Height of substrate
a	7	Length of waveguide
b	3.5	Width of waveguide
a1	47	length of horn
b1	37	length of flare
Sr	0.6	Slit radius
Sg	0.2	Slits gap
Pl	20	Length of patch
Pw	10	Width of patch

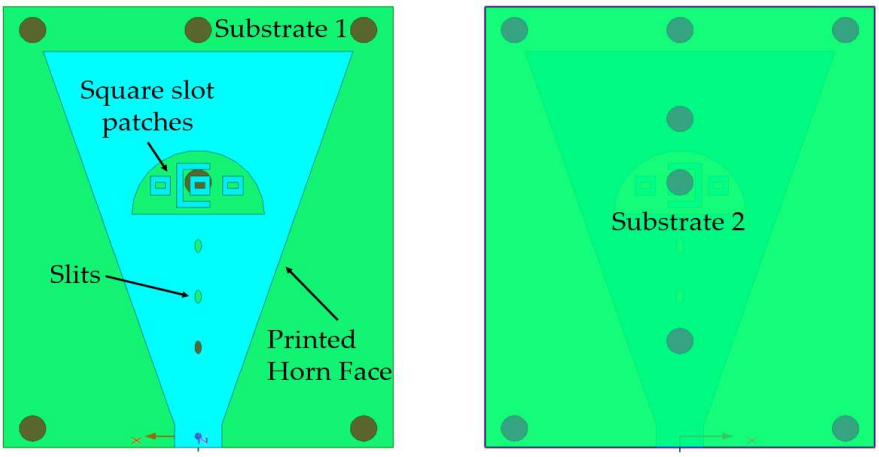

Figure 6.3 Description of the proposed antenna (a) Front view, (b) Back view.

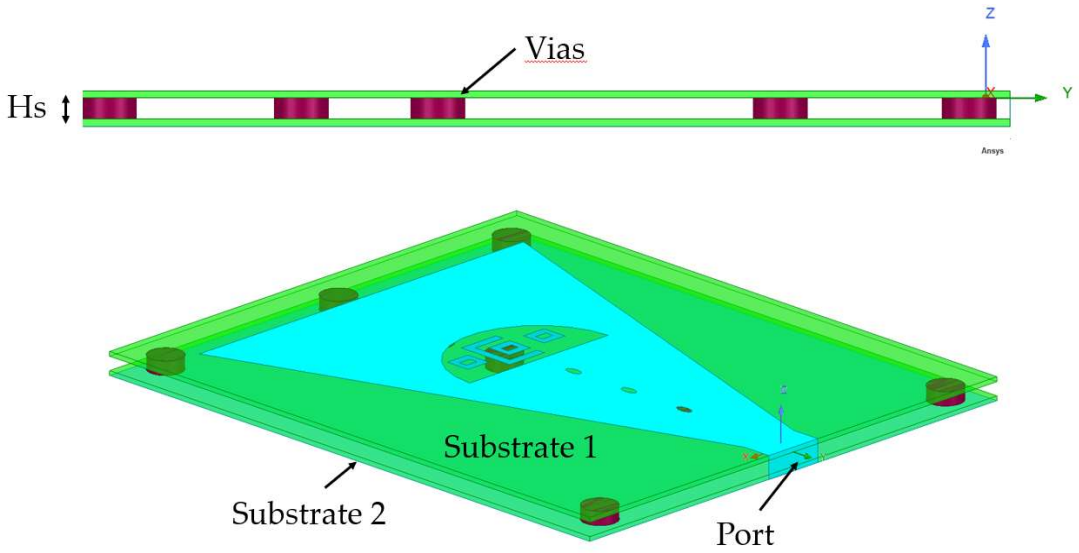

Figure 6.4 Substrate layering of proposed antenna.

6.3.3 Working Principle and Optimization

Based on a thorough analysis of the literature, it is determined that wireless 5G applications require a wideband, high-gain, affordable, low-profile, and small antenna. The low-profile, small-footprint, and simple-to-integrate substrate integrated horn antennas used in millimetre wave communications are emphasised. Horn antennas are a desirable option for constructing substrate integrated horn (SIW) shape patch antennas for 5G applications because of their directional nature and greater bandwidth capabilities, making them suited for high-gain broadband applications. An alternate approach where various correction structures, including as horn walls, metal through arrays, and SIW gap technologies [113,114,115] have been used to increase gain in substrate integrated horn antennas, was considered, however they frequently have a constrained impedance bandwidth.

In the proposed antenna design, a sandwich structure using RO3003(tm) dielectric substrates and stainless-steel columns is suggested as an alternative to the SIW

structure. For 5G applications requiring high data rates, approaches like slotted patches have been investigated to increase impedance bandwidth in low-profile microstrip antennas.

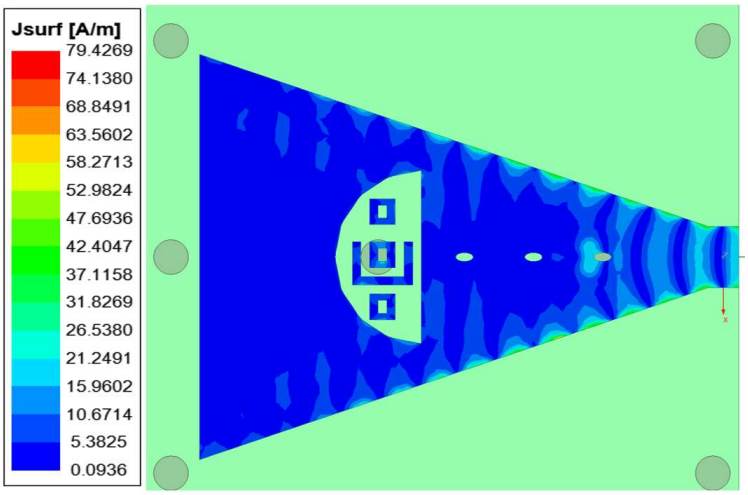

Figure 6.5 Surface current distribution of proposed antenna.

It is suggested to combine square patches with slits to create a sandwich substrate structure. Square patch and slit size are adjusted to maintain the desired radiation pattern while achieving high gain and good impedance matching performance. The upper metallic surface of the horn aperture has 0.23mm-wide holes etched into it. The slots are spaced apart by w1 and are arranged in a column. Slits are designed with the goal of achieving superior radiation performance. The square-shaped slots in the centre patch provide a boost to maintain the bandwidth. To increase the effectiveness of the radiation, WxL-sized gaps surrounding the patch are used to suppress the surface wave current.

(a) *Impact of Slits Topology*

The effect of slits on the functionality of horn antennas is discussed. Figure 6.5 depicts simulated surface current distributions at 33 GHz for the purpose of analysing the role of the down extra slits. Slits contribute to an almost uniform current distribution. Additionally, Figure 6.5 shows the simulated distributions of the surface current along the horn aperture. A more stable current distribution is

attained as a result of the slit's. These findings demonstrate that the substrate layering with slits topological structure may successfully modify the current distributions over the horn aperture. The results confirm that the substrate layering with slits topology structure effectively adjusts both the phase and amplitude distributions of the field over the horn aperture.

Figure 6.6 shows the simulated $|S_{11}|$ (reflection coefficient) of the antennas with and without the slits, demonstrating that the slits have no impact on the impedance matching, yet they maintain a high gain. Figure 6.7 clearly illustrates the gain of the antenna with and without the inclusion of slits and patches while maintaining the clarity of the patterns. The design incorporates the concept of a complementary source horn and achieves a wide bandwidth of 56% for $|S_{11}| < -10$ dB (from 22.5 to 40 GHz), covering the frequency bands relevant to fifth-generation mobile communications.

6.3.4 Experimental Results

The suggested antenna's performance and features have been examined. The antenna's total dimensions are 69.4 mm 58.8 mm 2.5 mm. The goal of this project is to improve the gain and operating bandwidth of the H-plane sectoral horn patch. To accomplish this, a multi-layered and slotted substrate topology with a printed H-plane sectoral horn is used. A multi-layered sandwich substrate with a slotted horn patch is used in the suggested design. Due to the constraints of the antenna's gain and impedance bandwidth with traditional construction, a multi-layered topology was implemented. This design significantly enhances the bandwidth while keeping a steady radiation pattern, ensuring performance below 10dB. The horn patch is on the top substrate, and the ground patch is present.

The simulation findings match up nicely, as illustrated in Figure 6.8, which shows a broadside radiation pattern like that of a waveguide horn antenna with a wide impedance bandwidth. Because it offers better gain, a narrow beam antenna radiation pattern is preferred in long-range communication systems. The narrow beam focuses the antenna's energy in a specific direction, allowing for long-

distance transmission and reception with increased signal strength. This type of antenna is commonly used in applications where a concentrated, directed signal is necessary to establish communication over significant distances.

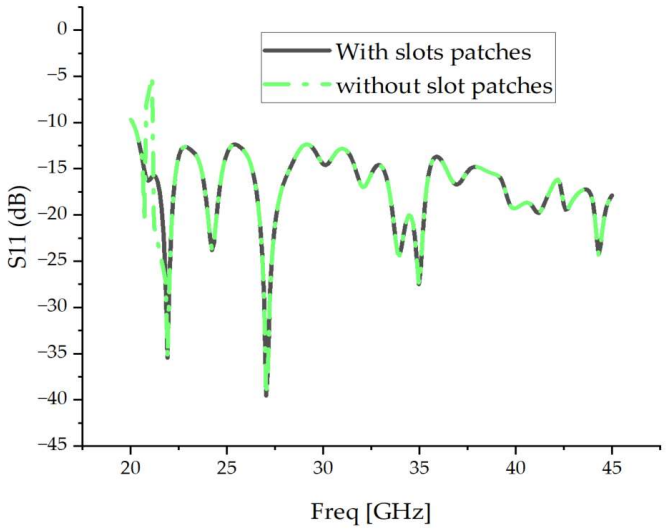

Figure 6.6 Return loss of proposed antenna.

On the other hand, for short-range communication systems, a wide beam pattern is more advantageous. A wide beam pattern allows for broader coverage, as the antenna disperses its energy over a wider area. This is beneficial in scenarios where the communication range is shorter, and the goal is to provide coverage to a larger area or multiple devices simultaneously. The choice of a narrow or wide beam antenna radiation pattern depends on the specific requirements of the communication system and the desired coverage area. Long-range systems prioritize high gain and targeted signal delivery, while short-range systems focus on wide coverage for multiple devices or a broader area.

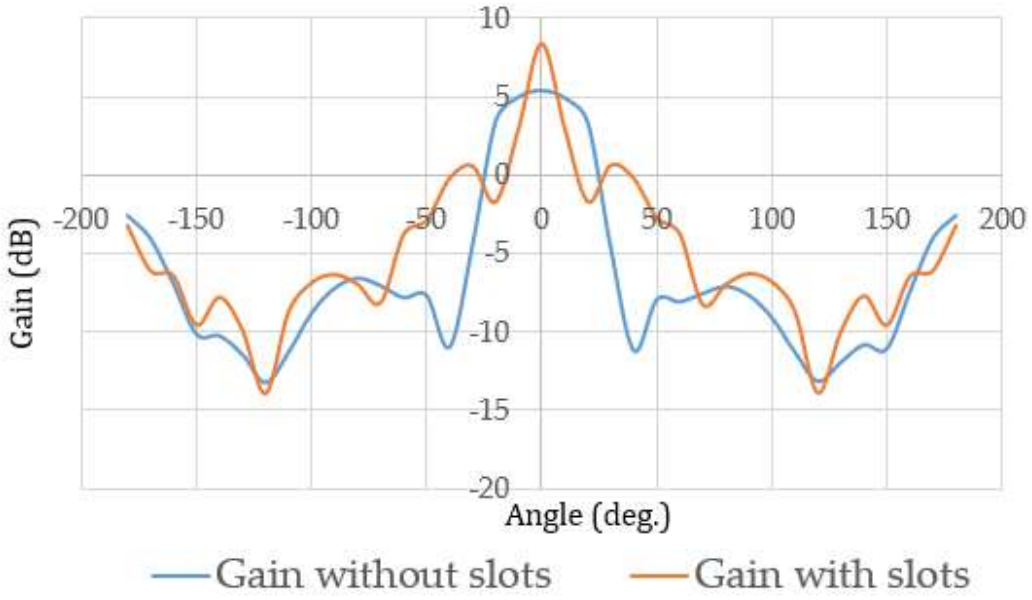

Figure 6.7 Gain of the proposed antenna at 28GHz.

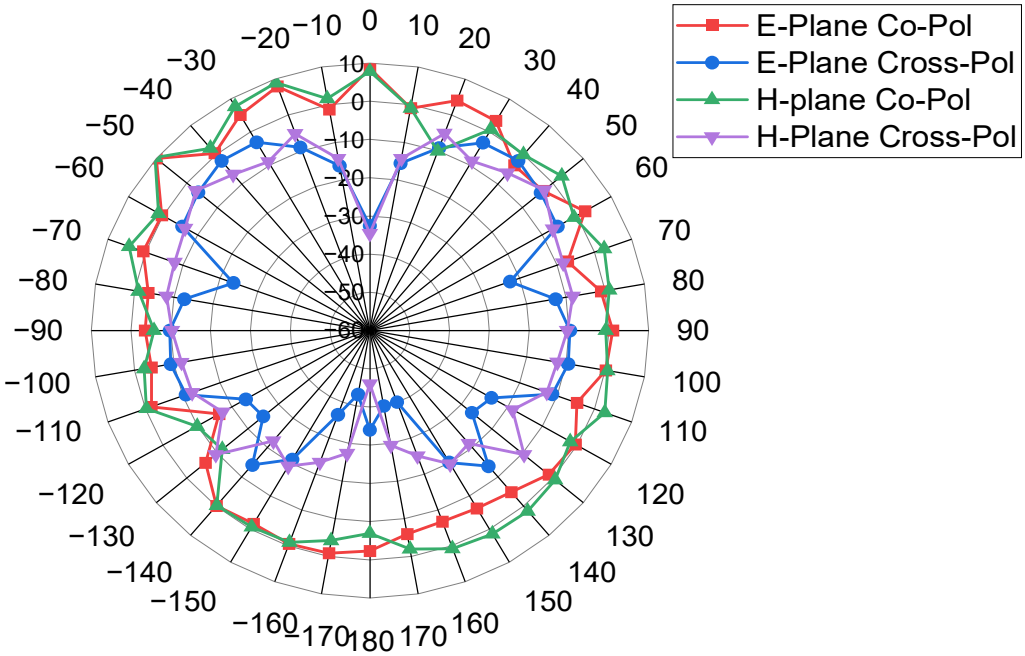

(a)

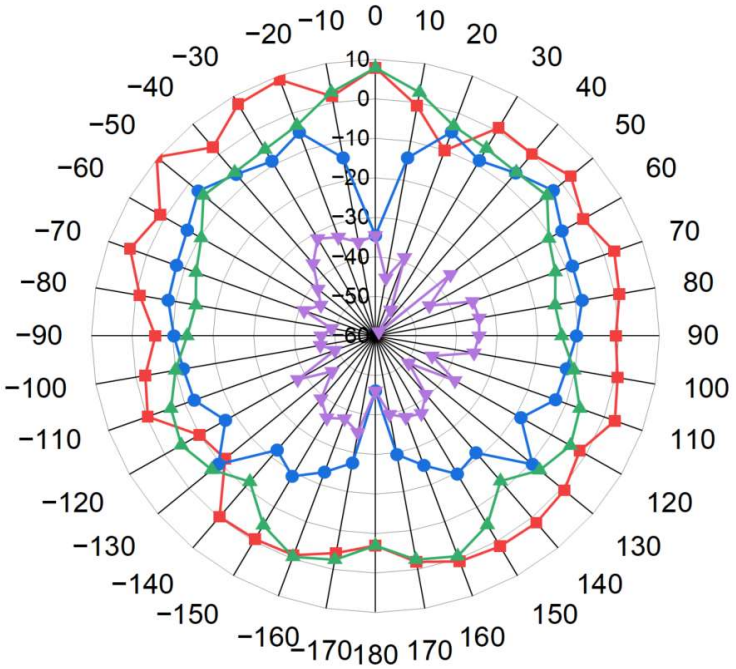
0
10
20
30
40
50
60
70
80
90
100
110
120
130
140
150
160
170
180
−170
−160
−150
−140
−130
−120
−110
−100
−90
−80
−70
−60
−50
−40
−30
−20
−10
10
0
−10
−20
−30
−40
−50
−60

(b)

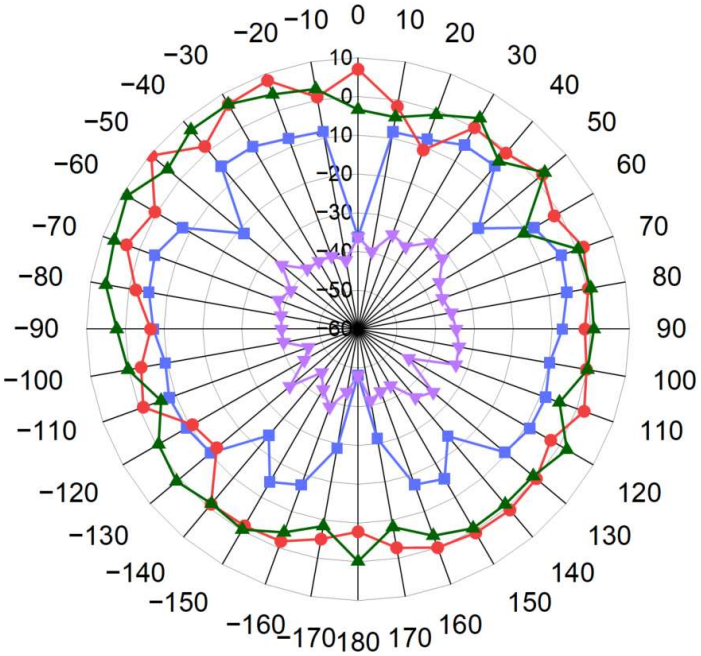
0
10
20
30
40
50
60
70
80
90
100
110
120
130
140
150
160
170
180
−170
−160
−150
−140
−130
−120
−110
−100
−90
−80
−70
−60
−50
−40
−30
−20
−10
10
0
−10
−20
−30
−40
−50
−60

(c)

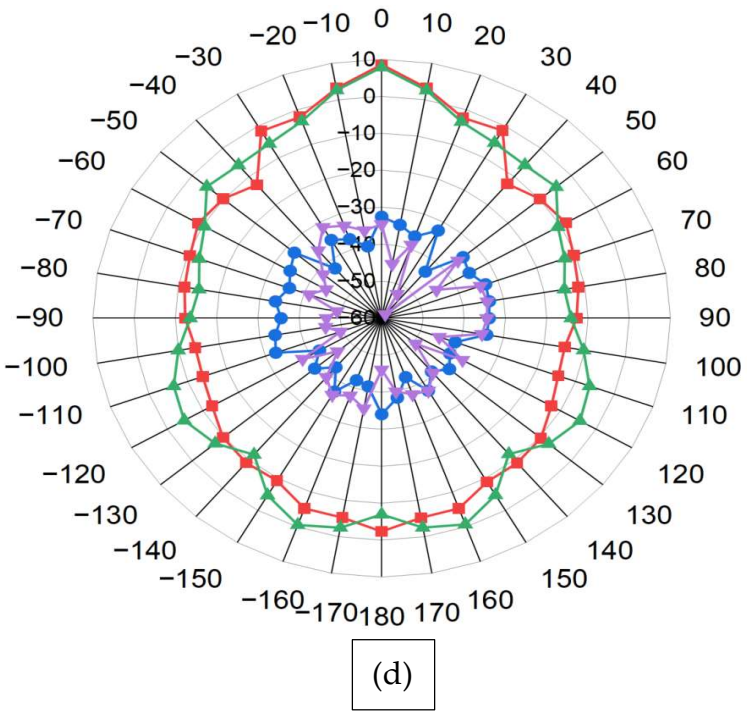

Figure 6.8 Radiation patterns of proposed antenna (a) 32 GHz (b) 36GHz (c) 40 GHz (d) 28GHz (design Freq).

Table 6.2: Comparison of Proposed antennas.

No.	Antenna Description	Frequency	Gain (dB)	Bandwidth
1	WR28 full horn antenna	28 GHz	20.2	18-40 GHz
2	Single substrate printed horn antenna	28 GHz	5.8	26.5-30.8 GHz
3	Proposed multilayered antenna	28 GHz	8.64	20-35 GHz (onward)

6.4 Summary

For a multitude of reasons, millimetre-wave (mmWave) antennas are vital for 5G broadcast applications. When compared to lower frequency bands utilised in conventional cellular networks, mmWave frequencies provide noticeably greater

bandwidths. This makes it possible for 5G broadcast applications to reach considerably higher data rates, enabling the delivery of significant volumes of multimedia material, such as high-definition video and virtual reality experiences. These high data speeds are supported by mmWave antennas, which also offer the capacity required for effective broadcast services. As 5G broadcast applications require a high capacity to serve a large number of simultaneous users. mmWave technology provides a solution by enabling the deployment of dense small cell networks. Beamforming and beam steering techniques are possible with mmWave antennas, which frequently take the form of phased array antenna systems. These features increase capacity and coverage, providing effective distribution of broadcast material to several consumers in a certain region.

MmWave signals incur increased route loss due to their shorter wavelengths, making them more vulnerable to obstruction from objects like trees and buildings. In order to deliver reliable coverage, mmWave antennas are frequently used in tiny cells that are positioned near to customers. This method enables the effective transmission of broadcast material to users in particular places, such as conference rooms, music halls, and sports stadiums.

MmWave antennas may be designed to have directional features, enabling the transmission and reception of targeted signals. In order to direct and shape the antenna's radiation pattern towards the targeted users, beamforming techniques are used, which strengthens the signal and lowers interference. When content delivery targeting is required for 5G broadcast applications, this functionality is especially helpful.

Chapter 7: Future Works for Next Generation Multi-Band Technologies

7.1 Future Trends in 5G Base Station Antennas

The foundation of any BSA antenna is the radiating elements in the arrays. Therefore, it is important to select wideband radiating elements with stable radiation patterns. Table 7.1 contains some of the recent state-of-the-art radiating elements that show wideband performance. Some of the design concepts used in the design of these elements can be used as the basis to develop more improved radiating elements for current and future 5G antennas.

The massive MIMO is one of the most popular topics among the 5G BSA community. Currently the massive MIMO used in the 5G network is typically standalone i.e. contains only one frequency band commonly referred to as mid band (2.6GHz-4.2GHz) with 32 or 64 ports (8 dual polarized columns with 2 or 4 rows). No other bands are integrated in those active antennas. The massive MIMO antennas require the radios to be used for each of the ports. Despite the high throughput advantage of these massive MIMO antennas, the extreme power consumption puts a significant loading on the electrical network. The operators can't remove the existing 4G BSAs to reduce the power consumption since the current 5G massive MIMO antennas can't still serve all the frequency bands. Therefore, the industry is leaning towards integrating legacy multiband 4G antennas with 5G massive MIMO antennas. One potential approach is to reduce the number of ports in massive MIMO BSAs from 32 to 16 and provide some space to integrate a legacy antenna. The aim is to strike a balance with operational cost and performance. The combination of legacy 4G and 5G massive MIMO still poses the challenges highlighted in the work. For example, the low band (under 1GHz) needs to be decoupled in an even wider band from 1.4 GHz-4.2GHz, which is very difficult. Moreover, the antenna profile is required to be slimmer for less wind loading, making the technical design more difficult. Possibilities remain open to design novel wideband frequency selective surfaces to overcome some of these

challenges of reducing coupling and improving patterns, since more bands are now required to be integrated under one radome.

Table 7.1: Comparison of a selected set of wideband radiating elements used in BSAs.

References	Antenna Element Type	Frequency Band (GHz)	Size *	Impedance Bandwidth	Isolation (dB)	HPBW	XPD (dB)	Gain(dBi)
[26]	Cross-dipole antenna with U-shaped parasitic element	1.68–3.23	0.38λ × 0.38 λ	63%	>32	65 + 5°	<16	8.5
[54]	Octagon shape folded dipoles	1.69–2.71	0.50λ × 0.50λ	46.4%	>28	66.5° ± 5.5°	25	9.8
[55]	Magneto-electric loop antenna	1.7–2.7	0.43λ × 0.43λ	45.5%	NG[#]	66.5° ± 3.5°	>20	NG [#]
[3]	Folded dipole with coplanar stripline	1.7–2.25	0.52λ × 0.52λ	27.8%	>25	66.3° ± 2.9°	>16	>8
[22]	Loop radiator, cross shaped feeding with loop parasitic element	1.7–2.9	0.56λ × 0.56λ	52%	>26	66.2° ± 3.7°	NG [#]	8.5
[11]	Octagonal shaped loop radiator with Y- shaped feeding line	1.7–2.7	0.39λ × 0.39λ	45%	>25	68° ± 2°	NG [#]	8.2
[21]	Slotted patch with shorting strips	0.82–0.99	0.42λ × 0.42λ	18.7%	>30	65° ± 10°	NG [#]	9.9
[20]	Spline edged bowtie radiator	1.42–2.9	0.50λ × 0.50λ	68%	>20	65° ± 11°	20	8
[16]	crossed stepped-width loop dipoles	1.68–2.94	0.41λ × 0.41λ	54.5%	>28.5	66.2° ± 3.7°	NG [#]	8.5
[43]	Square-loop shape dipole	1.63–2.95	0.36λ × 0.36λ	58%	>31	58.1° ± 12°	<27	8.8
[1]	Folded dipole	0.79–1	0.44λ × 0.44λ	23.5%	>30	69°	NG [#]	7.7
[19]	Orthogonal dipoles with fan-shaped slots	2.27–2.53	0.49λ × 0.49λ	52.6%	>25.4	60°	NG [#]	7.6
[23]	Leaf clover antenna with round metal disks and U-shape slot	1.39–2.8	0.42λ × 0.42λ	67%	30	65° ± 5°	NG [#]	9

* size in terms of wavelength(λ) at mid-band frequency, [#] not given.

7.2 Materials for the Antenna and Mechanical Characteristics of the Base Station

In order to send and receive signals from mobile devices, wireless communication systems rely on base station antennas. The best signal coverage is achieved when these antennas are positioned on high points like buildings, towers, or poles. When

it comes to the mechanical and electrical properties of base station antennas, the materials employed in their construction are critical.

Metals, composites, and plastics are just some of the many materials utilised to make base station antennas. Aluminium, steel, and fibreglass are the most prevalent components of base station antennas.

- Base station antennas are often made of aluminium due to the material's low weight, resilience, and resistance to corrosion. Because of its high electrical conductivity, it is also useful for signal transmission and reception. However, aluminium corrodes easily, therefore the antenna's strength degrades over time.
- Steel is often utilised in the building of base station antennas. It is hardy and long-lasting, and it won't rust or corrode. It is however heavier and trickier to manage than aluminium.
- Glass fibres and plastic resin are combined to create fibreglass, a composite material. It is perfect for use in base station antennas due to its low weight, high strength, and resistance to corrosion. Fibreglass, furthermore, is a versatile material that can be shaped into any design.

The design and materials of a base station antenna are what give it its mechanical properties. The antennas need to be sturdy enough to survive the elements, including wind, rain, and the antenna's own weight. To ensure the antenna can endure these stresses, the mechanical qualities of the antenna materials are crucial. A material's mechanical characteristics describe how well it holds together in the face of mechanical stress and deformation. The mechanical properties of an antenna system for a 5G base station will be determined by various different elements, including the design of the antenna, the size of the antenna, and the kind of mounting mechanism that is used. Nevertheless, the following is a list of some generic mechanical features that could be applicable to an antenna system for a 5G base station:

Size and weight: 5G base station antennas may come in a variety of sizes and forms, but in general, they are bigger and heavier than antennas from earlier generations. This is because of the increased number of components that are necessary to support multiple frequency bands and beamforming.

Mounting: Antennas for 5G base stations may be installed on a variety of various kinds of buildings, including roofs, poles, and towers. The mounting mechanism requires sufficient strength to sustain the weight of the antenna as well as resist the stresses caused by wind.

Protection from the elements: The antenna and any related electronics need to be shielded from the environment, particularly in regions that are prone to experiencing severe weather conditions. Features like hermetically sealed enclosures and materials that are resistant to corrosion may be included in weatherproofing.

Ability to be adjusted: In order to get the most performance out of 5G base station antennas, they may need to be adjusted or slanted. The mounting method must make it possible to adjust in a straightforward manner without needing the antenna to be taken apart.

Maintenance: The antenna system should be built to be simple to maintain, with components that are easy to reach and diagnostic tools that allow troubleshooting to be carried out in a timely and effective manner.

5G networks are expected to support very high data rates so the mechanical properties of a 5G base station antenna system should be assessed to ensure dependable and long-lasting performance in a broad variety of climatic circumstances. Base station antenna materials rely on a number of mechanical qualities, including:

- Resistance to deformation or failure under stress as a measure of a material's strength.

- Stiffness referring to a material's resistance to being deformed when stressed.
- Ductility is a material's capacity to undergo plastic deformation in the presence of stress without rupturing.
- Toughness is a measure of a material's resistance to cracking under stress.
- The capacity of a material to sustain repeated loading and unloading cycles without deterioration is known as its fatigue resistance.

When it comes to the mechanical and electrical properties of base station antennas, the materials employed in their construction are critical. In order to provide the best possible signal coverage and dependability, an antenna must be able to tolerate a wide range of climatic and mechanical stresses.

7.3 Summary

All parts of an antenna system, such as the radiating elements, the support members, the radomes, the feed harness and connections, and the hardware and mounting, must be meticulously planned out and constructed. The efficiency and dependability of the antenna system are dependent on each individual component.

In future works the radome design for base station antenna could be a very good option as discussed in section 7.2 Importance for mechanical characteristics of BSA. Radomes used in base station applications are often constructed from fibreglass or plastic to resist severe weather and other environmental factors. Altering the radiation pattern and adding losses to the signal are two ways in which the radome’s design may impact the antenna's performance. Antenna size and weight, as well as mounting location and ambient circumstances, influence hardware and installation decisions. Supporting the antenna at the necessary height and orientation may need the use of towers or masts or other specialised mounting structures.

In addition to the advanced technologies outlined in the future work, there remains ample opportunity to enhance the performance attributes of cellular base station

antennas. The configurations of antenna elements explored in Chapters 3, 4, and 5 could undergo further refinement to decrease antenna profile and size, all the while maintaining high-performance standards. Such enhancements would mitigate mutual coupling, modify antenna arrangement within arrays, and alleviate wind and tower load concerns in practical settings. Further emphasis should be placed on refining HV (horizontal and vertical dipoles) techniques or exploring alternative methods to achieve wideband scattering suppression capabilities while minimizing any adverse effects on antenna matching.

7.4 References

[1] H. Huang, Y. Liu, and S. Gong, "A Novel Dual-Broadband and Dual-Polarized Antenna for 2G/3G/LTE Base Stations," *IEEE Transactions on Antennas and Propagation,* vol. 64, no. 9, pp. 4113-4118, 2016, doi: 10.1109/TAP.2016.2589966.

[2] Y. He, Z. Pan, X. Cheng, Y. He, J. Qiao, and M. M. Tentzeris, "A Novel Dual-Band, Dual-Polarized, Miniaturized and Low-Profile Base Station Antenna," *IEEE Transactions on Antennas and Propagation*, vol. 63, no. 12, pp. 5399-5408, 2015, doi: 10.1109/TAP.2015.2481488.

[3] D. Wen, D. Zheng, and Q. Chu, "A Dual-polarized Planar Antenna Using Four Folded Dipoles and Its Array for Base Stations," *IEEE Transactions on Antennas and Propagation*, vol. 64, no. 12, pp. 5536-5542, 2016, doi: 10.1109/TAP.2016.2623660.

[4] Y. Liu, S. Wang, N. Li, J. Wang, and J. Zhao, "A Compact Dual-Band Dual-Polarized Antenna with Filtering Structures for Sub-6 GHz Base Station Applications," *IEEE Antennas and Wireless Propagation Letters,* vol. 17, no. 10, pp. 1764-1768, 2018, doi: 10.1109/LAWP.2018.2864604.

[5] A. Mandhyan. *4G and 5G capacity solutions comparative study*, Commscope.

[6] I. Kelly, M. Zimmerman, R. Butler, and Y. Zheng, "Base station antenna selection for LTE networks," Commscope, 2017.

[7] H. Zhu, H. Sun, C. Ding, and Y. J. Guo, "Butler Matrix Based Multi-Beam Base Station Antenna Array," i*n 2019 13th European Conference on Antennas and Propagation (EuCAP),* 31 March-5 April 2019, 2019, pp. 1-4.

[8] M. Ansari, B. Jones, H. Zhu, N. Shariati, and Y. J. Guo, "A Highly Efficient Spherical Luneburg Lens for Low Microwave Frequencies Realized with a Metal-Based Artificial Medium," *IEEE Transactions on Antennas and Propagation*, vol. 69, no. 7, pp. 3758-3770, 2021, doi: 10.1109/TAP.2020.3044638.

[9] A. F. A. Fournier. Recommendation on base station antenna standards, NGMN Alliance

[10] K. M. Mak, H. W. Lai, and K. M. Luk, "A 5G Wideband Patch Antenna With Antisymmetric L-shaped Probe Feeds," *IEEE Transactions on Antennas and Propagation*, vol. 66, no. 2, pp. 957-961, 2018, doi: 10.1109/TAP.2017.2776973.

[11] Q. Chu, D. Wen, and Y. Luo, "A Broadband± 45 Dual-Polarized Antenna With Y-Shaped Feeding Lines," *IEEE Transactions on Antennas and Propagation*, vol. 63, no. 2, pp. 483-490, 2015, doi: 10.1109/TAP.2014.2381238.

[12] W. Wang, X. Liu, Y. Wu, and Y. Liu, "A Broadband Filtering Patch Antenna Using T-Probe, Transverse Stubs, and U-Slots," *IEEE Access*, vol. 7, pp. 7502-7509, 2019, doi: 10.1109/ACCESS.2018.2889743.

[13] W. Wu, R. Fan, Z. Zhang, W. Zhang, and Q. Zhang, "A shorted dual-polarized cross bowtie dipole antenna for mobile communication Systems," in *2014 XXXIth URSI General Assembly and Scientific Symposium (URSI GASS)*, 16-23 Aug. 2014 2014, pp. 1-4, doi: 10.1109/URSIGASS.2014.6929509.

[14] A. Elsherbini, J. Wu, and K. Sarabandi, "Dual Polarized Wideband Directional Coupled Sectorial Loop Antennas for Radar and Mobile Base-Station Applications," *IEEE Transactions on Antennas and Propagation*, vol. 63, no. 4, pp. 1505-1513, 2015, doi: 10.1109/TAP.2015.2392773.

[15] R. Li, T. Wu, B. Pan, K. Lim, J. Laskar, and M. M. Tentzeris, "Equivalent-Circuit Analysis of a Broadband Printed Dipole with Adjusted Integrated Balun and an Array for Base Station Applications," *IEEE Transactions on Antennas and Propagation*, vol. 57, no. 7, pp. 2180-2184, 2009, doi: 10.1109/TAP.2009.2021967.

[16] D. Zheng and Q. Chu, "A Wideband Dual-Polarized Antenna with Two Independently Controllable Resonant Modes and Its Array for Base-Station Applications," *IEEE Antennas and Wireless Propagation Letters,* vol. 16, pp. 2014-2017, 2017, doi: 10.1109/LAWP.2017.2693392.

[17] Q. Chu and Y. Luo, "A Broadband Unidirectional Multi-Dipole Antenna with Very Stable Beamwidth," *IEEE Transactions on Antennas and Propagation*, vol. 61, no. 5, pp. 2847-2852, 2013, doi: 10.1109/TAP.2013.2243898.

[18] D. Zheng and Q. Chu, "A Multimode Wideband ± 45° Dual-Polarized Antenna with Embedded Loops," *IEEE Antennas and Wireless Propagation Letters*, vol. 16, pp. 633-636, 2017.

[19] H. Huang, Y. Liu, and S. Gong, "A Broadband Dual-Polarized Base Station Antenna with Anti-Interference Capability," *IEEE Antennas and Wireless Propagation Letters*, vol. 16, pp. 613-616, 2017, doi: 10.1109/LAWP.2016.2594095.

[20] Q. Zhang and Y. Gao, "A Compact Broadband Dual-Polarized Antenna Array for Base Stations," *IEEE Antennas and Wireless Propagation Letters*, vol. 17 no. 6, pp. 1073-1076, 2018.

[21] L. Y. Nie et al., "A Low-Profile Coplanar Dual-Polarized and Dual-Band Base Station Antenna Array," *IEEE Transactions on Antennas and Propagation,* vol. 66, no. 12, pp. 6921-6929, 2018.

[22] D. Wen, D. Zheng, and Q. Chu, "A Wideband Differentially Fed Dual-Polarized Antenna with Stable Radiation Pattern for Base Stations," *IEEE Transactions on Antennas and Propagation*, vol. 65, no. 5, pp. 2248-2255, 2017, doi: 10.1109/TAP.2017.2679762.

[23] Y. Cui, L. Wu, and R. Li, "Bandwidth Enhancement of a Broadband Dual-Polarized Antenna for 2G/3G/4G and IMT Base Stations," *IEEE Transactions on Antennas and Propagation,* vol. 66, no. 12, pp. 7368-7373, 2018, doi: 10.1109/TAP.2018.2867046.

[24] J. D. Kraus and R. J. Marhefkas, *Antennas: For All Applications*, 3rd ed. ed.: Tempe, AZ, USA: McGrw-Hill, 2002, pp. 165–196.

[25] L. H. Ye, X. Y. Zhang, Y. Gao, and Q. Xue, "Wideband Dual-Polarized Four-Folded-Dipole Antenna Array with Stable Radiation Pattern for Base-Station Applications," *IEEE Transactions on Antennas and Propagation*, vol. 68, no. 6, pp. 4428-4436, 2020, doi: 10.1109/TAP.2020.2969749.

[26] C. F. Ding, X. Y. Zhang, and M. Yu, "Simple Dual-Polarized Filtering Antenna with Enhanced Bandwidth for Base Station Applications," *IEEE Transactions on Antennas and Propagation,* vol. 68, no. 6, pp. 4354-4361, 2020, doi: 10.1109/TAP.2020.2975282.

[27] R. Wu and Q. Chu, "Resonator-Loaded Broadband Antenna for LTE700/GSM850/GSM900 Base Stations," *IEEE Antennas and Wireless Propagation Letters*, vol. 16, pp. 501-504, 2017, doi: 10.1109/LAWP.2016.2586079.

[28] Q. Xue, S. W. Liao, and J. H. Xu, "A Differentially Driven Dual-Polarized Magneto-Electric Dipole Antenna," *IEEE Transactions on Antennas and Propagation*, vol. 61, no. 1, pp. 425-430, 2013, doi: 10.1109/TAP.2012.2214998.

[29] Y. Liu, S. Wang, X. Wang, and Y. Jia, "A Differentially Fed Dual-Polarized Slot Antenna With High Isolation and Low Profile for Base Station Application," *IEEE Antennas and Wireless Propagation Letters,* vol. 18, no. 2, pp. 303-307, 2019, doi: 10.1109/LAWP.2018.2889645.

[30] L. Zhao and K. Wu, "A Dual-Band Coupled Resonator Decoupling Network for Two Coupled Antennas," *IEEE Transactions on Antennas and Propagation*, vol. 63, no. 7, pp. 2843-2850, 2015, doi: 10.1109/TAP.2015.2421973.

[31] X. Tang, K. Mouthaan, and J. C. Coetzee, "Dual-band decoupling and matching network design for very closely spaced antennas," in *2012 42nd European Microwave Conference, 29 Oct.-1 Nov. 2012, 2012*, pp. 49-52, doi: 10.23919/EuMC.2012.6459307.

[32] H. Huang, Y. Liu, and S. Gong, "A Dual-Broadband, Dual-Polarized Base Station Antenna for 2G/3G/4G Applications," *IEEE Antennas and Wireless Propagation Letters,* vol. 16, pp. 1111-1114, 2017, doi: 10.1109/LAWP.2016.2623315.

[33] M. Li, X. Chen, A. Zhang, and A. A. Kishk, "Dual-Polarized Broadband Base Station Antenna Backed With Dielectric Cavity for 5G Communications," I*EEE Antennas and Wireless Propagation Letters*, vol. 18, no. 10, pp. 2051-2055, 2019, doi: 10.1109/LAWP.2019.2937201.

[34] M. Mavridou, A. P. Feresidis, and P. Gardner, "Tunable Double-Layer EBG Structures and Application to Antenna Isolation," *IEEE Transactions on Antennas and Propagation*, vol. 64, no. 1, pp. 70-79, 2016, doi: 10.1109/TAP.2015.2496619.

[35] C. Chiu, C. Cheng, R. D. Murch, and C. R. Rowell, "Reduction of Mutual Coupling Between Closely-Packed Antenna Elements," *IEEE Transactions on Antennas and Propagation*, vol. 55, no. 6, pp. 1732-1738, 2007, doi: 10.1109/TAP.2007.898618.

[36] Y. Zhang, X. Y. Zhang, L. Ye, and Y. Pan, "Dual-Band Base Station Array Using Filtering Antenna Elements for Mutual Coupling Suppression," *IEEE Transactions on Antennas and Propagation*, vol. 64, no. 8, pp. 3423-3430, 2016, doi: 10.1109/TAP.2016.2574872.

[37] Y. M. Pan, P. F. Hu, X. Y. Zhang, and S. Y. Zheng, "A Low-Profile High-Gain and Wideband Filtering Antenna With Metasurface," *IEEE Transactions on Antennas and Propagation*, vol. 64, no. 5, pp. 2010-2016, 2016, doi: 10.1109/TAP.2016.2535498.

[38] J. Y. Jin, S. Liao, and Q. Xue, "Design of Filtering-Radiating Patch Antennas With Tunable Radiation Nulls for High Selectivity," *IEEE Transactions on Antennas and Propagation*, vol. 66, no. 4, pp. 2125-2130, 2018, doi: 10.1109/TAP.2018.2804661.

[39] T. L. Wu, Y. M. Pan, P. F. Hu, and S. Y. Zheng, "Design of a Low Profile and Compact Omnidirectional Filtering Patch Antenna," *IEEE Access*, vol. 5, pp. 1083-1089, 2017, doi: 10.1109/ACCESS.2017.2651143.

[40] G. Sun, S. Wong, L. Zhu, and Q. Chu, "A Compact Printed Filtering Antenna With Good Suppression of Upper Harmonic Band," *IEEE Antennas and Wireless Propagation Letters,* vol. 15, pp. 1349-1352, 2016, doi: 10.1109/LAWP.2015.2508918.

[41] W. Yang, S. Chen, Q. Xue, W. Che, G. Shen, and W. Feng, "Novel Filtering Method Based on Metasurface Antenna and Its Application for Wideband High-Gain Filtering Antenna With Low Profile," *IEEE Transactions on Antennas and Propagation*, vol. 67, no. 3, pp. 1535-1544, 2019, doi: 10.1109/TAP.2018.2889028.

[42] S. J. Yang, Y. F. Cao, Y. M. Pan, Y. Wu, H. Hu, and X. Y. Zhang, "Balun-Fed Dual-Polarized Broadband Filtering Antenna Without Extra Filtering Structure," I*EEE Antennas and Wireless Propagation Letters*, vol. 19, no. 4, pp. 656-660, 2020, doi: 10.1109/LAWP.2020.2975844.

[43] Z. Bao, Z. Nie, and X. Zong, "A Novel Broadband Dual-Polarization Antenna Utilizing Strong Mutual Coupling," *IEEE Transactions on Antennas and Propagation*, vol. 62, no. 1, pp. 450-454, 2014, doi: 10.1109/TAP.2013.2287010.

[44] Y. Chen, J. Zhao, and S. Yang, "A Novel Stacked Antenna Configuration and its Applications in Dual-Band Shared-Aperture Base Station Antenna Array Designs," *IEEE Transactions on Antennas and Propagation,* vol. 67, no. 12, pp. 7234-7241, 2019, doi: 10.1109/TAP.2019.2930136.

[45] Y. Zhu, Y. Chen, and S. Yang, "Decoupling and Low-Profile Design of Dual-Band Dual-Polarized Base Station Antennas Using Frequency-Selective Surface," *IEEE Transactions on Antennas and Propagation*, vol. 67, no. 8, pp. 5272-5281, 2019, doi: 10.1109/TAP.2019.2916730.

[46] P. Afanasyev et al., "Multi-beam Luneburg lens antenna for cellular communications," in *2015 9th European Conference on Antennas and Propagation (EuCAP)*, 13-17 April 2015, 2015, pp. 1-4.

[47] L. Matytsine, P. Lagoiski, M. Matytsine, and S. Matitsine, "Large size, lightweight, Luneburg Lenses for multi-beam antenna applications," in *2012 6th European Conference on Antennas and Propagation (EUCAP),* 26-30 March 2012 2012, pp. 2266-2270, doi: 10.1109/EuCAP.2012.6206510.

[48] D. Su, D. Fu, T. N. C. Wang, and H. Yang, "Broadband Polarization Diversity Base Station Antenna for 3G Communication System," in *2007 International Symposium on Microwave, Antenna, Propagation and EMC Technologies for Wireless Communications*, 16-17 Aug. 2007 2007, pp. 593-596, doi: 10.1109/MAPE.2007.4393689.

[49] S. Daoyi, J. J. Qian, Y. Hua, and D. Fu, "A novel broadband polarization diversity antenna using a cross-pair of folded dipoles," *IEEE Antennas and Wireless Propagati*on Letters, vol. 4, pp. 433-435, 2005, doi: 10.1109/LAWP.2005.860191.

[50] W. Fu, D. Thalakotuna, and P. Liversidge, "Stadium antenna," Patent WO 201 605 4672 A1, 2016.

[51] C. Wu and C. F. Yang, "Method and apparatus for improving antenna radiation patterns.," Patent US Patent 7 081 865 B2, 2006.

[52] I. Timofeev, X. Ai, and A. Teillet, "Dual polarized three-sector base station antenna with variable beam tilt," Patent US Patent 7 196 674 B2, 2007.

[53] P. Bisiules and A. S. Shooshtari, "Full wave dipole array having improved squint performance," Patent WO 2016 137 526 A1, 2017.

[54] H. Sun, C. Ding, B. Jones, and Y. J. Guo, "A Wideband Base Station Antenna Element With Stable Radiation Pattern and Reduced Beam Squint," *IEEE Access*, vol. 5, pp. 23022-23031, 2017, doi: 10.1109/ACCESS.2017.2763177.

[55] C. Ding, H. Sun, R. W. Ziolkowski, and Y. J. Guo, "A Dual Layered Loop Array Antenna for Base Stations With Enhanced Cross-Polarization Discrimination," I*EEE Transactions on Antennas and Propagation*, vol. 66, no. 12, pp. 6975-6985, 2018, doi: 10.1109/TAP.2018.2869216.

[56] J. Y. Yin and L. Zhang, "Design of a Dual-Polarized Magnetoelectric Dipole Antenna With Gain Improvement at Low Elevation Angle for a Base Station," *IEEE Antennas and Wireless Propagation Letters,* vol. 19, no. 5, pp. 756-760, 2020, doi: 10.1109/LAWP.2020.2979343.

[57] H. H. Sun, C. Ding, H. Zhu, B. Jones, and Y. J. Guo, "Suppression of Cross-Band Scattering in Multiband Antenna Arrays," *IEEE Transactions on Antennas and Propagation*, vol. 67, no. 4, pp. 2379-2389, 2019, doi: 10.1109/TAP.2019.2891707.

[58] O. Isik, P. Gripo, D. Thalakotuna, and P. Liversidge, "Cloaked low band elements for multiband radiating arrays," Patent US Patent 10 439 285 B2, 2019.

[59] J. C. Soric, A. Monti, A. Toscano, F. Bilotti, and A. Alù, "Dual-Polarized Reduction of Dipole Antenna Blockage Using Mantle Cloaks," *IEEE Transactions on Antennas and Propagation*, vol. 63, no. 11, pp. 4827-4834, 2015, doi: 10.1109/TAP.2015.2476468.

[60] T. Li, Q. Li, M. Zhang, A. X. Zhang, J. Zhang, and X. Chen, "Four-beam Antenna Array with Low Side-lobe for Base Station Application," in *2019 Photonics & Electromagnetics Research Symposium - Fall (PIERS - Fall),* 17-20 Dec. 2019 2019, pp. 2796-2805, doi: 10.1109/PIERS-Fall48861.2019.9021549.

[61] D. M. N. Hamdy. *An introduction to LTE Smart base station antennas,* .

[62] Z. Wu, B. Wu, Z. Su, and X. Zhang, "Development challenges for 5G base station antennas," in *2018 International Workshop on Antenna Technology (iWAT)*, 5-7 March 2018 2018, pp. 1-3, doi: 10.1109/IWAT.2018.8379163.

[63] X. Zhang, D. Xue, L. Ye, Y. Pan, and Y. Zhang, "Compact Dual-Band Dual-Polarized Interleaved Two-Beam Array With Stable Radiation Pattern Based on Filtering Elements," I*EEE Transactions on Antennas and Propagation*, vol. 65, no. 9, pp. 4566-4575, 2017, doi: 10.1109/TAP.2017.2723914.

[64] H. Zhu, H. Sun, B. Jones, C. Ding, and Y. J. Guo, "Wideband Dual-Polarized Multiple Beam-Forming Antenna Arrays," *IEEE Transactions on Antennas and Propagation*, vol. 67, no. 3, pp. 1590-1604, 2019, doi: 10.1109/TAP.2018.2888728.

[65] L. Shen, H. Wang, W. Lotz, and H. Jamali, "Dual Polarization 4x4 MIMO Sub-6GHz Multi-Beam Base Station Antennas," in 2*019 International Symposium on Antennas and Propagation (ISAP),* 27-30 Oct. 2019, 2019, pp. 1-3.

[66] L. Gu, W. Yang, W. Che, D. Chen, Y. Zhang, and W. Feng, "A Dual-Steerable-Beam Multi-Slot Coupled Metasurface Antenna," in 2*018 IEEE International Conference on Computational Electromagnetics (ICCEM)*, 26-28 March 2018, 2018, pp. 1-3, doi: 10.1109/COMPEM.2018.8496675.

[67] M. Sanad and N. Hassan, "A Sub-6 GHz Multi-Beam Base Station Antenna for 5G with an Arbitrary Beam-Tilting for Each Beam," in 2*019 IEEE Radio and Wireless Symposium (RWS),* 20-23 Jan. 2019, 2019, pp. 1-4, doi: 10.1109/RWS.2019.8714542.

[68] H. A. Kayani, Q. Gueuning, N. Goreux, D. Vanhoenacker-Janvier, C. Oestges, and C. Craeye, "Reconfigurable Cellular Base Station Antenna Consisting of Parasitic Radiators," I*EEE Transactions on Industrial Electronics*, vol. 67, no. 8, pp. 7083-7093, 2020, doi: 10.1109/TIE.2019.2935991.

[69] H. Walter, "Sub-6 GHz mMIMO base stations meet 5G's size and weight challenges," *Microwave Journal*, vol. 62, no. 2, pp. 40-52, 2019.

[70] F. Tefiku and C. A. Grimes, "Design of broad-band and dual-band antennas comprised of series-fed printed-strip dipole pairs," I*EEE Transactions on Antennas and Propagation*, vol. 48, no. 6, pp. 895-900, 2000, doi: 10.1109/8.865221.

[71] X. Qi, Z. Fushun, S. Baohua, Z. Yanlin, and L. Qizhong, "A novel dual-band Yagi-Uda antenna for wireless communications," i*n Proceedings of the 9th International Symposium on Antennas, Propagation and EM Theory*, 29 Nov.-2 Dec. 2010, 2010, pp. 289-292, doi: 10.1109/ISAPE.2010.5696456.

[72] Y. Cui, R. Li, and P. Wang, "Novel Dual-Broadband Planar Antenna and Its Array for 2G/3G/LTE Base Stations," *IEEE Transactions on Antennas and Propagation*, vol. 61, no. 3, pp. 1132-1139, 2013, doi: 10.1109/TAP.2012.2229377.

[73] Y. Li, C. Wang, H. Yuan, N. Liu, H. Zhao, and X. Li, "A 5G MIMO Antenna Manufactured by 3-D Printing Method," *IEEE Antennas and Wireless Propagation Letters*, vol. 16, pp. 657-660, 2017, doi: 10.1109/LAWP.2016.2596297.

[74] G. Ding, M. Zimmerman , J. Yu , and H. Qin, "Base station antennas including wiper phase shifters," Patent EP Patent 3 588 670 A1, 2020.

[75] W. Xiao, Z. Xiao, and W. Su, "Base station antenna," Patent US Patent 2016/0248156 A1, 2016.

[76] Y. He, J. Li, S. W. Wong, X. Pan, L. Zhang, and Z. N. Chen, "A Miniaturized Base Station Antenna With Novel Phase Shifter for 3G/LTE Applications," *IEEE Access,* vol. 6, pp. 52877-52888, 2018, doi: 10.1109/ACCESS.2018.2866482.

[77] S. Basaran, U. Olgun, and K. Sertel, "Multiband monopole antenna with complementary split-ring resonators for WLAN and WiMAX applications," *Electronics Letters*, vol. 49, no. 10, pp. 636-638, 2013.

[78] Y.-T. Wan, D. Yu, F.-S. Zhang, and F. Zhang, "Miniature multi-band monopole antenna using spiral ring resonators for radiation pattern characteristics improvement," *Electronics Letters*, vol. 49, no. 6, pp. 382-384, 2013.

[79] H. Cheribi, F. Ghanem, and H. Kimouche, "Metamaterial-based frequency reconfigurable antenna," *Electronics Letters*, vol. 49, no. 5, pp. 315-316, 2013.

[80] C. Sim, H. Chen, K. Chiu, and C. Chao, "Coplanar waveguide-fed slot antenna for wireless local area network/worldwide interoperability for microwave access applications," *IET Microwaves, Antennas & Propagation,* vol. 6, no. 14, pp. 1529-1535, 2012.

[81] He, Y.; Tian, W.; and Zhang, L., "A novel dual-broadband dual-polarized electrical downtilt base station antenna for 2G/3G applications," *IEEE Access*, 5, 15241–15249, 2017.

[82] Soric, J. C.; Monti, A.; Toscano, A.; Bilotti, F.; Alu, A., Dual-Polarized Reduction of Dipole Antenna Blockage Using Mantle Cloaks. *IEEE Transactions on Antennas and Propagation,* 63 (11), 4827-4834, 2015.

[83] Ding, C.; Sun, H.; Zhu, H.; and Guo, Y., "Achieving Wider Bandwidth with Full-Wavelength Dipoles for 5G Base Stations", *IEEE Trans. Antenna Propag*., , 68 (2), 1119-1127, 2020.

[84] Lalbakhsh, A.; Mohamadpour, G.; Roshani, S.; Ami, M.; Roshani, S.; Sayem, A.S.M.; Alibakhshikenari, M.; Koziel, S. Design of a Compact Planar Transmission Line for Miniaturized Rat-Race Coupler With Harmonics Suppression. I*EEE Access*, 9, 129207–129217, 2021.

[85] S. J. Yang and X. Y. Zhang, "Frequency Selective Surface-Based Dual-Band Dual-Polarized High-Gain Antenna," *IEEE Trans. on Ant. and Propag*., vol. 70, no. 3, pp. 1663-1671, 2022.

[86] Ding, H. Sun, R. W. Ziolkowski, and Y. J. Guo, "Simplified Tightly-Coupled Cross-Dipole Arrangement for Base Station Applications," *IEEE Access*, vol. 5, pp. 27491-27503, 2017

[87] Osseiran, A.; Parkvall, S.; Persson, P.; Zaidi, A.; Magnusson, S.; Balachandran, K. 5G Wireless Access: An Overview; 1/28423-FGB1010937; Ericsson: Sweden:2020

[88] Huang, H.; Li, X.; Liu, Y. A dual-broadband base station antenna with ikebana-like arrangement scheme. *Microwave and Optical Technology Letters,* 62, 708-713, 2020.

[89] Farasat, M.; Thalakotuna, D.N.; Hu, Z.; Yang, Y. A review on 5G sub-6 GHz base station antenna design challenges. *Electronics 2021*, 10, 2000

[90] Beckman, C.; Lindmark, B. The evolution of base station antennas for mobile communications. I*n Proceedings of the 2007 International Conference on Electromagnetics in Advanced Applications*, 2007; pp. 85-92

[91] Thalakotuna, D.N.; Karmokar, D.K.; Hu, Z.; Esselle, K.P.; Matekovits, L. Improving Cross-Band Isolation in MultiBand Antennas. In Proceedings of the 2021 International Conference on Electromagnetics in Advanced Applications (ICEAA),; pp. 068-068, 2021.

[92] Sun, H.-H.; Zhu, H.; Ding, C.; Jones, B.; Guo, Y.J. Scattering suppression in a 4G and 5G base station antenna array using spiral chokes. *IEEE Antennas and Wireless Propagation Letters* 2020, 19, 1818-1822.

[93] Sun, H.-H.; Jones, B.; Guo, Y.J.; Lee, Y.H. Dual-Band Base Station Antenna Array with Suppressed Cross-Band Mutual Scattering. *In Proceedings of the 2021 IEEE International Symposium on Antennas and Propagation and USNC-URSI Radio Science Meeting (APS/URSI)*, 2021; pp. 1-2

[94] Ding, C.; Jones, B.; Guo, Y.J.; Qin, P.Y. Wideband Matching of Full-Wavelength Dipole with Reflector for Base Station. *IEEE Transactions on Antennas and Propagation* 2017, 65, 5571-5576.

[95] Farasat, M.; Thalakotuna, D.; Hu, Z.; Yang, Y. A Simple and Effective Approach for Scattering Suppression in Multiband Base Station Antennas. *Electronics 2022*, 11, 3423.

[96] Zhao, L.; Qian, K.W.; Wu, K.L. A Cascaded Coupled Resonator Decoupling Network for Mitigating Interference Between Two Radios in Adjacent Frequency Bands. IEEE Transactions on Microwave Theory and Techniques 2014, 62, 2680-2688.

[97] Sun, H.-H.; Jones, B.; Guo, Y.J.; Lee, Y.H. Suppression of cross-band scattering in interleaved dual-band cellular base-station antenna arrays. *IEEE Access 2020*, 8, 222486-222495.

[98] Zhang, Y.; Zhang, X.Y.; Ye, L.; Pan, Y. Dual-Band Base Station Array Using Filtering Antenna Elements for Mutual Coupling Suppression. *IEEE Trans. Antennas Propag*. 2016, 64, 3423–3430.

[99] G. An and S. Lee, "Design and implementation of based wireless access point controller using RPC," 2*017 Ninth International Conference on Ubiquitous and Future Networks (ICUFN)*, Milan, , pp. 601-603, 2017.

[100] R. Garg Et. al., Microstrip Antenna Design Handbook. Artech House, Boston, London, 2001.

[101] Y.-L. Kuo and K.-L. Wong, Printed double-T monopole antenna for 2.4/5.2 GHz dual-band WLAN operations, *IEEE Trans Antennas Propag*, 51, 2187–2192, 2003.

[102] R. Zaker, Ch. Ghobadi, and J. Nourinia, A modified microstrip-fed two-step tapered monopole antenna for UWB and WLAN applications*, Prog Electromagn Res,* 77 ,137–148, 2007.

[103] Al-Hasan, M.J., T.A. Denidniand A. Sebak, "A New UC-EBG Based-dielectric Resonator Antennafor Millimeter-wave Applications", I*EEE International Symposium on Antennas and Propagation (APSURSI),* Washington, USA, pp. 1274-1276, 2011.

[104] Elsheakh, D.N., H.A. Elsadek, E.A. Abdallah,M.F. Iskander, and H. Elhenawy,"Ultra wide Bandwidth Umbrella-Shaped Microstrip Monopole Antenna Using Spiral Artificial Magnetic Conductor(SAMC)", *IEEE Antennas and Wireless PropagationLetters*, vol. 8, pp. 1255-1258, June 2009.

[105] Nornikman, H., B.H. Ahmad, M.Z, A. Aziz, F. Malek, H. Imran, and A.R. Othman, "Study and Simulation of an Edge Couple Split Ring Resonator Absorber", *Progress In Electromagnetics Research*, vol.10, pp.319-334, 2012.

[106] H. Nornikman, B. H. Ahmad, M. Z. A. Abd Aziz, A. R. Othman,"Effect of Single Complimentary Split Ring Resonator Structure on Microstrip Patch Antenna Design", I*EEE Symposium on Wireless Technology and Applications (ISWTA)*, pp.239-244, September 2012.

[107] J.B. Pendry, A.J. Holden, D.J. Robins, and W.J. Stewart, Magnetism from conductors and enhanced nonlinear phenomena, *IEEE Trans Microwave Theory Tech*, 47, 2075–2084, 1999.

[108] Y.E. Erdemli and A. Sondas, Dual-polarized frequency-tunable composite left-handed slab, *J Electromagn Wav*es *Appl 19*, 1907– 1918, 2005.

[109] C. Cenk, A. Sondas, and Y.E. Erdemli, Tunable split ring resonator microstrip filter design, I*n: Proceedings of Mediterranean Microwave Symposium,* Genoa, Italy, September, pp. 19–21, 2006.

[110] S.C. Basaran and Y.E. Erdemli, Dual-band split-ring antenna design for WLAN applications, *Turk J Electr Eng Comput Sci*, 16, 79–86, 2008.

[111] R. H. Elabd, H. H. Abdullah, and M. Abdelazim, "Compact Highly Directive MIMO Vivaldi Antenna for 5G Millimeter-Wave Base Station," *Journal of Infrared, Millimeter, and Terahertz Waves*, vol. 42, no. 2, pp. 173-194, 2021/02/01 2021, doi: 10.1007/s10762-020-00765-4.

[112] S. Esfandiarpour and A. Mallahzadeh, "Wideband planar horn antenna using substrate integrated waveguide technique," *in Asia-Pacific Microwave Conference 2011*, 5-8 Dec. 2011 2011, pp. 1969-1972.

[113] K. Fan, Z. C. Hao, and Q. Yuan, "A Low-Profile Wideband Substrate-Integrated Waveguide Cavity-Backed E-Shaped Patch Antenna for the Q-LINKPAN Applications," *IEEE Transactions on Antennas and Propagation,* vol. 65, no. 11, pp. 5667-5676, 2017, doi: 10.1109/TAP.2017.2748181.

[114] N. Bayat-Makou and A. A. Kishk, "Substrate Integrated Horn Antenna with Uniform Aperture Distribution," *IEEE Transactions on Antennas and Propagation*, vol. 65, no. 2, pp. 514-520, 2017, doi: 10.1109/TAP.2016.2640144.

[115] J. Wang, Y. Li, and J. Wang, "Wideband Dipole Array Loaded Substrate-Integrated Horn Array with Improved Sidelobe Performance," *IEEE Antennas and Wireless Propagation Letters*, vol. 18, no. 3, pp. 556-560, 2019, doi: 10.1109/LAWP.2019.2896600.

[116] Luo, Y., Chu, Q. X., & Wen, D. L. "A ±45. dual-polarized base-station antenna with enhanced cross- polarization discrimination via addition of four parasitic elements placed in a square contour," *IEEE Transactions on Antennas and Propagation,* vol, 64, pp.1514–1519, 2016.

[117] Y. Gao, R. Ma, Y. Wang, Q. Zhang, and C. Parini, "Stacked patch antenna with dual-polarization and low mutual coupling for massive MIMO," *IEEE Transactions on Antennas and Propagation*, vol. 64, no. 10, pp. 4544-4549, 2016.

[118] H. Huang, X. Li, and Y. Liu, "5G MIMO antenna based on vector synthetic mechanism," I*EEE Antennas and Wireless Propagation Letters*, vol. 17, no. 6, pp. 1052-1055, 2018.

[119] M. A. Al‐Tarifi, M. S. Sharawi, and A. Shamim, "Massive MIMO antenna system for 5G base stations with directive ports and switched beamsteering capabilities," *IET Microwaves, Antennas & Propagation*, vol. 12, no. 10, pp. 1709-1718, 2018.

[120] A. Alieldin, Y. Huang, M. Stanley, S. D. Joseph, and D. Lei, "A 5G MIMO antenna for broadcast and traffic communication topologies based on pseudo inverse synthesis," *IEEE Access*, vol. 6, pp. 65935-65944, 2018.

[121] K. Yee, "Numerical solution of initial boundary value problems involving Maxwell's equations in isotropic media," *IEEE Transactions on antennas and propagation*, vol. 14, no. 3, pp. 302-307, 1966.

[122] Q.-X. Chu, D.-L. Wen, and Y. Luo, "A Broadband $\pm 45^{\circ} $ Dual-Polarized Antenna With Y-Shaped Feeding Lines," *IEEE Transactions on Antennas and Propagation*, vol. 63, no. 2, pp. 483-490, 2014.

[123] Y. Cui, R. Li, and H. Fu, "A broadband dual-polarized planar antenna for 2G/3G/LTE base stations," *IEEE transactions on antennas and propagation*, vol. 62, no. 9, pp. 4836-4840, 2014.

[124] Y. Gou, S. Yang, J. Li, and Z. Nie, "A compact dual-polarized printed dipole antenna with high isolation for wideband base station applications," *IEEE Transactions on Antennas and Propagation*, vol. 62, no. 8, pp. 4392-4395, 2014.

[125] X. Liu, S. He, H. Zhou, J. Xie, and H. Wang, "A novel low-profile, dual-band, dual-polarization broadband array antenna for 2G/3G base station," in *2006 IET International Conference on Wireless*, Mobile and Multimedia Networks, 2006: IET, pp. 1-4.

[126] B. Li, Y.-Z. Yin, W. Hu, Y. Ding, and Y. Zhao, "Wideband dual-polarized patch antenna with low cross polarization and high isolation," *IEEE Antennas and Wireless Propagation Letters*, vol. 11, pp. 427-430, 2012.

[127] G. Cui, S.-G. Zhou, G. Zhao, and S.-X. Gong, "A compact dual-band dual-polarized antenna for base station application," *Progress in Electromagnetics Research C*, vol. 64, pp. 61-70, 2016.

[128] J. J. Xie, Y. Z. Yin, J. H. Wang, and X. L. Liu, "Wideband dual‐polarised electromagnetic‐fed patch antenna with high isolation and low cross‐polarisation," *Electronics Letters*, vol. 49, no. 3, pp. 171-173, 2013.

[129] F. Zhu et al., "Ultra-wideband dual-polarized patch antenna with four capacitively coupled feeds," *IEEE Transactions on Antennas and Propagation*, vol. 62, no. 5, pp. 2440-2449, 2014.

[130] B. F. Costa and T. Abrão, "Closed-form directivity expression for arbitrary volumetric antenna arrays," *IEEE Transactions on Antennas and Propagation*, vol. 66, no. 12, pp. 7443-7448, 2018.

[131] M. S. Sharawi, M. Ikram, and A. Shamim, "A two concentric slot loop based connected array MIMO antenna system for 4G/5G terminals," *IEEE Transactions on Antennas and Propagation,* vol. 65, no. 12, pp. 6679-6686, 2017.

[132] S. J. Nawaz, N. M. Khan, M. N. Patwary, and M. Moniri, "Effect of directional antenna on the Doppler spectrum in 3-D mobile radio propagation environment," *IEEE Transactions on Vehicular Technology*, vol. 60, no. 7, pp. 2895-2903, 2011.

[133] G. Coviello, A. Florio, G. Avitabile, C. Talarico, and J. M. Wang-Roveda, "Distributed full synchronized system for global health monitoring based on flsa," *IEEE Transactions on Biomedical Circuits and Systems*, vol. 16, no. 4, pp. 600-608, 2022.

[134] H. Sun, Y.-X. Guo, and Z. Wang, "60-GHz circularly polarized U-slot patch antenna array on LTCC," *IEEE Transactions on Antennas and Propagation*, vol. 61, no. 1, pp. 430-435, 2012.

[135] K.-S. Chin, W. Jiang, W. Che, C.-C. Chang, and H. Jin, "Wideband LTCC 60-GHz antenna array with a dual-resonant slot and patch structure," *IEEE Transactions on Antennas and Propagation,* vol. 62, no. 1, pp. 174-182, 2013.

[136] N. Ghassemi, K. Wu, S. Claude, X. Zhang, and J. Bornemann, "Low-cost and high-efficient W-band substrate integrated waveguide antenna array made of printed circuit board process," *IEEE Transactions on Antennas and Propagation*, vol. 60, no. 3, pp. 1648-1653, 2011.

[137] Y. Li and K.-M. Luk, "Wideband perforated dense dielectric patch antenna array for millimeter-wave applications," I*EEE Transactions on Antennas and Propagation*, vol. 63, no. 8, pp. 3780-3786, 2015.

[138] Y. Li and K.-M. Luk, "60-GHz dual-polarized two-dimensional switch-beam wideband antenna array of aperture-coupled magneto-electric dipoles," *IEEE Transactions on Antennas and Propagation*, vol. 64, no. 2, pp. 554-563, 2015.

[139] L. Wang, X. Yin, S. Li, H. Zhao, L. Liu, and M. Zhang, "Phase corrected substrate integrated waveguide H-plane horn antenna with embedded metal-via arrays," *IEEE Transactions on Antennas and Propagation*, vol. 62, no. 4, pp. 1854-1861, 2014.

[140] L. Wang, M. Esquius-Morote, H. Qi, X. Yin, and J. R. Mosig, "Phase Corrected Plane Horn Antenna in Gap SIW Technology," *IEEE Transactions on Antennas and Propagation,* vol. 65, no. 1, pp. 347-353, 2016.